

Oxidation of Volatile Organic Compounds in Aqueous Solution and at the Air-water Interface of Aqueous Microdroplets

Thesis by

Fathima Rifkha Kameel

In Partial Fulfillment of the Requirements

for the Degree of

Doctor of Philosophy

California Institute of Technology

Pasadena, California

2015

(Defended Oct 8th, 2014)

© 2014

Fathima Rifkha Kameel

All Rights Reserved

ACKNOWLEDGMENTS

First of all, I would like to extend my heart-filled gratitude to my advisor, Prof. Michael R. Hoffmann, for the support, enthusiastic encouragement and the guidance provided during my graduate study. Your valuable comments and encouragement made me a better and a stronger scientist. I thank you for giving me the opportunity to join your group and for trusting my capabilities. I also value your advice on balancing my education with family life. I would also like to thank my committee members, Prof. Paul Wennberg, Prof. Mitchio Okumura, Prof. William A. Goddard III and Prof. Simona Bordoni for valuable insights and guidance.

I would also like to express my great appreciation to Dr. Agustín J. Colussi for his guidance, encouragement, insightful comments, feedback and support throughout my stay at Caltech. I am very grateful for his constructive suggestions and planning of my research work. His willingness to give his time so generously is deeply appreciated. I would also like to thank Dr. Nathan Dalleska for technical support and for providing the resources I needed in my research project.

I also would like to acknowledge all group members for their help and support, which enabled me to successfully complete my graduate study. I especially want to thank Tammy Campbell and Jina Choi for their company. I miss you guys a lot. I would also like to thank my lab mates, Chong Woo, Dae Jung, Asghar Aryanfar and Clement Cid, for helping me on numerous occasions. I would also like to express my sincere thanks to my friend Francesca Riboni, a visiting student from Milan, Italy, for her

support both in the lab and outside of academics. I really miss you, and wish you were here with me. I am also grateful and would also like to extend my special thanks to Jae Hong for his help in course work, especially during my first year at Caltech.

I would also like to thank Natalie Gilmore, Assistant Graduate Dean, for supporting me financially when I needed it most and for her guidance about how to successfully complete my studies at Caltech.

Finally, I would like to thank my family, especially my husband Thilina Piyadasa for his unconditional love, support and encouragement. He was always my best supporter. I do not think I could have made it this far without you. Thank you for everything that you brought into my life; I do appreciate it a lot. I am so blessed to have you in my life. I would also like to extend my heartfelt gratitude towards my parents, who helped me with my daughters so that I could complete my studies without any difficulties. Last but not least, I would like to extend my thank you to my in-laws as well for helping me out on numerous occasions.

ABSTRACT

Isoprene (ISO), the most abundant non-methane VOC, is the major contributor to secondary organic aerosols (SOA) formation. The mechanisms involved in such transformation, however, are not fully understood. Current mechanisms, which are based on the oxidation of ISO in the gas-phase, underestimate SOA yields. The heightened awareness that ISO is only partially processed in the gas-phase has turned attention to heterogeneous processes as alternative pathways toward SOA.

During my research project, I investigated the photochemical oxidation of isoprene in bulk water. Below, I will report on the $\lambda > 305$ nm photolysis of H_2O_2 in dilute ISO solutions. This process yields $\text{C}_{10}\text{H}_{15}\text{OH}$ species as primary products, whose formation both requires and is inhibited by O_2 . Several isomers of $\text{C}_{10}\text{H}_{15}\text{OH}$ were resolved by reverse-phase high-performance liquid chromatography and detected as MH^+ ($m/z = 153$) and MH^+-18 ($m/z = 135$) signals by electrospray ionization mass spectrometry. This finding is consistent with the addition of $\cdot\text{OH}$ to ISO, followed by $\text{HO}\cdot$ -ISO \cdot reactions with ISO (in competition with O_2) leading to second generation $\text{HO}(\text{ISO})_2\cdot$ radicals that terminate as $\text{C}_{10}\text{H}_{15}\text{OH}$ via β -H abstraction by O_2 .

It is not generally realized that chemistry on the surface of water cannot be deduced, extrapolated or translated to those in bulk gas and liquid phases. The water density drops a thousand-fold within a few Angstroms through the gas-liquid interfacial region and therefore hydrophobic VOCs such as ISO will likely remain in these relatively

'dry' interfacial water layers rather than proceed into bulk water. In previous experiments from our laboratory, it was found that gas-phase olefins can be protonated *on* the surface of pH < 4 water. This phenomenon increases the residence time of gases at the interface, an event that makes them increasingly susceptible to interaction with gaseous atmospheric oxidants such as ozone and hydroxyl radicals.

In order to test this hypothesis, I carried out experiments in which ISO(g) collides with the surface of aqueous microdroplets of various compositions. Herein I report that ISO(g) is oxidized into soluble species via Fenton chemistry on the surface of aqueous Fe(II)Cl₂ solutions simultaneously exposed to H₂O₂(g). Monomer and oligomeric species (ISO)₁₋₈H⁺ were detected via online electrospray ionization mass spectrometry (ESI-MS) on the surface of pH ~ 2 water, and were then oxidized into a suite of products whose combined yields exceed ~ 5% of (ISO)₁₋₈H⁺. MS/MS analysis revealed that products mainly consisted of alcohols, ketones, epoxides and acids. Our experiments demonstrated that olefins in ambient air may be oxidized upon impact *on the surface* of Fe-containing aqueous acidic media, such as those of typical to tropospheric aerosols.

Related experiments involving the reaction of ISO(g) with ·OH radicals from the photolysis of dissolved H₂O₂ were also carried out to test the surface oxidation of ISO(g) by photolyzing H₂O₂(aq) at 266 nm at various pH. The products were analyzed via online electrospray ionization mass spectrometry. Similar to our Fenton experiments, we detected (ISO)₁₋₇H⁺ at pH < 4, and new m/z⁺ = 271 and m/z⁻ = 76 products at pH > 5.

TABLE OF CONTENTS

Abstract		v
Table of Contents		vii
List of Figures		viii
List of Illustrations		xii
Chapter 1	Introduction and Summary	1
Chapter 2	Polarity and Oxidation Level of Visible Absorbers in Model Organic Aerosol	21
Chapter 3	OH Radical-Initiated Chemistry of Isoprene in Aqueous Media: Atmospheric Implications	46
Chapter 4	Fenton Oxidation of Gas-Phase Isoprene on Aqueous Surfaces	76

LIST OF FIGURES

Figure	page
Figure 2.1: A typical chromatogram of a P1-T1 solution with product detection via UV absorption at 400 nm, 254 nm and total (negative) ion current (TIC) ESI mass spectrometry.	33
Figure 2.2: UV-Visible absorption spectra of species absorbing into the visible in P1-T1 mixtures (aged at 60 °C for 16 h).	34
Figure 2.3: Negative ion chromatogram of species in P1-T1 mixtures (aged at 60 °C for 16 h). A: eluting within 4.5-8.5 min. B: 35-40 min; C: 40-50 min.	35
Figure 2.4a: Negative extracted ion chromatogram (EIC) of some of the most abundant polar species in P1-T1 mixtures (aged at 60 °C for 16 h). The insert zooms in the 25-50 min retention time range	36
Figure 2.4b: Negative extracted ion chromatogram (EIC) of some of the most abundant weakly polar species in P1-T1 mixtures (aged at 60 °C for 16 h). The insert zooms in the 0-25 min	36
Figure 2.5a: Negative extracted $m/z = 289$ ion chromatogram (EIC) in P1 and P1-T1 solutions.	37
Figure 2.5b: Negative extracted $m/z = 269$ ion chromatogram (EIC) in P1 and P1-T1 solutions.	37
Figure 3.1: Chromatograms of the products of the $\lambda > 305$ nm photolysis of aqueous (5 mM ISO in 50 mM H ₂ O ₂) under air for 1 hr.	

a(b) traces correspond to total positive (negative) ion count (TIC) signals detected by ESI-MS. 60

Figure 3.2a: ESI positive ion mass spectrum of the products eluted between 10.70 and 10.84 min, in the photolysis of (10 mM ISO in 50 mM H₂O₂) solutions under air for 1 hr. 61

Figure 3.2b: ESI positive ion mass spectrum of the products eluted between 11.77 and 11.92 min, in the photolysis of (10 mM ISO in 50 mM H₂O₂) solutions under air for 1 hr. 62

Figure 3.3: Extracted ion chromatograms (EIC) of the products $m/z^+ = 135$ (a) and $m/z^+ = 153$ (b) of the photolysis of (10 mM ISO in 50 mM H₂O₂) solutions under air for 1 hr. 63

Figure 3.4: Extracted $m/z^+ = 153$ ion chromatograms of the products of the photolysis of (10 mM ISO in 50 mM H₂O₂) solutions under air for 1 hr. 64

Figure 3.5: $m/z^+ = 153$ ion current as a function of photolysis time for products 1 to 7 (labels as in Fig. 4) in the photolysis of (10 mM ISO in 50 mM H₂O₂) solutions under air. 65

Figure 3.6: Extraction ion chromatograms ($m/z^+ = 135$ [a,b] and 153 [c,d]) of the products of photolysis of Ar-purged versus air-sparged 10 mM ISO samples. 66

Figure 3.7: Extraction Ion chromatograms of 153^+ m/z of the photolysis products of aqueous ISO solutions (1 [a], 2 [b], 5[c] and 10 μ l[d] ISO+ 10 μ l H₂O₂ in 3.5ml MQ H₂O) in the presence of air. The inset shows the area under the trace of 153^+ m/z formed under the different initial amounts of added ISO. 67

Figure 4.1: Negative ESI-MS of FeCl₂ microjets exposed to: N₂(g) (grey trace) ISO(g)/N₂(g)(blue trace), H₂O₂(g)/N₂(g)(green trace), and ISO(g)/H₂O₂(g)/N₂(g)(red trace) streams. The inset represents the mass range where the m/z = 265 product appears. 92

Figure 4.2: MS² of m/z⁻ = 265. 93

Figure 4.3: Positive ESI-MS of 1 μ M FeCl₂ at pH 2 (grey traces) exposed to ISO(g)/N₂(g) (blue traces), H₂O₂(g)/N₂(g) (green traces), ISO(g)/H₂O₂(g)/N₂(g) (red traces). 4.3A: spectra in the m/z = 50 – 600 Da range. 94

4.3B: spectra of the less abundant product species in the m/z=150–350 Da range. Note the 250:1 Y-axis scale expansion in B relative to A. The largest (ISO)₁₋₈H⁺ signals of A were subtracted from the blue and red trace spectra of B for clarity.

Figure 4.4: MS² of (ISO)₂H⁺, m/z=137⁺. 95

Figure 4.5: Zooming in on the evolution of specific mass spectral peaks as functions of gas composition, and the presence of *t*-BuOH as ·OH radical scavenger. ISO(g): blue trace. ISO(g)/ H₂O₂(g)/N₂(g): red trace. ISO(g)/H₂O₂(g) in the

presence of excess dissolved *t*-BuOH (see text): light blue trace. A: $m/z^+ = 155$. B: $m/z^+ = 169$. C: $m/z^+ = 153$. D: $m/z^+ = 171$. 96

Figure 4.6: MS^2 of the $m/z^+ = 153$ and $m/z^+ = 171$ product signals. 97

Figure 4.7: Negative ES-MS of $1\mu\text{M Fe}^{2+}$ at pH 2, exposed to ISO(g)/ H₂O₂(g)/N₂(g) (red line), ISO(g)/ H₂O₂(g)/N₂(g) in the presence of excess dissolved *t*-BuOH ($\sim 100 \times [\text{FeCl}_2]$) (light blue line) in the $m/z=100-350$ Da. 98

LIST OF ILLUSTRATIONS

- Scheme 2.1: Proposed structures of the acids giving rise to the ESI mass spectral signals at $m/z = 269$ and their chromophore. 38
- Scheme 2.2: Proposed structures of the acids giving rise to the ESI mass spectral signals at $m/z = 289$ and their chromophore. 39
- Scheme 3.1: The initiation step leads to several HO-ISO \cdot isomers. 55
- Scheme 3.2: One of the many (propagation + termination) pathways leading to possible products. 56
- Scheme 4.1: Experimental setup – Microjets of 1 μM aqueous FeCl_2 at $\text{pH} \sim 2$ are continuously injected at $25 \mu\text{L min}^{-1}$ into the spraying chamber of an electrospray ionization mass spectrometer, where they are alternatively exposed to gas streams consisting of A: $\text{ISO}(\text{g})/\text{N}_2(\text{g})$, B: $\text{H}_2\text{O}_2/\text{N}_2(\text{g})$, or A + B. 82
- Scheme 4.2: Reaction scheme of further reactions that recycle $\text{Fe}(\text{II})$ and generate $\text{HOO}\cdot$ radicals and $\text{O}_2(\text{g})$ as additional reactants. 84
- Scheme 4.3: Possible structures for the 204 Da $(\text{ISO})_3$ sesquiterpenes and associated 266 Da $\text{C}_{15}\text{H}_{22}\text{O}_4$ products. 87

Chapter 1

Introduction and Summary

Aerosols affect the earth's climate by absorbing or reflecting the Sun's energy (direct effect) and influencing cloud formation (indirect effect). They also degrade the local air quality thereby leading to potential health effects especially lung diseases such as asthma and cancer. Aerosols may be organic or inorganic, but most aerosol or much of the mass is organic in nature, particularly the PM 2.5 fraction. The influence of organic compounds on atmospheric aerosols is far less understood and largely uncertain, predominantly in relation to that of the dominant inorganic aerosol components [1]. This is definitely caused by the large number (up to several hundred or a thousand) and structural complexity of the organic species involved, which are difficult to identify because of the difficulties associated with their collection, separation and the availability of suitable analytical methods. Primary organic aerosols, or POA, are directly emitted into the atmosphere through vehicle exhaust, cooking and biomass burning, whereas Secondary Organic Aerosols, or SOA, are formed from gas-to-particle conversion by oxidation of volatile organic compounds (VOC) present in the atmosphere. Oxidation mainly takes place with OH radicals, ozone or NO_x. SOA compounds are assumed to be largely water soluble or hydrophilic. Although the composition of SOA is the result of complex interactions between trace organic gases

and aerosols, some basic scenarios have been outlined using model systems that await validation.

Isoprene is the most abundant biogenic VOC. About $\sim 600 \text{ Tg/C}$ [2] are being emitted into the atmosphere annually. ISO significantly affects the oxidative capacity of the atmosphere. It has been generally assumed that condensed-phase reactions of hydrophobic substances, i.e., those having small Henry's law constants, would make a negligible contribution to SOA formation. ISO, which has a H constant = 0.036 M atm^{-1} [3], was not considered to produce SOA and was not included in traditional models of SOA formation. In the past, aqueous bulk phase reactions of polar organic compounds, such as glyoxal,[4, 5], methyl glyoxal and pyruvic acid, were proposed as potential sources of SOA. However, after the detection of tetrol species, the main tracer for SOA from isoprene under low NO_x regions in the Amazon forest ISO is being considered as a significant contributor for SOA formation[6]. Since then, ISO has been investigated as a major source of fog/haze and aerosol formation at the surface. During the daytime, photo-oxidation of ISO takes place with OH radicals. The mechanisms of SOA formation under high- NO_x is well understood; however, the mechanism of formation under low- NO_x conditions still remain to be fully characterized. In the low- NO_x regions such as forests, where there is a considerable amount of biogenic VOC emissions, the main mechanism for SOA formation would be the reaction between OH and ISO. In these regions, ISO forms epoxy diols (IEPOX)[7, 8] in the gas phase, and alkene tetrols and oligomers in the aqueous phase[8].

In the high-NO_x regions, apart from the formation of methyl vinyl ketone (MVK), methacrolein (MACR) and hydroxyacetone, ISO also leads to the regeneration of OH radicals through the formation of hydroxyl peroxy radicals[9]. These species also can be either primary or secondary in nature [10]. However, still the mechanism and the product formations are still not fully understood, and there are large discrepancies arising in modeled and measured ISO emission fluxes on the overlying boundary layer. In addition, the revelation that the laboratory generated aerosol underpredicts the oxygenated VOCs generated[11] and the masses of SOA[12, 13]. Field measurements have also revealed that the ·OH radical concentrations measured therein are much higher than those evaluated from current chemical mechanisms[11]. In this thesis, I argue that gas phase chemical reactions alone cannot fully account for all the SOA formed in the atmosphere[14]. Aqueous phase, gas/solid, emerging new concepts in the physical chemistry of interfaces,[15-18] and along with newly-found phenomena at the air-water interface[19-30] demonstrate some of the missing processes that can be used to fill in the mass balance gap. These deficiencies have led researchers to consider the possibility, seemingly by elimination, that other unspecified processors might close the gap[11]. In this thesis, I show that heterogeneous processors (HPs) may play an important role; however, this phenomenon awaits a complementary characterization in the field.

AQUEOUS PHASE REACTIONS

The photochemistry of organic species in the aqueous aerosol media is, in general, quite different from in the gas-phase, or in less polar or hydrogen-donating solvents, and also can be a potential contributor to SOA.

$\text{H}_2\text{O}_2(\text{g})$, having a Henry's law constant $H = 10^5 \text{ M atm}^{-1}$ [31], is extremely soluble in water [32]. Its gas-phase mixing ratio, i.e., the abundance of one component of a mixture relative to that of all the other components, may reach up to 1.5 ppbv (parts per 10^9 by volume), or more [33]. It has been calculated that, typically, ~ 1 ppbv gas-phase H_2O_2 concentrations will lead to 0.1 mM H_2O_2 in aqueous fog and aerosol droplets [34]. Furthermore, dissolved H_2O_2 can undergo solar photolysis generating OH radicals, which can lead to the formation of oxygenated species in the bulk.

Other OH radical precursors in the aqueous phase include Fe(II)/Fe(III) iron (Fenton reaction) species, and nitrate ions, which yield hydroxyl radical via photolysis [35, 36]. Isoprene in the aqueous bulk phase leads to the formation of polyols and other low-vapor pressure compounds (glyoxal, pyruvic acid [PA]), and these low-vapor pressure species undergo further oxidation to form higher mass oligomers. PA acid and GLA, which are highly water-soluble ($H = 3 \times 10^5 \text{ M/atm}$ [37, 38] and $H = 3.6 \times 10^5 \text{ M/atm}$ [39]) and under photo-oxidation, are capable of forming larger macromolecules that possess properties of HULIS (Humic Like Substances), and up to 50% of the aerosol mass consists of macromolecular organic substances [40].

Pyruvic acid is one of the most abundant of the α -dicarbonyls in the atmosphere both in the gas and in the aqueous phase. The α -dicarbonyls arise as a result of oxidation of isoprene (by the oxidation of VOC) and by the photochemical degradation of the colored organic matter in rivers, lakes, and oceans. Their fate is, however, uncertain. The ketonic functionality of the α -dicarbonyl moieties absorbs light above $\lambda \geq 300$ nm. Photolysis alone does not lead to oligomers[41]; rather it often leads to smaller species, but, at the same time, it is capable of producing colored species upon photolysis and aging [42], leading to a large sum of poly-functional high molecular weight oligomeric species [42-44] via slow dehydration of the alcohol functionalities.

HETEROGENEOUS REACTIONS AND MINERAL DUST AEROSOLS

Mineral dust aerosols, which can be another source of hydroxyl radical precursors, constitute an important fraction of the tropospheric aerosol budget. They originate from deserts by wind-blown erosion [45, 46], and fly ash emitted by power plants. Dust events originate in very dry environments in the northern hemisphere, especially the west coast of North Africa and extending through the Middle East into Central Asia, specifically in arid areas such as Sahara and the Gobi deserts. These events are responsible for both generation and deposition of the global airborne mineral dust[47].

Dust aerosols contain transition metal-based semiconductor particles such as Fe_2O_3 , ZnO and TiO_2 . Mineral aerosol sources of iron, i.e., soil particles suspended in the atmosphere by strong winds, represent approximately 95% of the globally-averaged

atmospheric budget, with the remaining fraction attributed to industry, biofuels, and biomass burning [48]. The largest natural source of iron has been identified as coming from the North African deserts, and thus the largest deposition to the oceans occurs in the North Atlantic and Mediterranean downwind of the North African coast [49]. The mass mixing ratio of TiO_2 is 0.1% to 10%, and varies depending on the location and source.

A fraction of the inorganic aerosol consists of semiconducting metal oxides, which can undergo long range transport and can be readily activated by UV-Vis solar radiation, leading to a diverse set of chemical transformations [5]. For example, $\alpha\text{-Fe}_2\text{O}_3$ has a band gap energy of 2.2 eV i.e., equivalent to a wavelength of 520 nm, while TiO_2 has a corresponding band gap energy of 3.2 eV, which is equivalent to a wavelength of 385 nm. When a photon of energy equal to or exceeding the band gap is irradiated onto the surface of a semi conductor, an electron from the valence band can be transferred to the conduction band, leaving a hole (h^+) behind. The 'exciton pair h^+ and e^- ', are capable of promoting a series of oxidation and reduction reactions on the surface of the semiconductor, leading to the *in situ* production of OH radicals, HO_2 radicals and O_2^- [50].

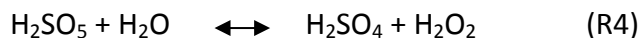
Thus, heterogeneous semiconductor photocatalysis via surface-activated photochemical processes in aqueous media may be a potent source of high-redox potential oxidants under dusty conditions.

INTERFACIAL CHEMISTRY

The troposphere contains airborne liquid water in the form of aerosol, clouds, fog and haze. The large specific surface areas ($S/V \sim 10^{-4}$ to 10^{-5} cm^{-1}) of such dispersions suggest that gas-liquid heterogeneous processes could play a significant role in atmospheric chemistry. Early recognition of this [51] and worldwide concern about atmospheric aerosols[52-55], however, have not translated into the inclusion of heterogeneous processes (HPs) as essential components of atmospheric chemistry until recently, especially over remote (i.e., low NO_x) forests[7].

Aerosol, in the form of water droplets, fog, cloud or haze particles, remains in the troposphere for a considerable period, depending on its size. Typically, droplets of $\sim 1 \mu\text{m}$ diameter will settle $\sim 25 \text{ m}$ per week under typical atmospheric conditions [56]. It also should be noted that the interfacial shells or the surfaces of these droplets, where water density drops a thousand fold within $\sim 1 \text{ nm}$, do not behave similar to bulk water[15, 17]. These interfaces are assumed to be drier than the bulk of the aerosol, and therefore, the properties are quite different from that of the bulk. Therefore, it is assumed that hydrophobic gases colliding with these interfacial shells tend to stick to the surface rather than proceed into bulk water[57]. All of these can increase the resident time at the interface. Having such a long lifetime and interfacial attractions will promote interfacial surface reactions, and the consequent modification of the aerosol's composition as a whole.

Sources of interfacial oxidants may include OH radicals from photolysis of H₂O₂ and OH from Fenton reactions. Generally, H₂O₂ production is associated with reactions occurring in the daytime, involving hydroxyl radical chemistry and species like HO_x, NO_x and ozone[58], with an H₂O₂ daytime production rate of 150 cm⁻³ s⁻¹[59]. However, a few authors have suggested the possibility that hydrogen peroxide is also produced during nighttime[59]; indeed, nitrate radicals, produced in the nighttime stratosphere oxidation of NO, react with hydrogen sulfate ions and produce hydrogen sulfate radicals (R1), whose fate is to dimerize to peroxydisulfuric acid (R2) and subsequently hydrate (R3) to Caro's acid (i.e., peroxymonosulfuric acid). Ultimately, the latter is in equilibrium with sulfuric acid and hydrogen peroxide (R4)[59]:



Given that H₂O₂ is very soluble in water (see above and [32]) and that, as we previously demonstrated, the production of OH radicals, through gas-liquid interface through Fenton reaction, potentially also occurs in the dark (i.e., with no incident

irradiation), isoprene oxidation in the nighttime can also be achieved also by means of processes other than the reactions with NO_3 [60].

FENTONS'S REAXTION

Iron is one of the most abundant elements on the earth surface and is found in cloud water and fog, as well as in mineral dust aerosols (sources include mineral dust from arid regions, anthropogenic emissions and biomass burning). It is also an important source of micronutrients to the ocean phytoplankton [61, 62]. As a redox-active metal, iron may be present in the oxidation states of Fe(II) and Fe(III), and can cycle between them through atmospheric processes, thus affecting the composition of the aerosol [63].

The amount of iron, present as Fe^{2+} in the atmosphere, varies between 0.4 ng/m^3 – 32820 ng/m^3 , and its speciation (oxidation state) is mainly influenced by photochemistry and pH [64]. Several studies have shown that photo-reduction of Fe^{3+} in the presence of organic compounds is an important source of Fe^{2+} in cloud and fog water [63, 65], and the concentration ratio of $\text{Fe}^{2+}/\text{Fe}^{3+}$ depends on the redox potential and the oxidation capacity (i.e. O_2 , O_3 , H_2O_2 and peroxyacids) [36].

The Fenton reaction is capable of producing $\cdot\text{OH}$ radicals via one-electron transfer (R5), and $\text{Fe}^{\text{IV}}\text{O}^{2+}$ species via a two-electron oxidation via O-atom transfe, as in the reaction R6 shown below [66]:



R5 can undergo further reaction to recycle Fe(II) and to generate HOO radicals[67-69] and O₂ as additional sources of oxidants.

Thus, when ISO molecules impinge on fog or haze aerosol containing Fe(II), they may react irreversibly with ·OH-radicals generated *in situ* via gas-phase interface Fenton reactions, either in the day- or nighttime (thus providing a possible contribution to the underestimate isoprene nighttime oxidation), with the rate of product formation depending on the efficiency of the OH radical generation within the aqueous aerosol.

The results presented in this thesis provide direct evidence, for the first time, that VOCs can be oxidized day and night on acidic aerosol via interfacial Fenton chemistry. This process represents an additional pathway for the conversion of organic gases into secondary organic aerosol matter.

SUMMARY

The research reported in my thesis concentrates on SOA formation pathways that are not included in traditional atmospheric chemistry models. This work reveals the potential importance of multiphase reactions in the formation of SOA. These pathways may provide clues as to the unaccounted sources of SOA both in the daytime/nighttime.

My thesis consists of 4 chapters. Chapter 1 provides a brief summary of background and research on aqueous aerosols. Chapters 2 to 4 describe research carried out in aqueous medium both in the bulk and at the interfaces.

In Chapter 2, we investigate the relationship between optical properties and the polarity of model organic aerosol using pyruvic acid as a surrogate to model organic aerosols. Our findings suggest that the visible absorptivity of the aerosol may be due to a small fraction of its chemical components, which are largely comprised of weakly polar species having a significantly smaller O/C ratio than the average. The finding also revealed that the average oxidation level of the aerosol may not be a good descriptor of its 'brownness'. This chapter was published in Chemical Physics letters in April 2014 [70].

In Chapter 3, we carry out an experimental study of the oxidation of aqueous ISO initiated by $\cdot\text{OH}$ radicals (from the photolysis of H_2O_2) in the presence and absence of dissolved O_2 under various experimental conditions. Here, we show that OH-initiated oxidation of ISO leads to the formation of $\text{C}_{10}\text{H}_{15}\text{OH}$ species as primary products, whose formation both require and is inhibited by O_2 . A minimum of seven $\text{C}_{10}\text{H}_{15}\text{OH}$ isomers were resolved by reverse-phase high-performance liquid chromatography and detected as MH^+ ($m/z = 153$). We also prove that the production of OH radicals in the aqueous phase via the photolysis of H_2O_2 is much faster than the gas phase production via photolysis of O_3 . Our calculations can further help to explain the enhanced SOA

concentration/visibility reductions during foggy conditions at sunrise. This chapter was published in the Journal of Physical Chemistry A in April 2013 [71].

In Chapter 4, we explore the possibility of ISO to undergo reactions on surfaces of aqueous droplets containing Fe^{2+} . We also find that gaseous isoprene $\text{ISO}(\text{g})$ is oxidized upon impacting the surface of aqueous FeCl_2 solutions simultaneously exposed to $\text{H}_2\text{O}_2(\text{g})$ via Fenton reaction. We observed the formation of monomer and oligomer species $(\text{ISO})_{1-8}\text{H}^+$ which are herein oxidized into myriad products whose combined yields amount to a minimum of $\sim 5\%$ of $(\text{ISO})_{1-8}\text{H}^+$. MS/MS analysis reveals that protonated species observed losses of H_2O and O neutrals, whereas the less abundant negative ion products undergo CO , H_2O and CO_2 losses. Addition of tert-butanol (as $\cdot\text{OH}$ scavenger) to FeCl_2 solutions significantly inhibited all of the oxidized species, demonstrating that unsaturated volatile gas compounds indeed oxidized upon impact on the surface of Fe-containing aqueous acidic media, such as those of typical tropospheric aerosols. This chapter was published in The Journal of Physical Chemistry C in July 2014 [72].

We also carried out the prospects of $\text{ISO}(\text{g})$ interaction with photolysed surfaces of aqueous H_2O_2 droplets under different pH conditions. ISO is oxidized with the OH radicals generated by photolysis of H_2O_2 at $\lambda = 266 \text{ nm}$. No new product formation was observed at $\text{pH} \leq 6$; However, a few products were observed both in positive and negative modes at $\text{pH} \geq 6$ particularly at $m/z^+ = 271$ and $m/z^- = 76$.

REFERENCE:

1. Fuzzi, S., et al., *Critical assessment of the current state of scientific knowledge, terminology, and research needs concerning the role of organic aerosols in the atmosphere, climate, and global change*. Atmospheric Chemistry and Physics, 2006. **6**: p. 2017-2038.
2. Guenther, A., *Estimates of global terrestrial isoprene emissions using MEGAN (Model of Emissions of Gases and Aerosols from Nature) (vol 6, pg 3181, 2006)*. Atmospheric Chemistry and Physics, 2007. **7**(16): p. 4327-4327.
3. Leng, C., et al., *Temperature-Dependent Henry's Law Constants of Atmospheric Organics of Biogenic Origin*. Journal of Physical Chemistry A, 2013. **117**(40): p. 10359-10367.
4. Galloway, M.M., et al., *Analysis of photochemical and dark glyoxal uptake: Implications for SOA formation*. Geophys Res Lett, 2011. **38**.
5. Carlton, A.G., et al., *Atmospheric oxalic acid and SOA production from glyoxal: Results of aqueous photooxidation experiments*. Atmos Environ, 2007. **41**(35): p. 7588-7602.
6. Claeys, M., et al., *Formation of secondary organic aerosols through photooxidation of isoprene*. Science, 2004. **303**(5661): p. 1173-1176.
7. Paulot, F., et al., *Unexpected Epoxide Formation in the Gas-Phase Photooxidation of Isoprene*. Science, 2009. **325**(5941): p. 730-733.
8. Surratt, J.D., et al., *Reactive intermediates revealed in secondary organic aerosol formation from isoprene*. Proceedings of the National Academy of Sciences of the United States of America, 2010. **107**(15): p. 6640-6645.
9. Surratt, J.D., *Radical regeneration from isoprene*. Nature Geoscience, 2013. **6**(12): p. 995-996.

10. Noziere, B., et al., *Atmospheric chemistry in stereo: A new look at secondary organic aerosols from isoprene*. Geophysical Research Letters, 2011. **38**.
11. Whalley, L., D. Stone, and D. Heard, *New Insights into the Tropospheric Oxidation of Isoprene: Combining Field Measurements, Laboratory Studies, Chemical Modelling and Quantum Theory*, in *Atmospheric and Aerosol Chemistry*, V.F. McNeill and P.A. Ariya, Editors. 2014. p. 55-95.
12. Heald, C.L., et al., *Satellite observations cap the atmospheric organic aerosol budget*. Geophysical Research Letters, 2010. **37**.
13. Ng, N.L., et al., *Organic aerosol components observed in Northern Hemispheric datasets from Aerosol Mass Spectrometry*. Atmospheric Chemistry and Physics, 2010. **10**(10): p. 4625-4641.
14. Barkley, M.P., et al., *Can a "state of the art" chemistry transport model simulate Amazonian tropospheric chemistry?* Journal of Geophysical Research-Atmospheres, 2011. **116**.
15. Donaldson, D.J. and K.T. Valsaraj, *Adsorption and Reaction of Trace Gas-Phase Organic Compounds on Atmospheric Water Film Surfaces: A Critical Review*. Environ. Sci. Technol., 2010. **44**(3): p. 865-873.
16. Valsaraj, K.T., *On the Physiochemical aspect of partitioning of Non-polar Hydrophobic Organics at the Air-water Interface*. Chemosphere, 1988. **17**(5): p. 875-887.
17. Valsaraj, K.T., *A Review of the Aqueous Aerosol Surface Chemistry in the Atmospheric Context*. Open Journal of Physical Chemistry 2012. **2**: p. 58-66.
18. Valsaraj, K.T., et al., *On the Enrichment of Hydrophobic Organic-Compounds in Fog Droplets*. Atmos Environ, 1993. **27**(2): p. 203-210.

19. Enami, S., M.R. Hoffmann, and A.J. Colussi, *How phenol and α -tocopherol react with ambient ozone at gas/liquid interfaces*. J. Phys. Chem. B, 2009. **in press**.
20. Enami, S., M.R. Hoffmann, and A.J. Colussi, *Simultaneous Detection of Cysteine Sulfenate, Sulfinic, and Sulfonate during Cysteine Interfacial Ozonolysis*. Journal of Physical Chemistry B, 2009. **113**(28): p. 9356-9358.
21. Enami, S., M.R. Hoffmann, and A.J. Colussi, *Absorption of Inhaled NO₂*. Journal of Physical Chemistry B, 2009. **113**(23): p. 7977-7981.
22. Enami, S., M.R. Hoffmann, and A.J. Colussi, *Prompt Formation of Organic Acids in Pulse Ozonation of Terpenes on Aqueous Surfaces*. Journal of Physical Chemistry Letters, 2010. **1**(15): p. 2374-2379.
23. Enami, S., M.R. Hoffmann, and A.J. Colussi, *Proton Availability at the Air/Water Interface*. Journal of Physical Chemistry Letters, 2010. **1**(10): p. 1599-1604.
24. Enami, S., M.R. Hoffmann, and A.J. Colussi, *Molecular Control of Reactive Gas Uptake "on Water"*. Journal of Physical Chemistry A, 2010. **114**(18): p. 5817-5822.
25. Enami, S., M.R. Hoffmann, and A.J. Colussi, *Dry deposition of biogenic terpenes via cationic oligomerization on environmental aqueous surfaces*. J. Phys. Chem. Lett., 2012. **3**: p. 3102-3108.
26. Enami, S., et al., *Protonation and Oligomerization of Gaseous Isoprene on Mildly Acidic Surfaces: Implications for Atmospheric Chemistry*. Journal of Physical Chemistry A, 2012. **116**(24): p. 6027-6032.
27. Enami, S., et al., *Superacid Chemistry on Mildly Acidic Water*. Journal of Physical Chemistry Letters, 2010. **1**(24): p. 3488-3493.

28. Enami, S., et al., *Global inorganic source of atmospheric bromine*. J. Phys. Chem. A, 2007. **111**: p. 8749-8752.
29. Mishra, H., et al., *Anions dramatically enhance proton transfer through aqueous interfaces*. Proceedings of the National Academy of Sciences of the United States of America, 2012. **109**(26): p. 10228-10232.
30. Mishra, H., et al., *Bronsted basicity of the air-water interface*. Proceedings of the National Academy of Sciences of the United States of America, 2012. **109**(46): p. 18679-18683.
31. *NASA-JPL Chemical Kinetics and Photochemical Data for Use in Atmospheric Studies, Evaluation Number 14*. 2003.
32. Vacha, R., et al., *Adsorption of atmospherically relevant gases at the air/water interface: Free energy profiles of aqueous solvation of N-2, O-2, O-3, OH, H2O, HO2, and H2O2*. Journal of Physical Chemistry A, 2004. **108**(52): p. 11573-11579.
33. Lelieveld, J. and P.J. Crutzen, *Influence Of Cloud Photochemical Processes on Tropospheric Ozone*. Nature, 1990. **343**(6255): p. 227-233.
34. Seinfeld, J.H. and S.N. Pandis, *Atmospheric chemistry and physics: from air pollution to climate change*. 2nd ed. 2006, Hoboken, N.J.: Wiley.
35. Wang, Y., et al., *Speciation of iron in atmospheric particulate matter by EXAFS*. Chinese Science Bulletin, 2006. **51**(18): p. 2275-2280.
36. Dedik, A.N., P. Hoffmann, and J. Enslin, *Chemical Characterization of Iron in Atmospheric Aerosols*. Atmospheric Environment Part a-General Topics, 1992. **26**(14): p. 2545-2548.

37. Khan, I., P. Brimblecombe, and S.L. Clegg, *The Henrys Law Constant of Pyruvic and Methacrylic Acids*. Environmental Technology, 1992. **13**(6): p. 587-593.
38. Staudinger, J. and P.V. Roberts, *A critical review of Henry's law constants for environmental applications*. Critical Reviews in Environmental Science and Technology, 1996. **26**(3): p. 205-297.
39. Zhou, X.L. and K. Mopper, *Apparent Partition-coefficient of 15 Carbonyl-compound between Seawater, Air and Fresh-water - Implications for Air Sea Exchange*. Environmental Science & Technology, 1990. **24**(12): p. 1864-1869.
40. Andreae, M.O. and A. Gelenczer, *Black carbon or brown carbon? The nature of light-absorbing carbonaceous aerosols*. Atmos. Chem. Phys. Discuss., 2006. **6**: p. 3419-3463.
41. Griffith, E.C., et al., *Photochemistry of aqueous pyruvic acid*. Proceedings of the National Academy of Sciences of the United States of America, 2013. **110**(29): p. 11714-11719.
42. Guzmán, M.I., A.J. Colussi, and M.R. Hoffmann, *Photoinduced Oligomerization of Aqueous Pyruvic Acid*. J. Phys. Chem. A, 2006. **110**: p. 3619-3626.
43. Rincon, A., A. Colussi, and M. Hoffmann, *Chemical identity and thermal behavior of polyfunctional Oligomers from pyruvic acid and photolysis in water and ammonium bisulfate*. 2009, California Institute of Technology: Pasadena.
44. Rincon, A.G., et al., *Optical Absorptivity versus Molecular Composition of Model Organic Aerosol Matter*. Journal Physicochemical A., 2009. **113**: p. 10512-10520.
45. Iuga, C., C.I. Sainz-Diaz, and A. Vivier-Bunge, *On the OH initiated oxidation of C2-C5 aliphatic aldehydes in the presence of mineral aerosols*. Geochimica Et Cosmochimica Acta, 2010. **74**(12): p. 3587-3597.

46. Andreae, M.O. and D. Rosenfeld, *Aerosol-cloud-precipitation interactions. Part 1. The nature and sources of cloud-active aerosols*. *Earth-Science Reviews*, 2008. **89**(1-2): p. 13-41.
47. Cwiertny, D.M., M.A. Young, and V.H. Grassian, *Chemistry and photochemistry of mineral dust aerosol*, in *Annual Review of Physical Chemistry*. 2008, Annual Reviews: Palo Alto. p. 27-51.
48. Louwse, M.J., P. Vassilev, and E.J. Baerends, *Oxidation of methanol by FeO₂⁺ in water: DFT calculations in the gas phase and ab initio MD simulations in water solution*. *Journal of Physical Chemistry A*, 2008. **112**(5): p. 1000-1012.
49. Mahowald, N.M., et al., *Atmospheric Iron Deposition: Global Distribution, Variability, and Human Perturbations*. *Annual Review of Marine Science*, 2009. **1**: p. 245-278.
50. Hoffmann, M.R., et al., *Environmental Applications of Semiconductor Photocatalysis*. *Chemical Reviews*, 1995. **95**(1): p. 69-96.
51. Schryer, D.R., *Heterogeneous Atmospheric Chemistry*. *Geophysical Monographs*. Vol. 26. 1982, Washington, D.C: American Geophysical Union.
52. Heald, C.L., et al., *A large organic aerosol source in the free troposphere missing from current models* *Geophys. Res. Lett.*, 2005. **32**: p. L18809.
53. Kanakidou, M., et al., *Organic aerosol and global climate modelling: a review*. *Atmos. Chem. Phys.*, 2005. **5**: p. 1053-1123.
54. Kroll, J.H. and J.H. Seinfeld, *Chemistry of secondary organic aerosol: Formation and evolution of low-volatility organics in the atmosphere*. *Atmos. Environ.*, 2008. **42**: p. 3593-3624.

55. Munger, J.W., et al., *Fogwater Chemistry in an Urban Atmosphere*. J. Geophys. Res., 1983. **88**(NC9): p. 5109-5121.
56. Finley, J.W., E.L. Wheeler, and S.C. Witt, *Oxidation of Glutathione by Hydrogen-Peroxide and other Oxidizing-Agents*. Journal of Agricultural and Food Chemistry, 1981. **29**(2): p. 404-407.
57. Goss, K.U., *Predicting Adsorption of Organic Chemicals at the Air-Water Interface*. J. Phys. Chem. A, 2009. **113**(44): p. 12256-12259.
58. Monks, P.S., *Gas-phase radical chemistry in the troposphere*. Chemical Society Reviews, 2005. **34**(5): p. 376-395.
59. Pedersen, T., *Nighttime Hydrogen-Peroxide Production on Sulfuric Acid-Aerosols involving Nitrate and Sulfate Radicals*. Geophysical Research Letters, 1995. **22**(12): p. 1497-1499.
60. Brown, S.S. and J. Stutz, *Nighttime radical observations and chemistry*. Chemical Society Reviews, 2012. **41**(19): p. 6405-6447.
61. Gao, Y., S.M. Fan, and J.L. Sarmiento, *Aeolian iron input to the ocean through precipitation scavenging: A modeling perspective and its implication for natural iron fertilization in the ocean*. Journal of Geophysical Research-Atmospheres, 2003. **108**(D7).
62. Sholkovitz, E.R., et al., *Fractional solubility of aerosol iron: Synthesis of a global-scale data set*. Geochimica Et Cosmochimica Acta, 2012. **89**: p. 173-189.
63. Pehkonen, S.O., et al., *Photoreduction of Iron Oxyhydroxides In the presence of important Atmospheric Organic-Compounds*. Environmental Science & Technology, 1993. **27**(10): p. 2056-2062.

64. Oakes, M., et al., *Characterization of soluble iron in urban aerosols using near-real time data*. Journal of Geophysical Research-Atmospheres, 2010. **115**.
65. Siefert, R.L., et al., *Iron Photochemistry of Aqueous Suspensions of Ambient Aerosols with added Organics-Acids*. Geochimica Et Cosmochimica Acta, 1994. **58**(15): p. 3271-3279.
66. Enami, S., Y. Sakamoto, and A.J. Colussi, *Fenton chemistry at aqueous interfaces*. Proc. Natl. Acad. Sci. U. S. A., 2014. **111**(2): p. 623-628.
67. Stark, M.S., *Addition of peroxy radicals to alkenes and the reaction of oxygen with alkyl radicals*. Journal of the American Chemical Society, 2000. **122**(17): p. 4162-4170.
68. Villano, S.M., H.H. Carstensen, and A.M. Dean, *Rate Rules, Branching Ratios, and Pressure Dependence of the HO₂ + Olefin Addition Channels*. Journal of Physical Chemistry A, 2013. **117**(30): p. 6458-6473.
69. Zador, J., S.J. Klippenstein, and J.A. Miller, *Pressure-Dependent OH Yields in Alkene plus HO₂ Reactions: A Theoretical Study*. Journal of Physical Chemistry A, 2011. **115**(36): p. 10218-10225.
70. Kameel, F.R., et al., *Polarity and oxidation level of visible absorbers in model organic aerosol*. Chemical Physics Letters, 2014. **603**: p. 57-61.
71. Kameel, F.R., M.R. Hoffmann, and A.J. Colussi, *OH Radical-Initiated Chemistry of Isoprene in Aqueous Media. Atmospheric Implications*. Journal of Physical Chemistry A, 2013. **117**(24): p. 5117-5123.
72. F. Rifkha Kameel , F.R., M. R. Hoffmann , Shinichi Enami , and A. J. Colussi *Fenton Oxidation of Gaseous Isoprene on Aqueous Surfaces*. J. Phys. Chem. C, 2014. 10.1021/jp505010e.

Chapter 2

Polarity and Oxidation Level of Visible Absorbers in Model Organic Aerosol

Sections reprinted with permission from F. Rifkha Kameel, S.H. Lee, M. R. Hoffmann,
and A. J. Colussi, *Chemical Physics Letters* April 2014

ABSTRACT

How to parameterize the absorptivity of organic aerosols in atmospheric models remains uncertain. Here, we report that the $\lambda = 400$ nm absorbers in model aerosol mixtures elute as weakly polar species in reversed-phase chromatography. Typical among them, the $m/z = 269$ ($C_{12}H_{13}O_7^-$, O/C = 0.58) isomers detected by mass spectrometry possess C=O groups linked by C=C bridges. More polar species, such as the $m/z = 289$ ($C_{11}H_{13}O_9^-$, O/C = 0.82) polyacids, are instead colorless. On this basis, we argue that visible absorptivity, which develops from extended conjugation among chromophores, may not increase monotonically with oxidation level.

INTRODUCTION

In addition to degrading air quality,¹ aerosols affect the Earth's radiation budget.²⁻³ They scatter incoming solar radiation, thereby having a cooling effect. Some,⁴⁻⁵ however, also absorb radiation and may have a significant warming effect on mid-troposphere.⁶ Absorptivity is mainly due to their organic matter content. The main absorber is primary Black Carbon (BC) emitted during the incomplete burning of biomass materials. Aerosols, however, also contain Brown Carbon (BrC) matter⁷ generated in the atmospheric processing of the volatile organic compound (VOC) emissions that dominate the tropospheric carbon budget.⁸

Much work has been dedicated to unravel the physical and chemical mechanisms by which secondary organic aerosols (SOA) are produced from volatile organic compound (VOC) emissions. The main goal was to account for the fraction of global VOC emissions converted to SOA on the basis of the aerosol yields produced in laboratory experiments.⁷ The key assumptions were that (1) the photochemical processing of VOCs in the gas-phase generates heavier species that may condense and become part of the aerosol,⁸ and (2) the molecular identification of the myriad condensable species produced in such experiments should suffice to characterize SOA and their role in the Earth's system.^{9,10}

Biogenic gases account for a larger fraction of VOCs emitted globally¹¹ and organic matter for most of the mass of atmospheric aerosols.¹² It is known that the exhaustive

chemical and biological degradation of natural organic substances in the environment yields extremely complex materials that have been described as humic-like substances (HULIS).¹³ Notably, HULIS isolated from soils, surface waters or atmospheric aerosols display similar properties to a certain extent despite their different origins and, hence, the wide variations in their chemical frameworks and functionalities.¹⁴ This observation suggests that the full speciation of such materials (1) should be difficult (and perhaps unfeasible) even by the most advanced analytical techniques,¹⁵ and (2) could be neither sufficient nor necessary for assessing their role in the environment. The implication is that HULIS properties may emerge from universal supramolecular interactions in mixtures of polyfunctional molecules exceeding a modicum of chemical complexity.

The photochemical oxidation of VOC's should produce BrC aerosol particles whose optical properties may not be generic, but could vary with their residence time and the oxidative power of the local troposphere. Thus, there is a need for assessing how the evolution of BrC absorptivity could be parametrized in current atmospheric radiative transfer models. Extreme chemical complexity precludes a bottom up approach in which absorptivity is evaluated from the contributions made by the myriad light absorbers.⁹⁻¹⁰ An alternative, more realistic approach is based on overall descriptors, such as overall polarity or oxidation level. Here, we show that visible absorptivity may be associated with the less polar fraction of BrC components rather than with specific compounds. We also argue on chemical grounds that such fraction consists of highly unsaturated rather

than highly oxidized species, and that the degree of unsaturation may be actually anti-correlated with oxidation beyond a certain level.

How chromophores, which absorb in the visible ($\lambda > 400$ nm), are produced in the photochemical oxidation of VOCs is not fully understood.¹¹⁻¹² It has been suggested that absorbance could involve unspecified interactions in the aerosol phase among discrete, low-molecular weight α -keto carboxylic acids,¹¹ such as the widespread pyruvic and mesoxalic acids byproducts of the oxidation of aromatics.^{8, 13-14} These acids absorb ($\lambda_{\text{max}} \sim 320$ nm) the solar radiation reaching the lower troposphere due to the fact that the carbonyl chromophore is conjugated with the adjacent carboxyl C=O group, and thereby may undergo photochemistry.¹⁵ Aqueous solutions of such acids and their photochemical transformations may in fact be considered model surrogates of typical aerosol matter. The photolysis of pyruvic acid solutions is known to produce small polyfunctional oligomers.¹⁶⁻²⁰ Previously, we had shown that visible absorptions develop during the thermal aging of such mixtures via the slow dehydration of alcohol functionalities.¹⁶⁻¹⁷ We hypothesized that such red-shifted absorptions arose from the conjugation of disjoint carbonyl chromophores via newly created π -orbital $>C=C<$ bridges in species, which, by being the products of dehydration, had lower O/C ratios than their precursors.

Here, we confirm such hypothesis by means of separative analyses of aged model aerosol mixtures via high-performance reversed-phase liquid chromatography with

tandem UV-visible absorption-electrospray/chemical ionization mass spectrometric detection, and also show that photolysis of pyruvic acid leads to HULIS substances.

EXPERIMENTAL DETAILS

Pyruvic acid (PA) solutions (0.1 M to 0.5 M, PA, 98% Sigma-Aldrich) were prepared in deionized water adjusted to pH 1 using 70% HClO₄, sparged with ultrapure air prior and subsequently photolyzed with $\lambda > 305$ nm light. Sample solutions (3.5 mL, magnetically stirred in 4 mL silica UV cuvettes kept at 298 K in a Peltier sample holder) (hereafter designated as P0) were irradiated for ~ 4 hours with light from a 1 kW high-pressure Xe-Hg lamp source filtered through a water cell (to remove infrared radiation) and a tandem $\lambda > 305$ nm long band-pass interference filter. After irradiation, photolyzed samples (P1) were aged in the dark at 60 °C for several hours (16 to 19 h). Some of these thermally aged samples (hereafter P1-T1) were photolyzed for 1 h into P1-T1-P2 samples. Some P1-T1-P2 samples were thermally aged for several hours (P1-T1-P2-T2). Some P1-T1 samples were diluted in 1:5, 1:25 and 1:100 with deionized water prior to analysis.

Samples were analyzed by injecting 50 μ l into a HPLC/UV/ESI (Agilent 1100 series) LC/MS system. Separation was performed using a ZORBAX Eclipse XDB-C18 RPLC reversed-phase column (l=250 mm, ID= 3.00, dp =5 micron, flow rate=0.4 l/min, t₀= 2.5 min) under various solvent gradient protocols. The eluent consisted of mixtures of

solution A (0.1% acetic acid/ Milli-Q water) plus MeOH (B) programmed as follows: 7.5% B until 8 min, increasing to 90% at 45 min. ESI-MS detection of both positive and negative singled-charged ions in the 100-800 Da range was performed at various fragmentation voltages. We also ran extracted ion chromatograms (EIC) at several m/z values. The structures of selected products were elucidated via MS/MS spectrometry using an Ion Trap detector (Agilent 6300 Series HPLC-MSⁿ/Bruker Ion Trap mass spectrometer) in positive and negative ion modes in the 30 to 800 Da mas range at fragmentation voltages of 1 V and 3V.

RESULTS AND DISCUSSION

We verified that PA solutions before (P0) or after being photolyzed (P1) do not absorb above $\lambda \sim 350$ nm, in accord with previous experiments from our laboratory performed under similar or identical conditions on PA samples as received from the supplier or distilled at low pressure.¹⁵⁻¹⁶ The accelerated aging at 60 °C undergone by P1-T1 samples is deemed to simulate the thermal processes occurring in actual aerosol particles during their atmospheric lifetimes, which range from days to weeks depending on particle size and meteorology.²¹ Previously, we had shown that the thermal ‘browning’ of such solution has an apparent activation energy $E_{\text{act}} \sim 55$ kJ mol⁻¹.¹⁷ Thus, aging at 60 °C for 16 hours is deemed equivalent to aging at 25 °C for ~ 5.6 days in the atmosphere.

In contrast with P0 and P1 samples, P1-T1 samples absorb appreciably up to ~ 450 nm. Figure 1 displays a chromatogram of P1-T1 solutions as simultaneously reported by absorbance at 400 nm (Fig. 2.1A) and 254 nm (Fig. 2.1B), and by the total negative ion current (TIC) detected by tandem ESI mass spectrometry (Fig. 2.1C). It is apparent that (with the exception of a small feature at 6 min) *all* of the species absorbing at 400 nm (1) elute after ~ 20 minutes; i.e., they are weakly polar,²²⁻²³ (2) are not well resolved under present conditions; i.e., they consist of a suite of molecular structures possessing a quasi-continuum of affinities for the column, and (3) they are acidic, but since they are weakly polar, the (carboxylic) acid groups appear to be attached to large, less polar backbones. Since $A_{254 \text{ nm}}/A_{400 \text{ nm}} \sim 10$ for most chromophores (Fig. 2.2), we overlaid the 10 x chromatogram at 400 nm (Fig. 2.1A) in Fig. 2.1B. Comparing the red and blue traces before 40 min in Fig. 1B, we infer that 400 nm absorbers represent a minor fraction of the species present in this system (cf. the red and blue traces in Fig. 2.1B). By the same token, we infer that nearly *all* species eluting after 40 min absorb at 400 nm. Fig. S2.1 shows the evolution of the 400 nm absorbers upon successive thermal aging and > 300 nm photolysis treatments. As a rule, thermal aging results in the deepening of color, which is nearly bleached upon photolysis in accord with previous reports from our laboratory.¹⁷

Figs. 2.3A-C show negative ion ESI mass spectra in the mass range $m/z = 50$ to 800 Da acquired between 8 and 10 minutes (yellow band in Fig. 1) in Fig. 2.3A, between 35 and 40 minutes (orange band in Fig. 1) Fig. 3B, and between 40 and 50 min (red band in

Fig. 1) Fig. 2.3C. Note the differences between the scales of the Y-axis of Figs. 3A-C, which give a measure of the relative abundances of the anions detected in each case. If not the most intense, the most congested mass spectrum is that corresponding to those species eluting between 35 and 40 minutes (Fig. 2.3B), which give rise to maximum absorbance at 400 nm (Fig. 2.1A). EICs are particularly informative about isomerism and polarity among the products (Figs. 2.4A and B). Among the more polar species (i.e., those eluting before ~ 20 min), we find the isomers of $m/z = 289$ (green trace) and $m/z = 245$ (blue trace) anions (Fig. 4A). Notably, $m/z = 177$ anions appear (mostly) at ~ 6 min, and also at ~ 36 min. It is hardly conceivable that such $m/z = 177$ signals could correspond to a very polar and a weakly polar isomer of the same molecular formula, respectively (see below).

Fig. 2.5A and B show the EICs of the polar $m/z = 289$ and of the less polar $m/z = 269$ anions in P1 (after photolysis) versus P1-T1 (i.e., after thermal aging) samples, respectively. Note that the $m/z = 289$ anions of Fig. 2.5A, which elute before 10 min, do not absorb appreciably at 400 nm (cf. Fig 1A), whereas some the less polar $m/z = 269$ anions elute in the > 20 min range, which overlaps the region of significant 400 nm absorbance (Fig. 2.1A). Also note that the intensities of $m/z = 289$ anions do not change much upon aging, whereas those of the $m/z = 269$ anions markedly increase under the same conditions. Thus, the formation of $m/z = 269$ anions, as a representative of the species absorbing in the visible, is concomitant with color development during thermal aging. Hence, *the anions of mass 269 Da ($C_{12}H_{13}O_7^-$) must possess several isomers of*

similar polarities that absorb in the visible region (Scheme 2.1). As a rule, each additional double bond in a conjugated π -electron system is known to shift the absorption maximum about 30 nm towards longer wavelength.²⁴⁻²⁵ It follows that conjugation should be less extended in the species that give rise to the $m/z = 289$ anions ($C_{11}H_{13}O_9^-$) (Scheme 2.2). We have confirmed that $m/z = 289$ anions correspond to C_{11} species because they shift to $m/z = 300.0916$ (versus 289.0565, as detected via high-resolution ESI mass spectrometry) in the photolysis of $^{13}CH_3^{13}C(O)^{13}C(O)OH$. The MS/MS spectra of representative $m/z = 247$ and 289 anions reveals systematic 44 (CO_2) and 18 (H_2O) neutral losses, which are characteristic of hydroxyl-acids. Basic chemistry tells us that the various geometric (*E*, *Z*) isomers of the 270 Da acids in Scheme 1 may have different polarities²⁶ and would absorb further into the visible than the 290 Da acids of Scheme 2.²⁷⁻²⁸ The absorption spectrum of the octa-3,5-diene-2,7-dione motif of most of the proposed structures for the 270 Da acids in fact has maxima at 280 and 350 nm; i.e., it extends significantly into the > 400 nm region.²⁹

It was found that the van Krevelen diagram of the H/C vs. O/C ratios of bulk organic aerosols (OA) from a variety of locations and environments has a slope of $S_{VK} \sim -1$.³⁰ Since the replacement of a $>CH_2$ group with $>C=O$ and $>C-OH$ functions leads to $S_{VK} = -2$ and 0, respectively, a $S_{VK} \sim -1$ slope is therefore consistent with the creation of both $>C=O$ and $>C-OH$ functionalities, i.e. with the formation of acids or hydroxy-ketones. This has been shown to be true for a wide range of OA types, including laboratory/ambient, biogenic/anthropogenic, urban/remote and freshly emitted/aged.

Thus, OA has a characteristic bulk elemental composition with an average $\text{CH}_{(2-x)}\text{O}_x$ empirical formula.³⁰ In this context, the empirical formula of colorless $\text{C}_{11}\text{H}_{14}\text{O}_9 \propto \text{CH}_{1.27}\text{O}_{0.82}$ species shows that they are slightly more oxygenated than the expected average: $\text{CH}_{1.27}\text{O}_{0.73}$, whereas the visible absorbers $\text{C}_{12}\text{H}_{14}\text{O}_7$ (270 Da) $\propto \text{CH}_{1.17}\text{O}_{0.58}$ are considerably less oxygenated than the average species having the same H/C = 1.17 ratio: $\text{CH}_{1.17}\text{O}_{0.83}$. In other words aerosol, 'browness' may not arise from its most oxidized components.^{11, 31} The basic requirement for bathochromic shifts is the extension of conjugation among preexisting chromophores, in this case C=O carbonyls. The required unsaturations are likely to be created via dehydration of α -hydroxy ketones, as we had proposed before.¹⁷ However, they can be partially bleached by the reverse photochemically induced rehydration,¹⁶⁻¹⁷ and would be destroyed by ozone and OH-radical attack. Thus, 'browness' is not an intrinsic feature of BrC aerosol, but it is expected to vary according to ambient relative humidity, i.e., water activity, and the oxidative power of ambient air, i.e., of insolation.

Notably, $m/z = 177$ signals appear as prominent peaks both at short and long retention times (cf. Figs. 2.3A and C). We had previously identified a C_6 -dicarboxylic acid ($\text{C}_6\text{H}_{10}\text{O}_6$, 2,3-dihydroxy-2,3-dimethylsuccinic acid, i.e., dimethyl-tartaric acid, DMT) as a major product of PA photolysis (i.e., at the P1 stage) whose mono-anion gave rise to $m/z = 177$ signals.¹⁵ Since DMT does not absorb above ~ 250 nm,¹⁵ it is likely the species eluting before 10 min. The possibility that the $m/z = 177$ signal appearing in Figs. 2.3B and C arises from less polar isomers of DMT, such as 2,3,3-trihydroxy-2-methyl-4-

oxopentanoic acid, is unlikely because such species can only be gem-diols that would dehydrate into more stable carbonyls. The resulting di-ketones, however, would have given rise to $m/z = 159$ signals, which are conspicuously absent from Figs. 3A-C. Thus, we are led to consider that the $m/z = 177$ signal in Figure 3B could be in fact a fragment of higher mass species. Note that the multiplicity of structures that would arise from assembling a suite of smaller molecules could account, in part, both for the unresolved features absorbing at 400 nm in Fig. 2.1A and the congested mass spectrum shown in Fig. 3B. The dissimilar retention times of the $m/z = 269$ vs. $m/z = 289$ anions could be accounted for by the fact that most conceivable structures of the $m/z = 269$ acids are amphiphilic. Thus, their hydrophobic domains are expected to bind more strongly to the hydrophobic C18-bonded-phase of the reversed-phase column.²³

Summing up, our findings suggest that (1) the visible absorptivity of the aerosol may be due to a small fraction of its chemical components, which is largely comprised of weakly polar species having a significantly smaller O/C ratio than the average, (2) the average oxidation level of the aerosol may not be a good descriptor of its 'brownness'. These conclusions, which are based on basic chemical concepts, should be therefore expected to hold both under laboratory and environmental conditions.

ACKNOWLEDGEMENTS: This work was supported by NSF (U.S.A.) Grant AC-1238977.

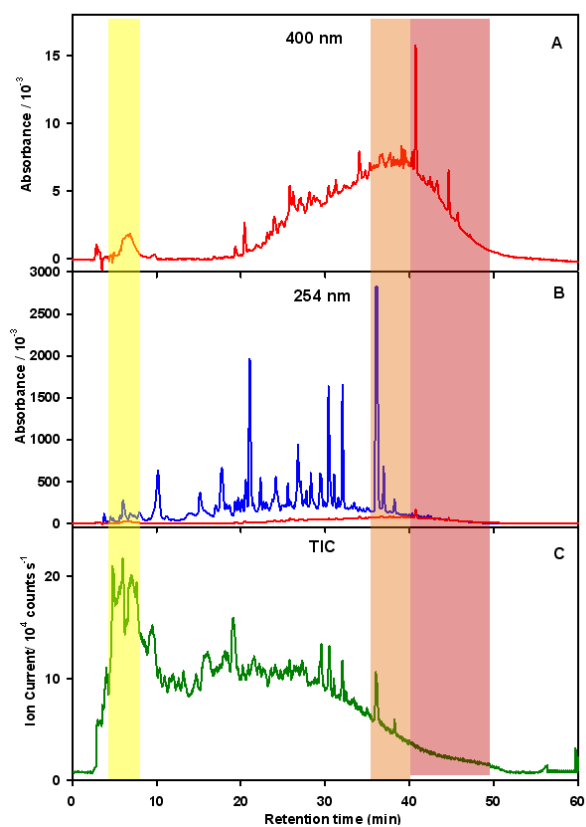


FIGURE 2.1: A typical chromatogram of a P1-T1 solution with product detection via UV absorption at 400 nm, 254 nm and total (negative) ion current (TIC) ESI mass spectrometry. Colored bands denote retention time ranges. **Yellow:** 8-10 min, **Orange:** 35-40 min, **Red:** 40-50 min.

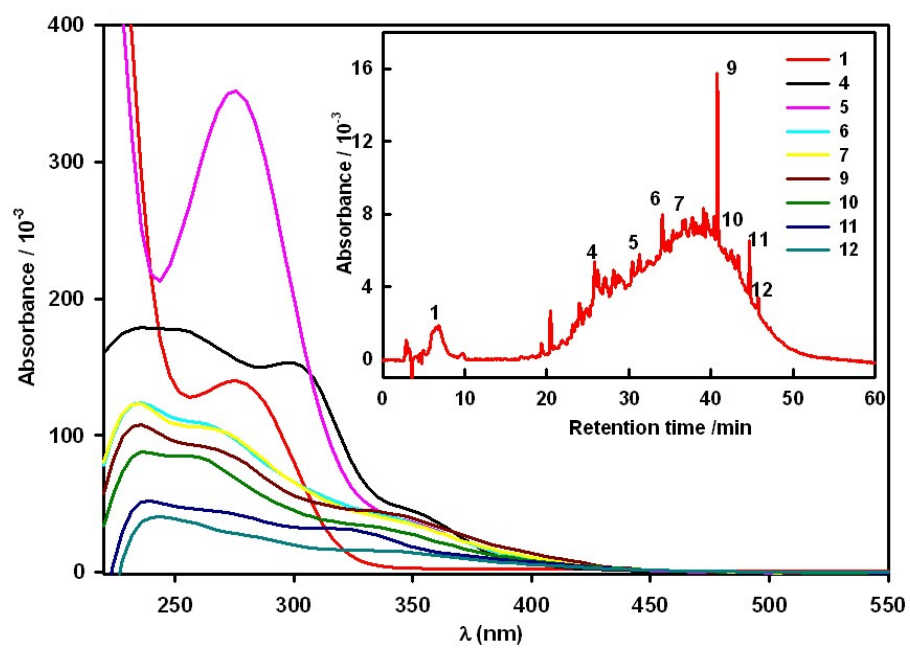


FIGURE 2.2: UV-Visible absorption spectra of species absorbing into the visible in P1-T1 mixtures (aged at 60 °C for 16 h).

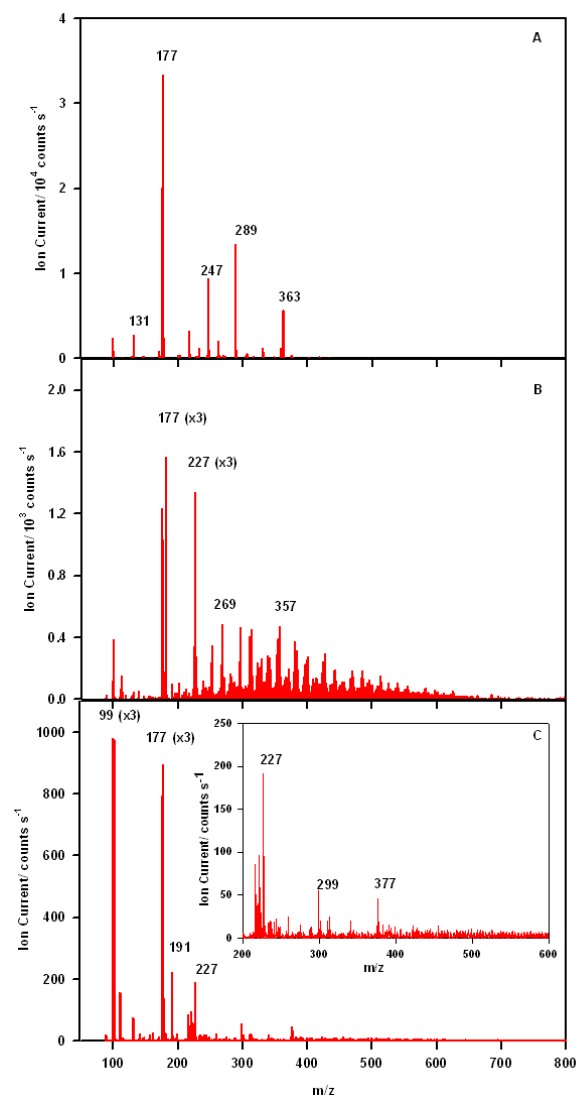


FIGURE 2.3: Negative ion chromatogram of species in P1-T1 mixtures (aged at 60 °C for 16 h). A: eluting within 4.5-8.5 min. B: 35-40 min; C: 40-50 min.

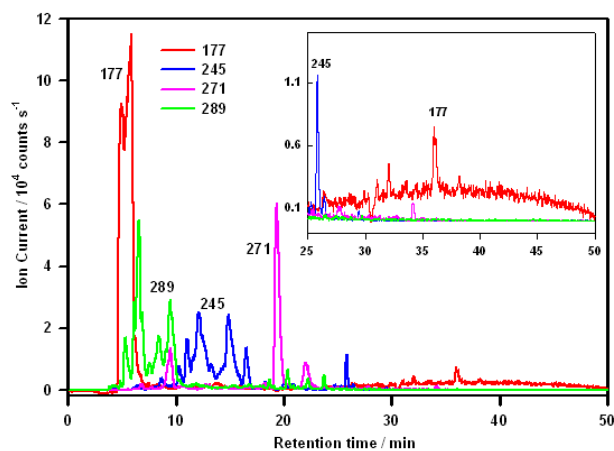


FIGURE 2.4A

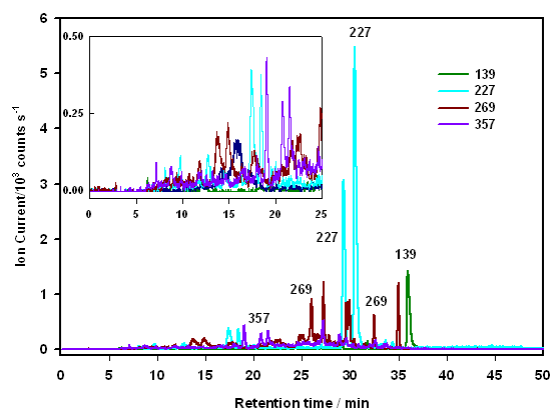


FIGURE 2.4B

FIGURE 2.4A: Negative extracted ion chromatogram (EIC) of some of the most abundant polar species in P1-T1 mixtures (aged at 60 °C for 16 h). The insert zooms in the 25-50 min retention time range.

FIGURE 2.4B: Negative extracted ion chromatogram (EIC) of some of the most abundant weakly polar species in P1-T1 mixtures (aged at 60 °C for 16 h). The insert zooms in the 0-25 min retention time range.

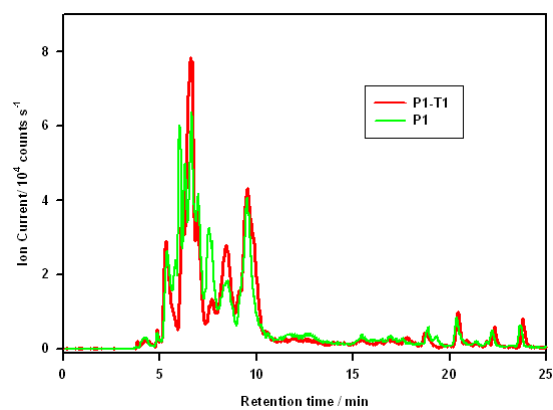
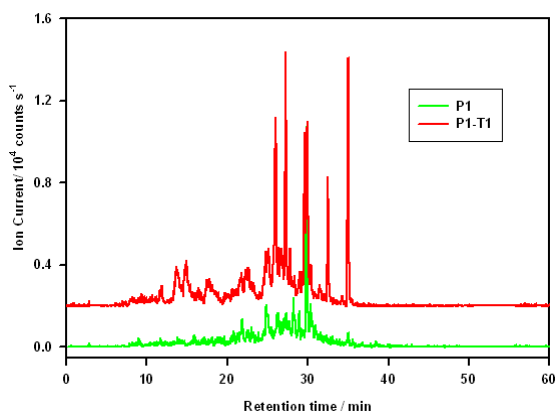
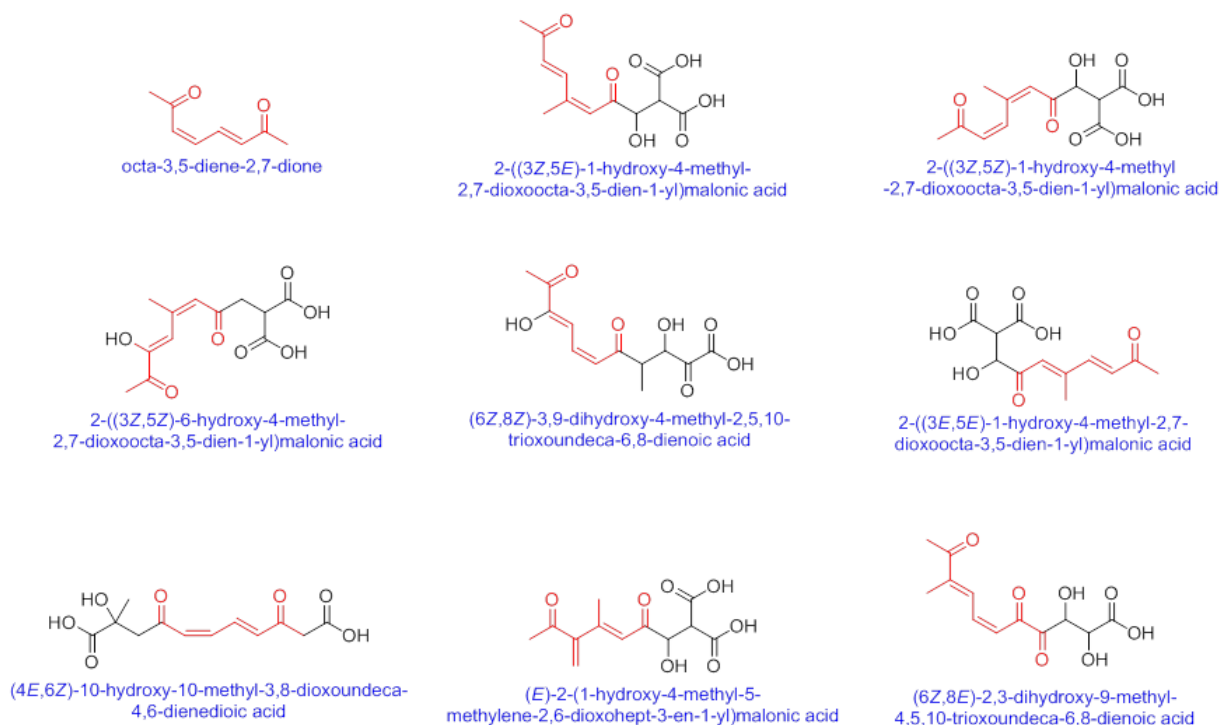
**FIGURE 2.5A****FIGURE 2.5B**

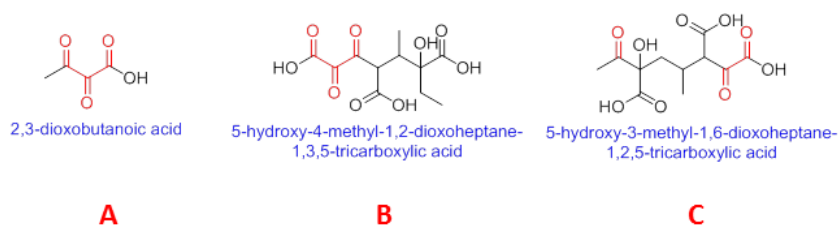
FIGURE 2.5A: Negative extracted $m/z = 289$ ion chromatogram (EIC) in P1 and P1-T1 solutions.

FIGURE 2.5B: Negative extracted $m/z = 269$ ion chromatogram (EIC) in P1 and P1-T1 solution



Scheme 1

Scheme 2.1: Proposed structures of the acids giving rise to the ESI mass spectral signals at $m/z = 269$ and their chromophore.



Scheme 2

Scheme 2.2: Proposed structures of the acids giving rise to the ESI mass spectral signals at $m/z = 289$ and their chromophore.

REFERENCES

1. Unger, N., Global Climate Forcing by Criteria Air Pollutants. In Annual Review of Environment and Resources, Vol 37, Gadgil, A.; Liverman, D. M., Eds. 2012; Vol. 37
2. Wang, C., Impact of anthropogenic absorbing aerosols on clouds and precipitation: A review of recent progresses. Atmospheric Research 2013, 122, 237-249.
3. Bond, T. C.; Doherty, S. J.; Fahey, D. W.; Forster, P. M.; Berntsen, T.; DeAngelo, B. J.; Flanner, M. G.; Ghan, S.; Karcher, B.; Koch, D.; Kinne, S.; Kondo, Y.; Quinn, P. K.; Sarofim, M. C.; Schultz, M. G.; Schulz, M.; Venkataraman, C.; Zhang, H.; Zhang, S.; Bellouin, N.; Guttikunda, S. K.; Hopke, P. K.; Jacobson, M. Z.; Kaiser, J. W.; Klimont, Z.; Lohmann, U.; Schwarz, J. P.; Shindell, D.; Storelvmo, T.; Warren, S. G.; Zender, C. S., Bounding the role of black carbon in the climate system: A scientific assessment. J Geophys Res-Atmos 2013, 118 (11), 5380-5552.

4. Ramanathan, V.; Chung, C.; Kim, D.; Bettge, T.; Buja, L.; Kiehl, J. T.; Washington, W. M.; Fu, Q.; Sikka, D. R.; Wild, M., Atmospheric brown clouds: Impacts on South Asian climate and hydrological cycle. *P. Natl. Acad. Sci. USA* 2005, 102 (15), 5326-5333.
5. Ramanathan, V.; Crutzen, P. J., New directions: Atmospheric brown "Clouds". *Atmos. Environ.* 2003 37, 4033-4035.
6. Dumka, U. C.; Moorthy, K. K.; Kumar, R.; Hegde, P.; Sagar, R.; Pant, P.; Singh, N.; Babu, S. S., Characteristics of aerosol black carbon mass concentration over a high altitude location in the Central Himalayas from multi-year measurements. *Atmospheric Research* 2010, 96 (4), 510-521.
7. Formenti, P.; Elbert, W.; Maenhaut, W.; Haywood, J.; Osborne, S.; Andreae, M. O., Inorganic and carbonaceous aerosols during the Southern African Regional Science Initiative (SAFARI 2000) experiment: Chemical characteristics, physical properties, and emission data for smoke from African biomass burning. *J. Geophys. Res-Atmos.* 2003, 108 (D13).
8. Kanakidou, M.; Seinfeld, J. H.; Pandis, S. N.; Barnes, I.; Dentener, F. J.; Facchini, M. C.; Van Dingenen, R.; Ervens, B.; Nenes, A.; Nielsen, C. J.; Swietlicki, E.; Putaud, J. P.; Balkanski, Y.; Fuzzi, S.; Horth, J.; Moortgat, G. K.; Winterhalter, R.; Myhre, C. E. L.; Tsigaridis, K.; Vignati, E.; Stephanou, E. G.; Wilson, J., Organic aerosol and global climate modelling: a review. *Atmos. Chem. Phys.* 2005, 5, 1053-1123.
9. Williams, B. J.; Goldstein, A. H.; Millet, D. B.; Holzinger, R.; Kreisberg, N. M.; Hering, S. V.; White, A. B.; Worsnop, D. R.; Allan, J. D.; Jimenez, J. L., Chemical speciation

of organic aerosol during the International Consortium for Atmospheric Research on Transport and Transformation 2004: Results from in situ measurements. *J. Geophys. Res-Atmos.* 2007, 112 (D10).

10. Nakayama, T.; Matsumi, Y.; Sato, K.; Imamura, T.; Yamazaki, A.; Uchiyama, A., Laboratory studies on optical properties of secondary organic aerosols generated during the photooxidation of toluene and the ozonolysis of alpha-pinene. *J. Geophys. Res-Atmos.* 2010, 115.

11. Lambe, A. T.; Cappa, C. D.; Massoli, P.; Onasch, T. B.; Forestieri, S. D.; Martin, A. T.; Cummings, M. J.; Croasdale, D. R.; Brune, W. H.; Worsnop, D. R.; Davidovits, P., Relationship between Oxidation Level and Optical Properties of Secondary Organic Aerosol. *Environ Sci Technol* 2013, 47 (12), 6349-6357.

12. Sun, H. L.; Biedermann, L.; Bond, T. C., Color of brown carbon: A model for ultraviolet and visible light absorption by organic carbon aerosol. *Geophys. Res. Lett.* 2007, 34 (17).

13. Kawamura, K.; Tachibana, E.; Okuzawa, K.; Aggarwal, S. G.; Kanaya, Y.; Wang, Z. F., High abundances of water-soluble dicarboxylic acids, ketocarboxylic acids and alpha-dicarbonyls in the mountaintop aerosols over the North China Plain during wheat burning season. *Atmos Chem Phys* 2013, 13 (16), 8285-8302.

14. Yu, J. Z.; Jeffries, H. E.; Sexton, K. G., Atmospheric photooxidation of alkylbenzenes .1. Carbonyl product analyses. *Atmos. Environ.* 1997, 31 (15), 2261-2280.

15. Guzmán, M. I.; Colussi, A. J.; Hoffmann, M. R., Photoinduced Oligomerization of Aqueous Pyruvic Acid. *J. Phys. Chem. A* 2006, 110, 3619-3626.
16. Rincon, A. G.; Guzman, M. I.; Hoffmann, M. R.; Colussi, A. J., Optical Absorptivity versus Molecular Composition of Model Organic Aerosol Matter. *J. Phys. Chem. A* 2009, 113, 10512-10520.
17. Rincon, A. G.; Guzman, M. I.; Hoffmann, M. R.; Colussi, A. J., Thermochromism of Model Organic Aerosol Matter. *J. Phys. Chem. Lett.* 2010, 1 (1), 368-373.
18. Altieri, K. E.; Seitzinger, S. P.; Carlton, A. G.; Turpin, B. J.; Klein, G. C.; Marshall, A. G., Oligomers formed through in-cloud methylglyoxal reactions: Chemical composition, properties, and mechanisms investigated by ultra-high resolution FT-ICR mass spectrometry. *Atmos. Environ.* 2008, 42 (7), 1476-1490.
19. Carlton, A. G.; Turpin, B. J.; Lim, H. J.; Altieri, K. E.; Seitzinger, S., Link between isoprene and secondary organic aerosol (SOA): Pyruvic acid oxidation yields low volatility organic acids in clouds. *Geophys. Res. Lett.* 2006, 33 (6).
20. Wiesen, E.; Barnes, I.; Becker, K. H., Study of the OH-Initiated Degradation of the Aromatic Photooxidation Product 3,4-Dihydroxy-3-Hexene 2,5-Dione. *Environ. Sci. Technol.* 1995, 29 (5), 1380-1386.
21. Seinfeld, J. H.; Pandis, S. N., *Atmospheric chemistry and physics: from air pollution to climate change*. 2nd ed.; Wiley: Hoboken, N.J., 2006.
22. Baker, J. K., Estimation of High-Pressure Liquid Chromatography Retention Indexes. *Anal. Chem.* 1979, 51 (11), 1693-1697.

23. Kaliszan, R., QSRR: Quantitative Structure-(Chromatographic) retention relationships. *Chem. Rev.* 2007, 107 (7), 3212-3246.
24. Nielsen, A. T., Correlation of Ultraviolet Absorption Spectra with Structure of Alpha, Beta-Unsaturated Acids and Derivatives. *J. Org. Chem.* 1957, 22 (12), 1539-1548.
25. Pavia, D. L., Introduction to spectroscopy. 4th ed.; Brooks/Cole: Belmont, CA, 2009.
26. Anslyn, E. V.; Dougherty, D. A., Modern Physical Organic Chemistry. University Science Books: Sausalito, California, 2006.
27. Francese, S.; Bradshaw, R.; Flinders, B.; Mitchell, C.; Bleay, S.; Cicero, L.; Clench, M. R., Curcumin: A Multipurpose Matrix for MALDI Mass Spectrometry Imaging Applications. *Anal. Chem.* 2013, 85 (10), 5240-5248.
28. Silverstein, R. M.; Webster, F. X.; Kiemle, D. J., Spectrometric identification of organic compounds. 7th ed. ed.; John Wiley & Sons: Hoboken, NJ, 2005.
29. Karrer, P.; Eugster, C. H.; Perl, S., *Mucosansaurealdehyd un Octadien-(3,5)-Dion-(2,7). *Helvetica Chimica Acta* 1949, 32 (3), 1013-1015.
30. Heald, C. L.; Kroll, J. H.; Jimenez, J. L.; Docherty, K. S.; DeCarlo, P. F.; Aiken, A. C.; Chen, Q.; Martin, S. T.; Farmer, D. K.; Artaxo, P., A simplified description of the evolution of organic aerosol composition in the atmosphere. *Geophys. Res. Lett.* 2010, 37.
31. Cappa, C. D.; Che, D. L.; Kessler, S. H.; Kroll, J. H.; Wilson, K. R., Variations in organic aerosol optical and hygroscopic properties upon heterogeneous OH oxidation. *J. Geophys. Res-Atmos.* 2011, 116.

SUPPORTING INFORMATION

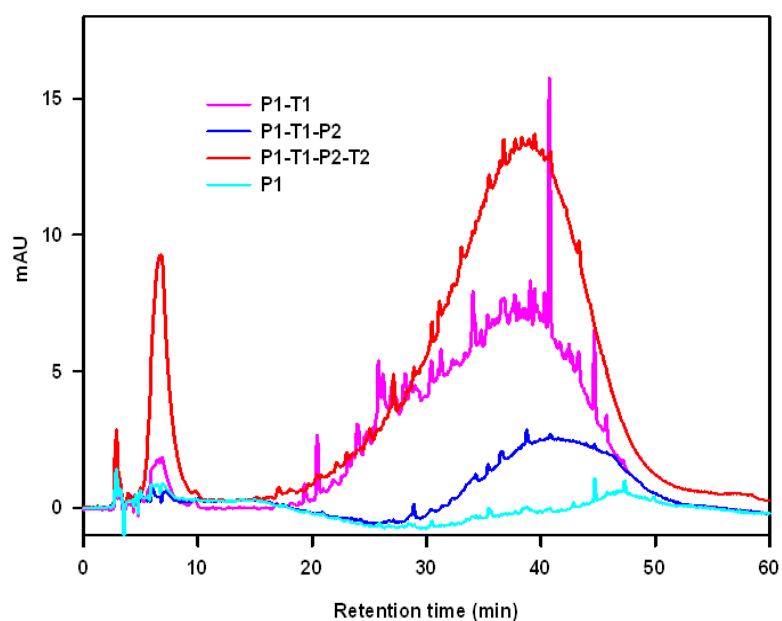


FIGURE S 2.1: UV absorption Chromatogram @ 400 nm of PA solution at different conditions. Figure S3 represents the UV chromatogram @ 400nm for P1(coloreless), P1-T1(yellow), P1-T1-P2 (1 of rephotolysis, pale yellow) and P1-T1-P2-T2 (dark yellow) PA solutions. The yellow color of the thermally-treated solution disappears upon photolysis and reappears upon thermal aging.

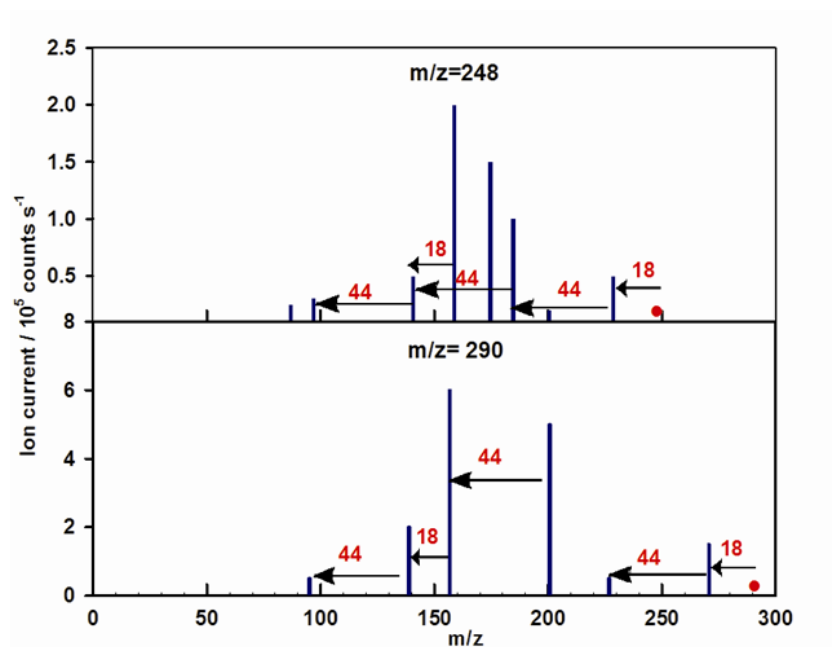


FIGURE S2.2: MS/MS spectrum of an isomers of $m/z=290$ ($M=289$ m/z) where 271 ($M - 1[H_2O]$), 245 ($M - 44[CO_2]$), 227 ($M - 62 = [44+18]$), 201 ($M - 88$), 157 ($M - 132 [= 88 + 44]$), 139 ($M - 150 [= 88 + 44 + 18]$), and 95 ($M - 194 [=88+44+18+44]$).

Chapter 3

OH Radical-Initiated Chemistry of Isoprene in Aqueous Media: Atmospheric Implications

Sections reprinted with permission from F. Rifkha Kameel, M. R. Hoffmann and A. J. Colussi*. *Journal of Physical Chemistry A* **2013**

ABSTRACT

The fate of isoprene (2-methyl-1,3-butadiene, ISO) emissions into the atmosphere is not fully understood. Increasing awareness that ISO is only partially processed in the gas-phase has turned attention to its reactive uptake by fog, cloud and aerosol droplets. As a hydrophobic gas, ISO would preferentially partition to the surface rather than the bulk of aqueous media. Such media also contain dissolved O_2 and water-soluble unsaturated organics, and support $\cdot OH$ generation rates (from the solar photolysis of H_2O_2 dissolved therein) that are several orders of magnitude faster than in the gas-phase. Hence, ISO should be converted to heavier products rather than into the C_4 - C_5 volatile compounds produced in the gas-phase. Here, we substantiate this scenario by reporting that the $\lambda > 305$ nm photolysis of H_2O_2 in aqueous dilute ISO solutions yields $C_{10}H_{15}OH$ species as primary products, whose formation both requires and is inhibited by O_2 . A minimum of seven $C_{10}H_{15}OH$ isomers are resolved by reverse-phase high-performance liquid chromatography and detected as MH^+ ($m/z = 153$) and MH^+-18 ($m/z = 135$) signals by electrospray ionization mass spectrometry. Our findings are consistent with the addition of $\cdot OH$ to ISO, followed by $HO-ISO\cdot$ reactions with ISO (in competition with O_2) leading to second generation $HO(ISO)_2\cdot$ radicals that terminate as $C_{10}H_{15}OH$ via β -H abstraction by O_2 . We show that a significant fraction of gas-phase olefins should be converted into less volatile species via this process on airborne wet particles.

INTRDUCTION

The surface area of airborne liquid water in the troposphere is about two orders of magnitude larger than that of the Earth's oceans. This counterintuitive statement is in fact a conservative estimate based on ground-based and satellite measurements of cloud optical densities.¹⁻² It should be realized that the interfacial shells or airborne liquid water, where water density drops a thousandfold within ~ 1 nm, do not behave as bulk water.³⁻⁴ Hydrophobic gases colliding with these relatively 'dry' shells therefore accumulate therein rather than proceed into bulk water.⁵ This idea has been previously floated in the literature.⁶⁻⁸

We have recently demonstrated experimentally that gases having proton affinities larger than water itself are protonated upon colliding with the surface of $\text{pH} < 4$ water.⁹⁻¹⁰ These conditions are within the range of fog and aerosol water acidities, whose surfaces therefore behave as superacidic toward incoming gases.⁹⁻¹⁴ In contrast to hydrophobic gases, hydrogen peroxide (HP, H_2O_2) produced in the gas-phase (Henry's law constant $H_{\text{HP}} \sim 10^5 \text{ M atm}^{-1}$) is concentrated in airborne liquid water. As a result, $\cdot\text{OH}$ radical production rates from H_2O_2 dissolved therein are significantly larger than those from the photolysis of O_3 in the gas-phase (see below).¹⁵ Not only is the chemical composition of airborne aqueous phases significantly different from the gas-phase, due to selective partitioning of hydrophobic versus hydrophilic species, but the higher mass density and specific interactions to drive chemical transformations along pathways is different from those in the gas-phase. For example, the chemically activated ('hot')

species generated in $\cdot\text{OH}$ and O_3 additions to alkenes¹⁶ are rapidly thermalized in condensed phases.¹⁷ These basic considerations seem to have been overlooked in atmospheric chemistry.^{4, 18-19}

The $\sim 600 \text{ Tg yr}^{-1}$ of isoprene, ISO, emitted by the biosphere represent the major injection of non-methane volatile organic compounds (VOC) into the troposphere.²⁰⁻²¹ Since ISO is barely soluble in bulk water ($H_{\text{ISO}} \sim 10^{-2} \text{ M atm}^{-1}$), it has been assumed that its relatively fast reaction with gas-phase $\cdot\text{OH}$ radicals ($\tau_{1/2} \sim 2 \text{ h}$) is the main mechanism of removal from the atmosphere.²²⁻²⁶ Such an assumption, which is incorporated into atmospheric chemistry models, however, has failed to account for actual removal rates.²⁷⁻²⁸ The rapid decay of ISO after sunset and the unexpectedly high levels of $\cdot\text{OH}$ radicals detected over forest canopies have pointed to additional, heterogeneous sinks that remain to be characterized.

Several studies have shown that ISO would also react at diffusionally-controlled rates with photo-catalytically generated OH-radicals on mineral surfaces to produce more complex polar compounds via both oxidation and polymerization processes. OH radical, the cleaning reagent of the atmosphere, is generated on dust aerosol containing semiconductor oxides. Semiconductor oxides, by absorbing supra band-gap photons, generate oxidizing holes and reducing electrons on the surface of dust particles [20]. As a result, interfacial H_2O is oxidized to OH radicals that may react with gases, impacting dust particles.

Herein, we report an experimental study of the oxidation of aqueous ISO initiated by $\cdot\text{OH}$ radicals (from the photolysis of H_2O_2) in the presence and absence of dissolved O_2 under various experimental conditions.

EXPERIMENTAL DETAILS

Isoprene (Aldrich, 98.0%) was purified by fractional distillation, collecting the fraction boiling between 35 and 40°C. A stock solution of deionized water (18 M Ω cm) saturated with liquid purified ISO was kept in the dark at 4° C ($[\text{ISO}]_{\text{sat}} = 10$ mM at 4° C). Photolysis samples, 5 mM in ISO, were prepared by diluting a known volume of stock solution with air-saturated deionized water in 3.5 mL (1 cm optical path length) fused silica cuvettes. Note that all photolysis experiments were performed at 10°C (see below). The effect of ISO concentration was tested in samples prepared by injecting variable amounts of neat ISO (1 to 10 μL) into deionized water. Samples were spiked with concentrated H_2O_2 (Sigma-Aldrich, 30% H_2O_2 by weight in water, $[\text{H}_2\text{O}_2] = 9.8$ M) to 50 mM in H_2O_2 and sealed before irradiation. Blank photolysis experiments were performed on 5 mM ISO samples in the absence of H_2O_2 . The effect of the dissolved O_2 concentration was tested on samples prepared by sparging 50 mM H_2O_2 solutions (held in cuvettes capped with silicone septa) with ultrapure $\text{Ar}(\text{g})$, zero air (20% O_2) or neat $\text{O}_2(\text{g})$ for 30 minutes, followed by the injection of 10 μL liquid ISO prior to photolysis. Samples were photolyzed (under continuous magnetic stirring) with light from a 1 kW high-pressure Xe-Hg lamp source that has been filtered through a water cell (to remove unwanted

infrared radiation), a tandem $\lambda > 305$ nm long band-pass interference filter, and attenuated as desired by neutral filters of known transmittance. We estimate (from previous actinometric measurements on this setup)²⁹ that $\sim 1 \times 10^{15}$ photons $\text{cm}^{-2} \text{s}^{-1}$ within $\lambda = 305$ and 320 nm, i.e., in the range where H_2O_2 absorbs significantly: $\langle \epsilon \rangle = 1.2 \text{ M}^{-1} \text{ cm}^{-1}$ (base e),³⁰ hit the front window of the cuvette. Under present conditions, H_2O_2 is photolyzed at $\sim 0.1 \mu\text{M s}^{-1}$ rates.

Analyses of organic products were carried out in a LC/MS system (Hewlett-Packard 1100 series) provided with spectral UV-visible absorption and tandem electrospray ionization mass spectrometric detection (HPLC/UV/ESI/MS). The (diode array) UV detector was typically set to record UV chromatograms at $\lambda = 254$ and 400 nm. The ESI mass spectrometer could be operated in either total ion count (TIC) or extracted ion count (EIC) modes and set to detect negative or positive ions from 50 Da to 500 Da. ESI mass spectra were run at stepped fragmentation voltages (50 V up to 100 m/z, 80 V from 100 to 400 m/z, and 100 V thereafter). Chromatograms involved injecting 25 - 50 μL of sample solutions into a ZORBAX SB-C18 reverse-phase liquid chromatography (RPLC) column ($L = 50$ mm, $\text{ID} = 2.1$ mm, $d_{\text{pore}} = 5$ μm) eluted at 0.4 L/min. The mobile phase consisted of (A) 0.1% acetic acid in deionized water plus (B) 100% MeOH solutions programmed to ramp B from 7.5% at 2 min to 95% from 18 to 20 min, followed by a 3 minute post-run column equilibrium period. Statistical data analyses were carried out using SigmaPlot 12 graphic software.

RESULTS AND DISCUSSION

Figure 3.1 shows chromatograms of photolyzed ISO solutions obtained with negative (red trace) and positive (blue trace) TIC detection. We found that positive ions, i.e., those resulting from the protonation of reaction products, were considerably more abundant than negative ones (from the anions of carboxylic acid products) under most conditions. Hereafter, the products giving rise to the positive ion signals eluting between 10 and 12.5 minutes will be labeled as group A (as indicated in Fig. 3.1) and those eluting between 12.5 and 18 min as group B.

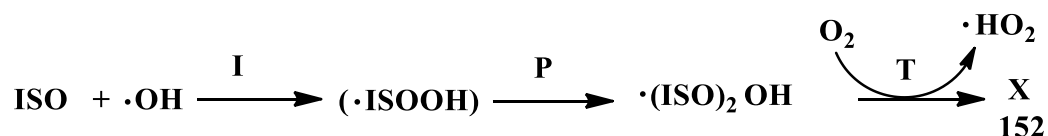
Figures 3.2a and b show positive-ion ESI mass spectra of group A products eluting between 10.70 and 10.84 min (a) and between 11.77 and 11.92 min, respectively. In both cases, major peaks appear at $m/z^+ = 153$ (M) and 135 (M - H₂O). The $m/z^+ = 153$ signal corresponds to the protonated form of neutral isomer products of molecular mass 152 Da. Remarkably, such product(s) were absent from the mass spectra of group B eluates. Figure 3.3 displays extraction ion chromatograms (EIC) at $m/z^+ = 135$ and 153. It is apparent that such signals belong to a discrete set of structural isomers that elute within a narrow interval. Seven isomers out of a possibly larger set were resolved under present conditions isomers (labeled from 1 to 7, Figure 3.4). Strong evidence that the $m/z^+ = 135$ signals correspond to daughter ions from the collisionally-induced loss of neutral H₂O from $m/z = 153$ parent products is provided by their anti-correlated dependence on fragmentation voltage (Figs. S3.1 a, b).

Isomers 1 to 7 are primary products, which undergo further reaction at longer photolysis times. This is apparent from Figure 3.5, in which all isomers are produced with non-zero initial rates and peak almost simultaneously at ~ 52 minutes. We infer that the oxidation of ISO is initiated by an unselective intermediate, such as the $\cdot\text{OH}$ -radical from the photolysis of H_2O_2 , which adds to ISO and reaction products 1-7 at similar rates. The relative yields of the different isomers reflect either statistical factors and/or the selectivity of first generation ISO-OH \cdot intermediates for adding to ISO. Furthermore, since (1) $\cdot\text{OH}$ radicals are quite unselective, i.e., they will react at nearly diffusionally controlled rates with ISO and all primary products, (2) species 1-7 are generated without delay, i.e., during the initial period when their concentrations are much smaller than ISO, we infer that the detected species 1-7 contain one O-atom per molecule, i.e., that introduced by $\cdot\text{OH}$ in the initiation step I.

Figure 3.6, which displays experiments on Ar-purged versus air (20% O_2)-sparged samples, shows that O_2 is essential for the appearance of photolysis products. However, figures S3.2 - S3.4, reveal that pure O_2 fully inhibits the formation of such products. Similar observations have been reported in a recent study on the $\bullet\text{OH}$ -initiated oligomerization of methyl vinyl ketone in aqueous solution.¹⁹ Experiments in which the initial ISO concentration was varied between 3 and 30 mM (Figure 7) indicate that product formation rates are roughly proportional to [ISO]. We verified the absence of methyl vinyl ketone (MVK) and methacrolein (MACR) among the products of reaction via GC/MS analysis of head-space gases. Our results, which clearly correspond to the

initial phase of the OH-initiated oxidation of ISO in aqueous solution, are at variance with reports on the formation of organic acids, MVK and MACR in this system.^{24, 31} Accordingly, we found no evidence for the formation of isoprene-derived polyols, which must therefore be formed in later stages of the oxidation process.^{25, 32-34}

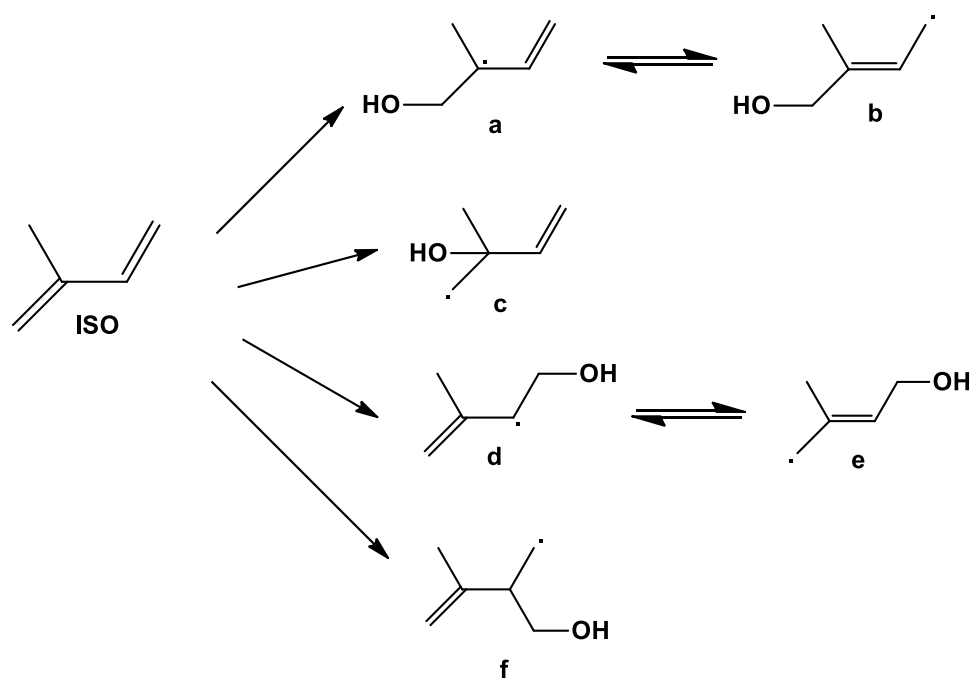
The above results are consistent with the following reaction scheme:



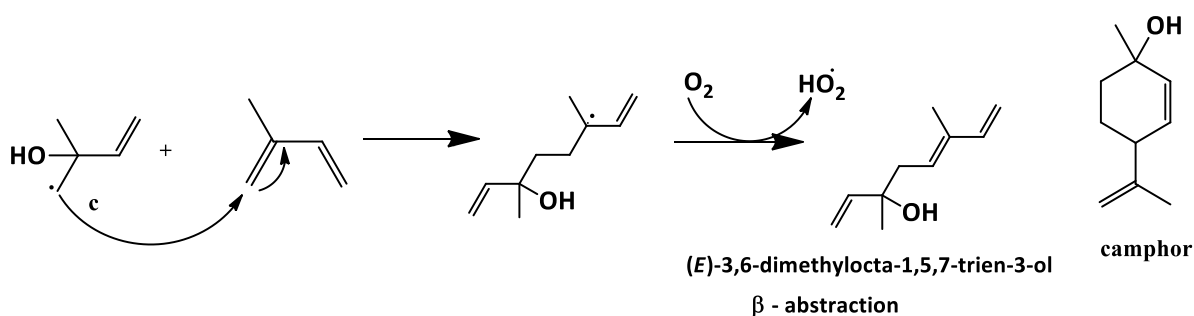
where X stands collectively for the suite of products of molecular mass 152 Da (see below Schemes 1 and 2 for possible $\cdot\text{ISOOH}$, $\cdot(\text{ISO})_2\text{OH}$ and X structures).

The initial radical adducts, HO-ISO \cdot (several isomers possible, Scheme 1) add to a second ISO (the propagation step P)³⁵ or, alternatively to other unsaturated compounds, UNS, likely present in real tropospheric aqueous phases³⁶⁻³⁹, leading to a suite of (ISO)₂OH \cdot isomers. The latter may undergo cyclization reactions (depending on their structures)⁴⁰ prior to reacting with O₂⁴¹, and terminate as the X species detected in our experiments. The propagation step clearly competes with inhibition by excess O₂, depending on the [ISO]/[O₂] ratio (or, more generally, the [UNS]/[O₂] ratio) into different intermediate products. Realistic concentrations of dissolved organics in fog water are typically ~ 250 mg C/L³⁹, of which $\sim 25\%$ is in the form of water-soluble unsaturated organic acids (such as maleic + fumaric)⁴²⁻⁴⁵, leading to [UNS] $\sim 0.5 - 1$ mM, which is within range of the [ISO]s in our experiments. It is apparent that O₂ competitive

abstracts β -hydrogens (to free radical centers) from $(\text{ISO})_2\text{OH}\cdot$ species, thereby eliminating $\text{HO}_2\cdot$ in the process. Given their mechanism of formation, X species must be unsaturated alkyl alcohols rather than vinylic alcohols (which should rapidly isomerize to saturated aldehydes). These alcohol functionalities can be protonated into the detected parent $m/z^+ = 153$ ions, which would readily split H_2O neutrals (via collisionally induced dissociation, Fig. S1) into the major $m/z^+ = 135$ ion fragments. Therefore, X species are formally monoterpenoids, $\text{C}_{10}\text{H}_{15}\text{OH}$, a class comprising hundreds of natural species (Scheme 2), such as camphor.⁴⁶



SCHEME 3.1: The initiation step leads to several HO-ISO \cdot isomers.



SCHEME 3.2: One of the many (propagation + termination) pathways leading to possible products.

ATMOSPHERIC IMPLICATIONS

Secondary Organic Aerosol (SOA) is an important component of the troposphere. In the past, aqueous phase reactions of polar organic compounds, such as glyoxal,⁴⁷⁻⁴⁸ methyl glyoxal and pyruvic acid, were proposed as potential sources of SOA. It has been generally assumed that condensed-phase reactions of hydrophobic substances, i.e., those having small Henry's law constants, would make a negligible contribution to SOA formation. Here, we adopt a more general perspective and emphasize that (1) aerosol phase reactions can occur both in the bulk liquid and at the air-liquid interface,³ (2) the partitioning of gases to the interface versus to the bulk liquid are vastly different, particularly for hydrophobic gases^{4-5, 49-50}, (3) hydrophobic gases are always physisorbed, but some species, such as unsaturated and oxygenated species, can also be chemisorbed at the interface^{10, 12}, (4) the rate of photochemical $\cdot\text{OH}$ -radical production in aqueous aerosols is orders of magnitude higher than in the gas-phase.

Water droplets, fog, cloud or haze particles remain in the troposphere for significant periods. As a reference, droplets of $\sim 1 \mu\text{m}$ diameter will settle $\sim 25 \text{ m}$ per week under typical atmospheric conditions.⁵¹ Notice that surface or energy accommodation coefficients, i.e., the probabilities that colliding molecules are adsorbed on the surface for finite times or, what is equivalent, the fraction of those impinging on the surface that are inelastically (rather than specularly) reflected without entering the bulk liquid, α_s , are larger than conventional mass accommodation coefficients, α_M .⁵² The latter describes the probability that the colliding species enters the bulk liquid prior to desorbing. While at the surface, the accommodated species may react with other species therein during residence times.⁴ It has been realized that less polar, more hydrophobic species such as VOCs will adsorb to the relatively drier interfaces in amounts higher than predicted by their Henry's law constants for partitioning into bulk water³, whereas the opposite conclusion applies to more polar oxygenated species.⁵ Adsorption, however, is not the only outcome of gas-liquid collisions. Recently, we have shown that unsaturated organics, such as ISO and biogenic terpenes in general, are protonated and remain as such on aqueous surfaces of $\text{pH} < 4$, with uptake coefficients $\gamma \sim 10^{-3} - 10^{-4}$.^{9-10, 12} The frequency of sticking collisions of ISO molecules (average speed $c_{\text{ISO}} \sim 3 \times 10^4 \text{ cm/s}$) with fog droplets, ω , is given by the kinetic theory of gases, equation E(1)

$$\omega = \frac{1}{4} \gamma c_{\text{ISO}} (S/V) \quad \text{E(1)}$$

For typical fogs, with specific surface areas: $(S/V) \sim 5 \times 10^{-5} \text{ cm}^{-1}$,^{23, 53} $\gamma \sim 5 \times 10^{-4}$, $\omega \sim 1.9 \times 10^{-5} \text{ s}^{-1}$, which is commensurate with the reciprocal of the lifetime of ISO toward reaction with $\cdot\text{OH}$ radicals in the gas-phase: $1/\tau_{\text{ISO}} \sim 2 \text{ h}$.²³

Once ISO molecules stick to fog or aquated haze aerosol, they will react irreversibly with $\cdot\text{OH}$ -radicals generated *in situ*. A key feature of airborne water chemistry is that the rate of $\cdot\text{OH}$ -radical generation from the solar photolysis of dissolved H_2O_2 is about several orders of magnitude faster than that ensuing the photolysis of $\text{O}_3(\text{g})$ in the gas-phase. $\text{H}_2\text{O}_2(\text{g})$ with a Henry's law constant: $H = 10^5 \text{ M atm}^{-1}$,³⁰ is extremely soluble in water.⁵⁴ Typical ~ 1 ppbv gas-phase H_2O_2 concentrations will lead to 0.1 mM H_2O_2 in aqueous fog and aerosol droplets.²³ By assuming that the frequency of H_2O_2 solar photolysis, $J(\text{OH})$, is about the same in gas and solution phase,⁵⁵ a representative value of $J(\text{OH}) = 8 \times 10^{-6} \text{ s}^{-1}$ (on June 30, at 35 °N, noon, 0 elevation, surface albedo 0.3)¹⁵ leads to: $R_{+\text{OH}}(\text{aq}) \sim 1 \times 10^{-9} \text{ M s}^{-1}$, for the rate of $\cdot\text{OH}$ -radical production in the aqueous phase. By comparison, in the gas-phase at 0.1 ppmv $\text{O}_3(\text{g})$, $J(\text{O}^1\text{D}) = 4 \times 10^{-5} \text{ s}^{-1}$ under the same conditions,¹⁵ $R_{+\text{O}^1\text{D}} \sim 1 \times 10^8 \text{ cm}^{-3} \text{ s}^{-1}$ or $1.6 \times 10^{-13} \text{ M s}^{-1}$. At 298 K, 50% relative humidity, the branching ratio of O^1D into OH -radicals is ~ 0.2 ,²³ leading to $R_{+\text{OH}}(\text{g}) \sim 3 \times 10^{-14} \text{ M s}^{-1}$, for the rate of $\cdot\text{OH}$ -radical production in the gas-phase, i.e., about 10^5 times smaller than $R_{+\text{OH}}(\text{aq})$.

On the basis of the above results and considerations, hydrophobic VOCs are expected to be oxidized faster under foggy than clear conditions. This expectation seems to have been confirmed by a recent field study, which found enhanced and

protracted SOA production during foggy versus non-foggy conditions.⁵⁶ The commonplace observation that early foggy conditions typically lead to optically thicker and more persistent urban haze (and associated health effects) during the day, remarkably, has so far lacked a plausible explanation.

CONCLUSION

The OH-initiated oxidation of ISO leads to the formation of C₁₀H₁₅OH species as primary products, whose formation both requires and is inhibited by O₂. A minimum of seven C₁₀H₁₅OH isomers were resolved by reverse-phase high-performance liquid chromatography and detected as MH⁺ (m/z = 153). We show that similar to isoprene, the overall uptake of other gas-phase olefins are enhanced by several factors that include: (1) the higher rates of photochemical ·OH-radical production in aqueous media, (2) the likelihood that aerosol phase reactions can occur both in the bulk liquid and at the air-liquid interface due to high surface areas that are available for reactions, and (3) the reaction products remain on aqueous acidic surfaces, where they are converted into less volatile species. The production of OH radical in the aqueous phase via the photolysis of H₂O₂ is much faster than the gas phase production via photolysis of O₃. Our calculations can help to explain the enhanced SOA concentration/visibility reductions during foggy conditions at sunrise.

ACKNOWLEDGEMENTS: This work was supported by NSF (U.S.A.) Grant AC-1238977

SUPPORTING INFORMATION AVAILABLE: Additional data and experimental details. This information is free of charge via the Internet at <http://pubs.acs.org>.

FIGURES

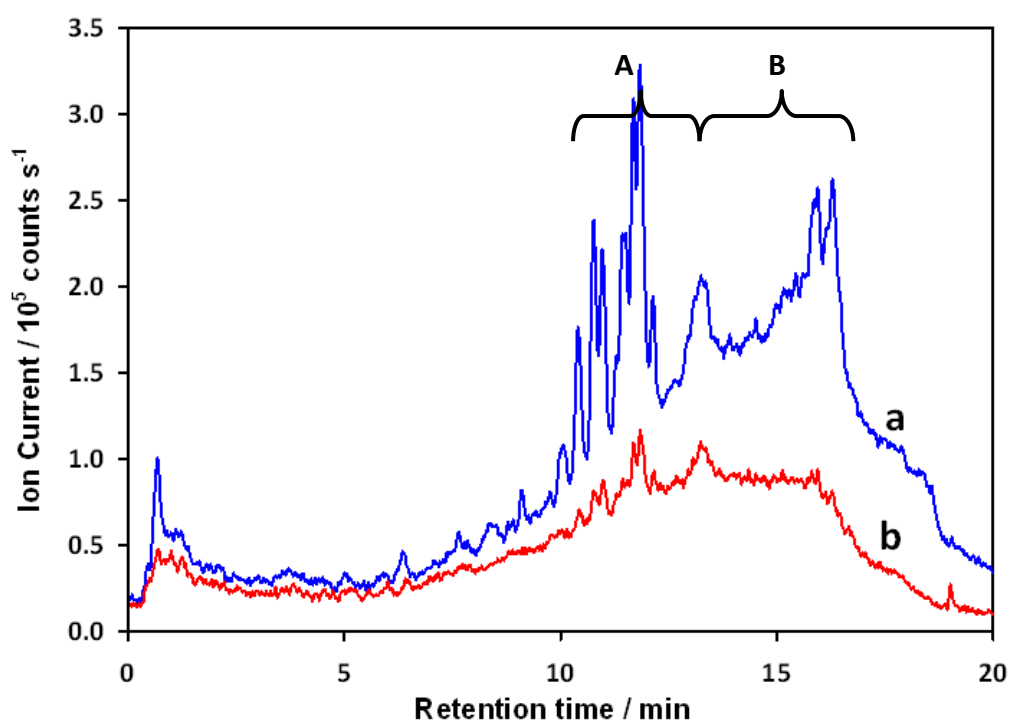


FIGURE 3.1: Chromatograms of the products of the $\lambda > 305$ nm photolysis of aqueous (5 mM ISO in 50 mM H₂O₂) under air for 1 hr. **a** (**b**) traces correspond to total positive (negative) ion count (TIC) signals detected by ESI-MS.

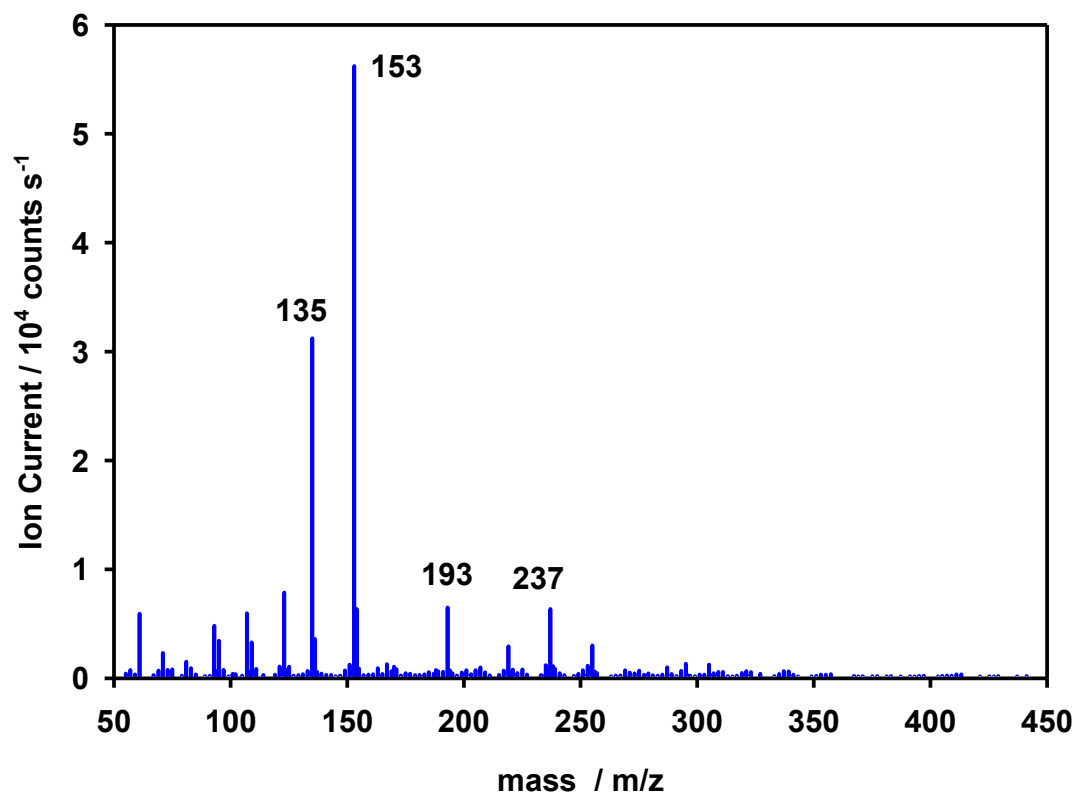


FIGURE 3.2a: ESI positive ion mass spectrum of the products eluted between 10.70 and 10.84 min, in the photolysis of (10 mM ISO in 50 mM H_2O_2) solutions under air for 1 hr.

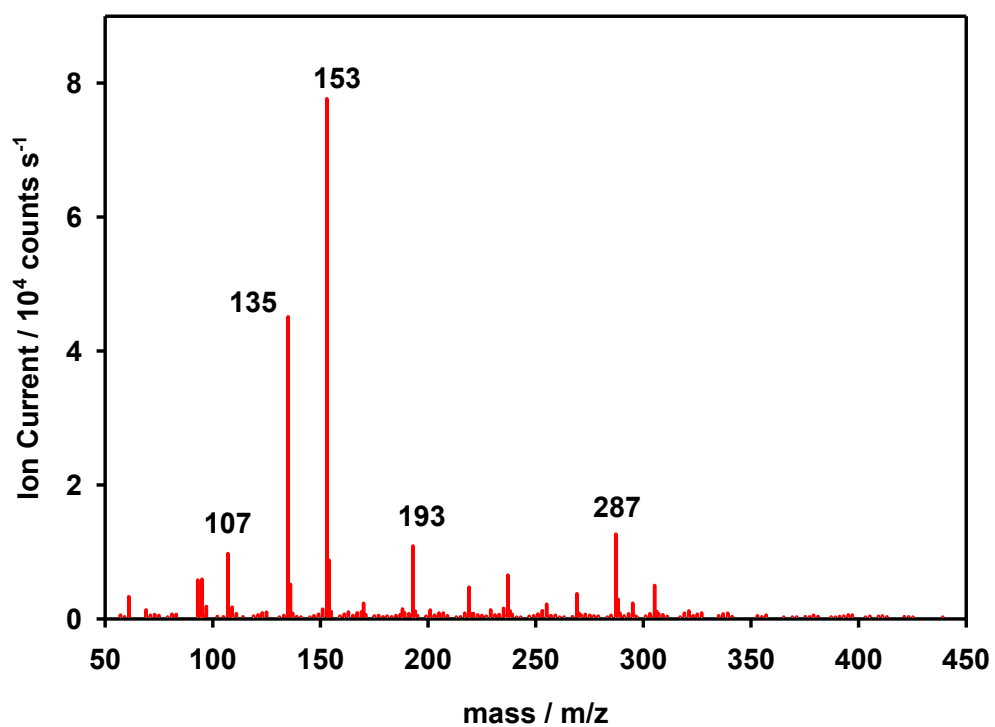


FIGURE 3.2b: ESI positive ion mass spectrum of the products eluted between 11.77 and 11.92 min, in the photolysis of (10 mM ISO in 50 mM H₂O₂) solutions under air for 1 hr.

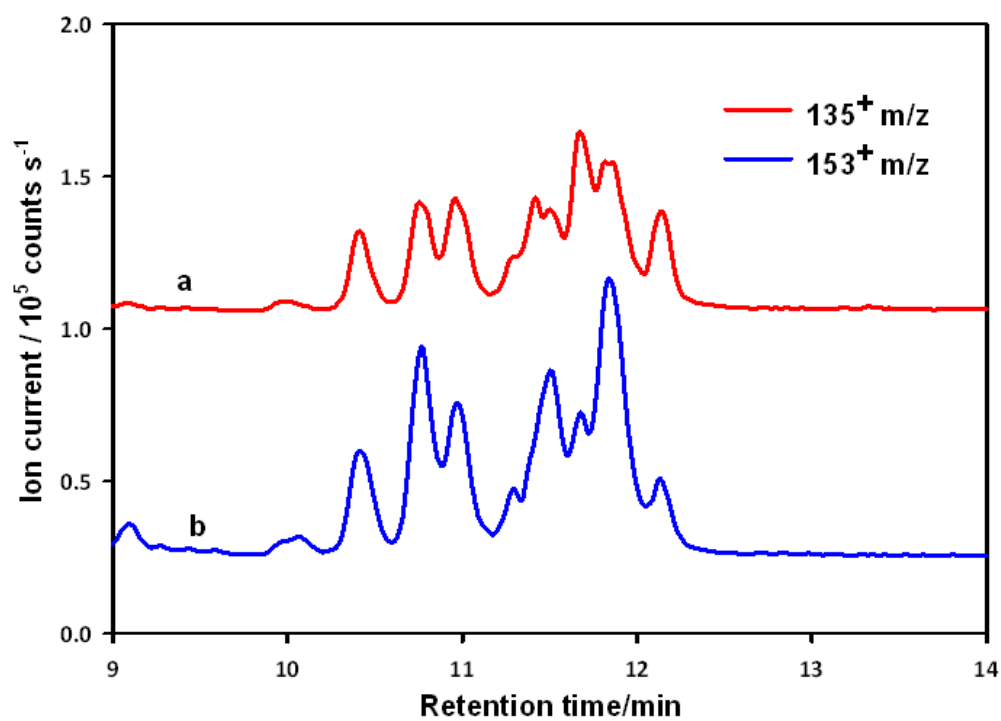


FIGURE 3.3: Extracted ion chromatograms (EIC) of the products $m/z^+ = 135$ (**a**) and $m/z^+ = 153$ (**b**) of the photolysis of (10 mM ISO in 50 mM H₂O₂) solutions under air for 1 hr.

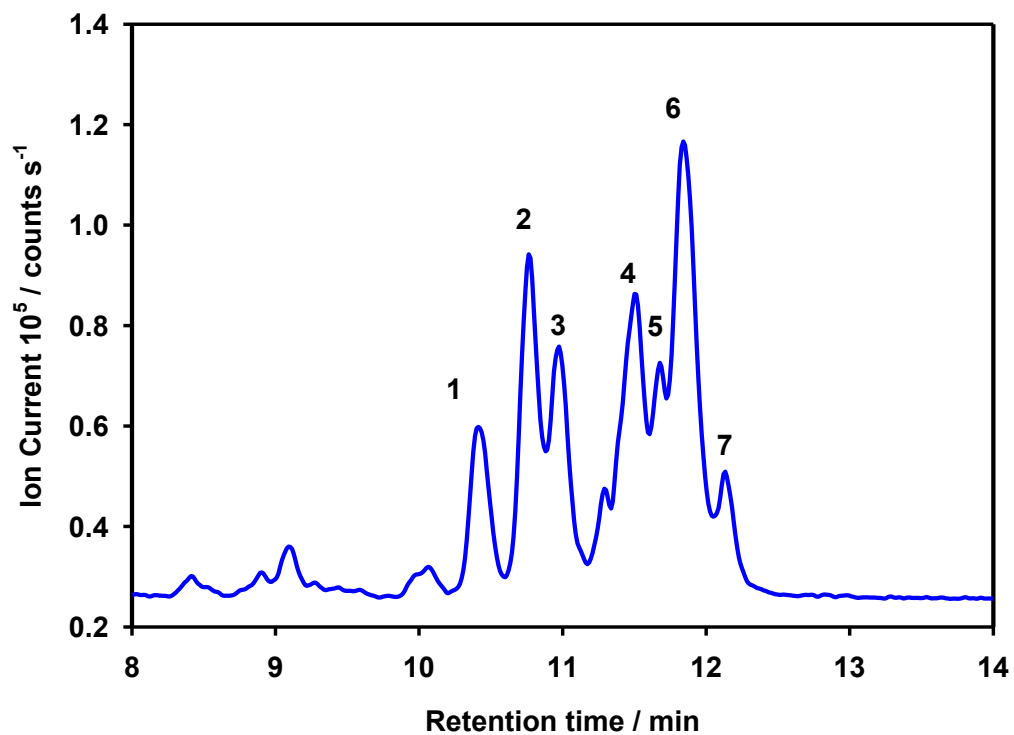


FIGURE 3.4: Extracted $m/z^+ = 153$ ion chromatograms of the products of the photolysis of (10 mM ISO in 50 mM H_2O_2) solutions under air for 1 hr.

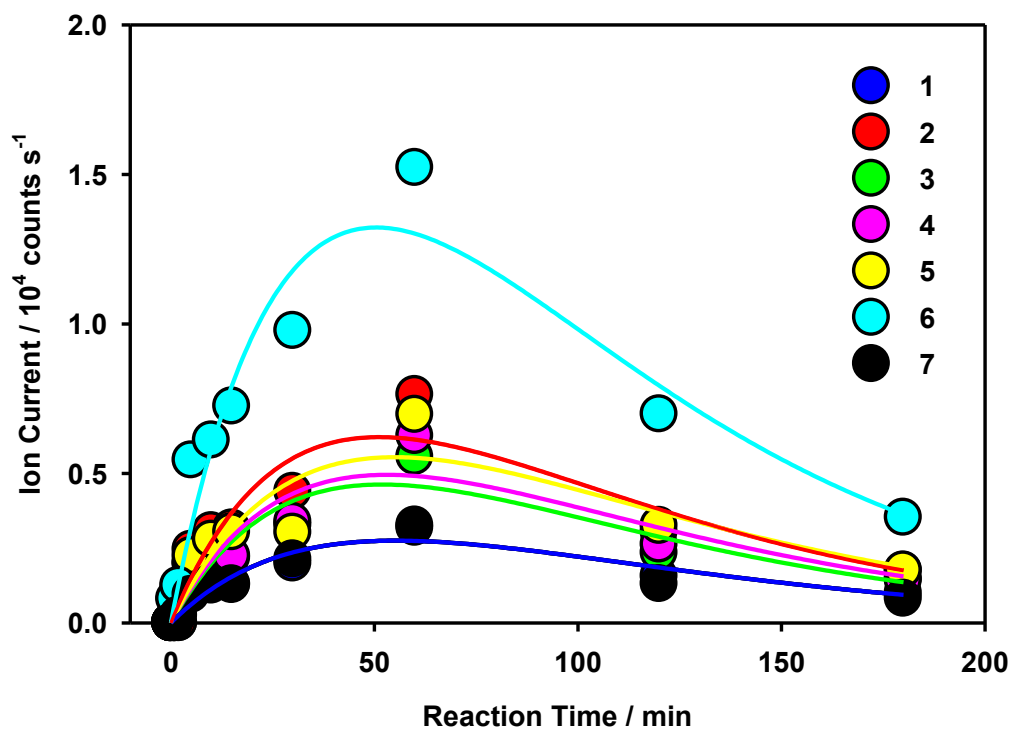


FIGURE 4.5: $m/z^+ = 153$ ion current as a function of photolysis time for products 1 to 7 (labels as in Fig. 4) in the photolysis of (10 mM ISO in 50 mM H_2O_2) solutions under air.

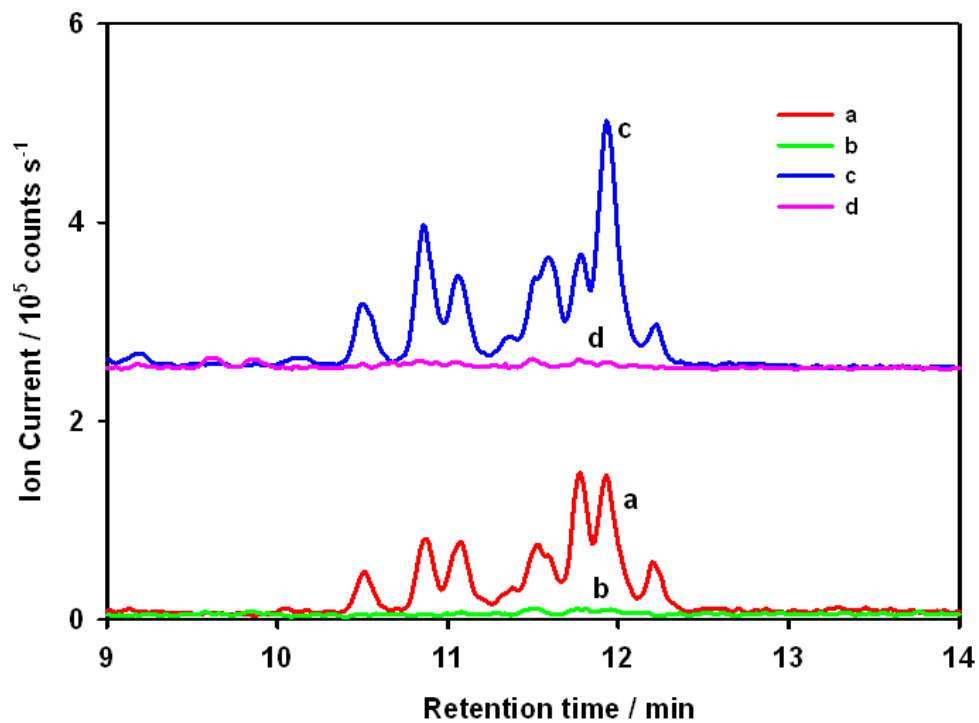


FIGURE 4.6: Extraction ion chromatograms ($m/z^+ = 135$ [**a,b**] and 153 [**c,d**]) of the products of photolysis of Ar-purged versus air-sparged 10 mM ISO samples.

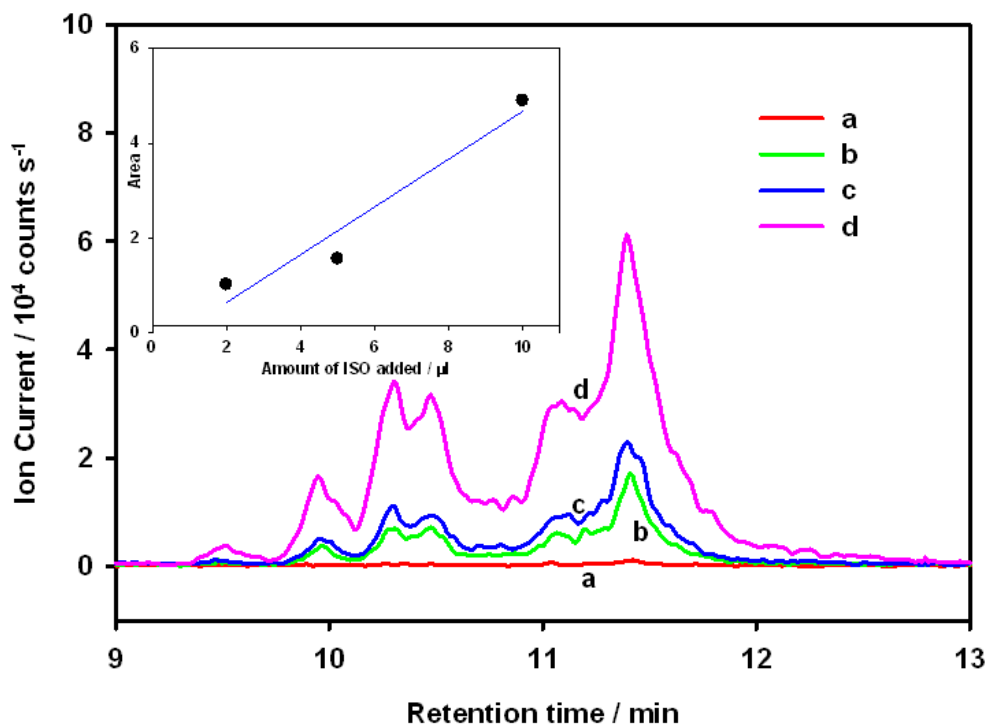


FIGURE 4.7: Extraction Ion chromatograms of 153^+ m/z of the photolysis products of aqueous ISO solutions (1 [a], 2 [b], 5 [c] and 10 μl [d] ISO+ 10 μl H_2O_2 in 3.5ml MQ H_2O) in the presence of air. The inset shows the area under the trace of 153^+ m/z formed under the different initial amounts of added ISO.

REFERENCES

1. Kim, B. G.; Schwartz, S. E.; Miller, M. A.; Min, Q. L., Effective radius of cloud droplets by ground-based remote sensing: Relationship to aerosol. *J. Geophys. Res-Atmos.* 2003, *108* (D23), Doi 10.1029/2003jd003721.
2. Wylie, D.; Jackson, D. L.; Menzel, W. P.; Bates, J. J., Trends in global cloud cover in two decades of HIRS observations. *J Climate.* 2005, *18* (15), 3021-3031.

3. Donaldson, D. J.; Valsaraj, K. T., Adsorption and Reaction of Trace Gas-Phase Organic Compounds on Atmospheric Water Film Surfaces: A Critical Review. *Environ. Sci. Technol.* 2010, *44* (3), 865-873.
4. Valsaraj, K. T., A Review of the Aqueous Aerosol Surface Chemistry in the Atmospheric Context. *Open Journal of Physical Chemistry* 2012, *2*, 58-66.
5. Goss, K. U., Predicting Adsorption of Organic Chemicals at the Air-Water Interface. *J. Phys. Chem. A* 2009, *113* (44), 12256-12259.
6. Ellison, G. B.; Tuck, A. F.; Vaida, V., Atmospheric processing of organic aerosols. *J. Geophys. Res-Atmos.* 1999, *104* (D9), 11633-11641.
7. Donaldson, D. J.; Vaida, V., The influence of organic films at the air-aqueous boundary on atmospheric processes. *Chem. Rev.* 2006, *106* (4), 1445-1461.
8. Rudich, Y., Laboratory perspectives on the chemical transformations of organic matter in atmospheric particles. *Chem. Rev.* 2003, *103* (12), 5097-5124.
9. Enami, S.; Hoffmann, M. R.; Colussi, A. J., Dry deposition of biogenic terpenes via cationic oligomerization on environmental aqueous surfaces. *J. Phys. Chem. Lett.* 2012, *3*, 3102-3108.
10. Enami, S.; Mishra, H.; Hoffmann, M. R.; Colussi, A. J., Protonation and Oligomerization of Gaseous Isoprene on Mildly Acidic Surfaces: Implications for Atmospheric Chemistry. *J. Phys. Chem. A.* 2012, *116* (24), 6027-6032.
11. Enami, S.; Hoffmann, M. R.; Colussi, A. J., Proton Availability at the Air/Water Interface. *J Phys Chem Lett* 2010, *1* (10), 1599-1604.

12. Enami, S.; Stewart, L. A.; Hoffmann, M. R.; Colussi, A. J., Superacid Chemistry on Mildly Acidic Water. *J. Phys. Chem. Lett.* 2010, *1* (24), 3488-3493.
13. Mishra, H.; Enami, S.; Nielsen, R. J.; Stewart, L. A.; Hoffmann, M. R.; Goddard, W. A.; Colussi, A. J., Bronsted basicity of the air-water interface. *P. Natl. Acad. Sci. USA* 2012, *109* (46), 18679-18683.
14. Shultz, M. J.; Vu, T. H.; Meyer, B.; Bisson, P., Water: A Responsive Small Molecule. *Accounts Chem. Res.* 2012, *45* (1), 15-22.
15. Tropospheric Ultraviolet and Visible (TUV) Radiation Model, http://cprm.acd.ucar.edu/Models/TUV/Interactive_TUV/
16. Johnson, D.; Marston, G., The gas-phase ozonolysis of unsaturated volatile organic compounds in the troposphere. *Chem. Soc. Rev.* 2008, *37* (4), 699-716.
17. Enami, S.; Hoffmann, M. R.; Colussi, A. J., Prompt Formation of Organic Acids in Pulse Ozonation of Terpenes on Aqueous Surfaces. *J. Phys. Chem. Lett.* 2010, *1* (15), 2374-2379.
18. Epstein, S. A.; Nizkorodov, S. A., A comparison of the chemical sinks of atmospheric organics in the gas and aqueous phase. *Atmos. Chem. Phys.* 2012, *12* (17), 8205-8222.
19. Renard, P.; Siekmann, F.; Gandolfo, A.; Socorro, J.; Salque, G.; Ravier, S.; Quivet, E.; Clément, J.-L.; Traikia, M.; Delort, A.-M.; Voisin, D.; Thissen, R.; Monod, A., Radical mechanisms of methyl vinyl ketone oligomerization through aqueous phase OH-

oxidation: on the paradoxical role of dissolved molecular oxygen. *Atmos. Chem. Phys. Discuss.* 2013, *13*, 2913-2954.

20. Chameides, W. L.; Fehsenfeld, F.; Rodgers, M. O.; Cardelino, C.; Martinez, J.; Parrish, D.; Lonneman, W.; Lawson, D. R.; Rasmussen, R. A.; Zimmerman, P.; Greenberg, J.; Middleton, P.; Wang, T., Ozone precursor relationships in the ambient atmosphere. *J. Geophys. Res.-Atmos.* 1992, *97* (D5), 6037-6055.

21. Guenther, A.; Karl, T.; Harley, P.; Wiedinmyer, C.; Palmer, P. I.; Geron, C., Estimates of global terrestrial isoprene emissions using MEGAN (Model of Emissions of Gases and Aerosols from Nature). *Atmos. Chem. Phys.* 2006, *6*, 3181-3210.

22. Fan, J. W.; Zhang, R. Y., Atmospheric Oxidation Mechanism of Isoprene. *Environ. Chem.* 2004, *1* (3), 140-149.

23. Seinfeld, J. H.; Pandis, S. N., Atmospheric chemistry and physics: from air pollution to climate change. 2nd ed.; Wiley: Hoboken, N.J., 2006.

24. Huang, D.; Zhang, X.; Chen, Z. M.; Zhao, Y.; Shen, X. L., The kinetics and mechanism of an aqueous phase isoprene reaction with hydroxyl radical. *Atmos. Chem. Phys.* 2011, *11* (15), 7399-7415.

25. Santos, L. S.; Dalmazio, I.; Eberlin, M. N.; Claeys, M.; Augusti, R., Mimicking the atmospheric OH-radical-mediated photooxidation of isoprene: formation of cloud-condensation nuclei polyols monitored by electrospray ionization mass spectrometry. *Rapid. Commun. Mass Sp.* 2006, *20* (14), 2104-2108.

26. Kleindienst, T. E.; Lewandowski, M.; Offenber, J. H.; Jaoui, M.; Edney, E. O., The formation of secondary organic aerosol from the isoprene plus OH reaction in the absence of NO_x. *Atmos. Chem. Phys.* 2009, *9* (17), 6541-6558.
27. Ervens, B.; Turpin, B. J.; Weber, R. J., Secondary organic aerosol formation in cloud droplets and aqueous particles (aqSOA): a review of laboratory, field and model studies. *Atmo. Chem. Phys.* 2011, *11* (21), 11069-11102.
28. Mouchel-Vallon, C.; Brauer, P.; Camredon, M.; Valorso, R.; Madronich, S.; Herrmann, H.; Aumont, B., Explicit modeling of volatile organic compounds partitioning in the atmospheric aqueous phase. *Atmos Chem Phys* 2013, *13* (2), 1023-1037.
29. Guzman, M. I.; Colussi, A. J.; Hoffmann, M. R., Photoinduced oligomerization of aqueous pyruvic acid. *J Phys Chem A* 2006, *110* (10), 3619-3626.
30. NASA-JPL Chemical Kinetics and Photochemical Data for Use in Atmospheric Studies, Evaluation Number 14. 2003.
31. Edney, E. O.; Kleindienst, T. E.; Jaoui, M.; Lewandowski, M.; Offenber, J. H.; Wang, W.; Claeys, M., Formation of 2-methyl tetrols and 2-methylglyceric acid in secondary organic aerosol from laboratory irradiated isoprene/NO(X)/SO(2)/air mixtures and their detection in ambient PM(2.5) samples collected in the eastern United States. *Atmos Environ* 2005, *39* (29), 5281-5289.
32. Claeys, M.; Graham, B.; Vas, G.; Wang, W.; Vermeylen, R.; Pashynska, V.; Cafmeyer, J.; Guyon, P.; Andreae, M. O.; Artaxo, P.; Maenhaut, W., Formation of

secondary organic aerosols through photooxidation of isoprene. *Science* 2004, 303 (5661), 1173-1176.

33. Claeys, M.; Wang, W.; Ion, A. C.; Kourtchev, I.; Gelencser, A.; Maenhaut, W., Formation of secondary organic aerosols from isoprene and its gas-phase oxidation products through reaction with hydrogen peroxide. *Atmos Environ* 2004, 38 (25), 4093-4098.

34. Ruppert, L.; Becker, K. H., A product study of the OH radical-initiated oxidation of isoprene: formation of C-5-unsaturated diols. *Atmos Environ* 2000, 34 (10), 1529-1542.

35. Fischer, H.; Radom, L., Factors controlling the addition of carbon-centered radicals to alkenes-an experimental and theoretical perspective. *Angew Chem Int Edit* 2001, 40 (8), 1340-1371.

36. Bao, L. F.; Matsumoto, M.; Kubota, T.; Sekiguchi, K.; Wang, Q. Y.; Sakamoto, K., Gas/particle partitioning of low-molecular-weight dicarboxylic acids at a suburban site in Saitama, Japan. *Atmos Environ* 2012, 47, 546-553.

37. Shakya, K. M.; Place, P. F.; Griffin, R. J.; Talbot, R. W., Carbonaceous content and water-soluble organic functionality of atmospheric aerosols at a semi-rural New England location. *J Geophys Res-Atmos* 2012, 117, Doi 10.1029/2011jd016113.

38. Kiss, G.; Varga, B.; Galambos, I.; Ganszky, I., Characterization of water-soluble organic matter isolated from atmospheric fine aerosol. *J Geophys Res-Atmos* 2002, 107 (D21), Doi 10.1029/2001jd000603.

39. Decesari, S.; Facchini, M. C.; Fuzzi, S.; Tagliavini, E., Characterization of water-soluble organic compounds in atmospheric aerosol: A new approach. *J Geophys Res-Atmos* 2000, *105* (D1), 1481-1489.
40. Park, J.; Jongsma, C. G.; Zhang, R. Y.; North, S. W., Cyclization reactions in isoprene derived beta-hydroxy radicals: implications for the atmospheric oxidation mechanism. *Phys. Chem. Chem. Phys.* 2003, *5* (17), 3638-3642.
41. Villano, S. M.; Huynh, L. K.; Carstensen, H. H.; Dean, A. M., High-Pressure Rate Rules for Alkyl + O₂ Reactions. 2. The Isomerization, Cyclic Ether Formation, and beta-Scission Reactions of Hydroperoxy Alkyl Radicals. *J Phys Chem A* 2012, *116* (21), 5068-5089.
42. Ho, K. F.; Cao, J. J.; Lee, S. C.; Kawamura, K.; Zhang, R. J.; Chow, J. C.; Watson, J. G., Dicarboxylic acids, ketocarboxylic acids, and dicarbonyls in the urban atmosphere of China. *J Geophys Res-Atmos* 2007, *112* (D22).
43. Ho, K. F.; Ho, S. S. H.; Lee, S. C.; Kawamura, K.; Zou, S. C.; Cao, J. J.; Xu, H. M., Summer and winter variations of dicarboxylic acids, fatty acids and benzoic acid in PM_{2.5} in Pearl Delta River Region, China. *Atmos Chem Phys* 2011, *11* (5), 2197-2208.
44. Kawamura, K.; Kasukabe, H.; Barrie, L. A., Secondary formation of water-soluble organic acids and alpha-dicarbonyls and their contributions to total carbon and water-soluble organic carbon: Photochemical aging of organic aerosols in the Arctic spring. *J Geophys Res-Atmos* 2010, *115*.

45. Kawamura, K.; Yasui, O., Diurnal changes in the distribution of dicarboxylic acids, ketocarboxylic acids and dicarbonyls in the urban Tokyo atmosphere. *Atmos Environ* 2005, 39 (10), 1945-1960.
46. NIST Chemistry WebBook. *NIST Standard Reference Database Number 69* 2011, <http://webbook.nist.gov/chemistry/>.
47. Galloway, M. M.; Loza, C. L.; Chhabra, P. S.; Chan, A. W. H.; Yee, L. D.; Seinfeld, J. H.; Keutsch, F. N., Analysis of photochemical and dark glyoxal uptake: Implications for SOA formation. *Geophys. Res. Lett.* 2011, 38, Doi 10.1029/2011gl048514.
48. Carlton, A. G.; Turpin, B. J.; Altieri, K. E.; Seitzinger, S.; Reff, A.; Lim, H. J.; Ervens, B., Atmospheric oxalic acid and SOA production from glyoxal: Results of aqueous photooxidation experiments. *Atmos. Environ.* 2007, 41 (35), 7588-7602.
49. Pankow, J. F., Partitioning of semi-volatile organic compounds to the air/water interface. *Atmos. Environ.* 1997, 31 (6), 927-929.
50. Valsaraj, K. T.; Thoma, G. J.; Reible, D. D.; Thibodeaux, L. J., On the Enrichment of Hydrophobic Organic-Compounds in Fog Droplets. *Atmos. Environ.* 1993, 27 (2), 203-210.
51. Finley, J. W.; Wheeler, E. L.; Witt, S. C., Oxidation of glutathione by hydrogen peroxide and other oxidizing agents. *J. Agr. Food. Chem.* 1981, 29 (2), 404-407.
52. Davidovits, P.; Kolb, C. E.; Williams, L. R.; Jayne, J. T.; Worsnop, D. R., Mass accommodation and chemical reactions at gas-liquid interfaces. *Chem. Rev.* 2006, 106, 1323-1354.

53. Kinugawa, T.; Enami, S.; Yabushita, A.; Kawasaki, M.; Hoffmann, M. R.; Colussi, A. J., Conversion of gaseous nitrogen dioxide to nitrate and nitrite on aqueous surfactants. *Phys. Chem.* 2011, *13* (11), 5144-5149.
54. Vacha, R.; Slavicek, P.; Mucha, M.; Finlayson-Pitts, B. J.; Jungwirth, P., Adsorption of atmospherically relevant gases at the air/water interface: Free energy profiles of aqueous solvation of N₂, O₂, O₃, OH, H₂O, HO₂, and H₂O₂. *J. Phys. Chem. A* 2004, *108* (52), 11573-11579.
55. Kahan, T. F.; Washenfelder, R. A.; Vaida, V.; Brown, S. S., Cavity-Enhanced Measurements of Hydrogen Peroxide Absorption Cross Sections from 353 to 410 nm. *J. Phys. Chem. A* 2012, *116* (24), 5941-5947.
56. Kaul, D. S.; Gupta, T.; Tripathi, S. N.; Tare, V.; Collett, J. L., Secondary Organic Aerosol: A Comparison between Foggy and Nonfoggy Days. *Environ. Sci. Technol.* 2011, *45* (17), 7307-7313.

Chapter 4

Fenton Oxidation of Gas-Phase Isoprene on Aqueous Surfaces

Sections reprinted with permission from **F. Rifkha Kameel, F. Riboni, Shinichi Enami, M. R. Hoffmann and A. J. Colussi^{1*}**, *Journal of Physical Chemistry C*

ABSTRACT

We report that gaseous isoprene ISO(g) is oxidized into soluble species on the surface of aqueous acidic FeCl₂ solutions simultaneously exposed to H₂O₂(g). In our experiments, ISO(g) and/or H₂O₂(g) streams intersect aqueous pH ~ 2 FeCl₂ microjets for ~ 10 microseconds. The products formed in these reactive encounters are identified *in situ* via online electrospray ionization mass spectrometry. We found that the (ISO)_nH⁺ oligomers generated from ISO(g) on the surface of pH < 4 water are oxidized into myriad products whose combined yields exceed 5% of (ISO)_nH⁺ reactants. MS² analysis reveals that the positive ions derived from the protonation of neutral products split H₂O and O neutrals, whereas the less abundant negative carboxylate ion products undergo CO, H₂O and CO₂ losses. Significantly, all products are fully quenched by the ·OH scavenger *tert*-butanol. These results are consistent with an oxidation process initiated by the addition of ·OH from (Fe²⁺[aq] + H₂O₂[g]) to (ISO)_nH⁺, followed by fast reactions involving dissolved H₂O₂, HO₂· and O₂ that lead to polyols, carbonyls and, to a lesser extent, carboxylic acids. Our experiments demonstrate that gas-phase olefins can be oxidized upon colliding on the surface of Fe-containing acidic aqueous media under typical tropospheric conditions.

INTRODUCTION

The troposphere contains vast amounts of airborne liquid water in the form of aerosol, clouds, fog and haze. The large specific surface areas ($S/V \sim 10^{-4}$ to 10^{-5} cm^{-1}) of such dispersions suggest that gas-liquid heterogeneous processes could play a significant role in atmospheric chemistry. Early recognition of this fact¹ and worldwide concern about atmospheric aerosols,²⁻⁵ however, have not yet translated into the inclusion of heterogeneous processes (HPs) as essential components of atmospheric chemistry. Recently, interest in HPs in atmospheric chemistry has been revived by the puzzling issues posed by the fate of biogenic volatile organic compounds (VOCs) over remote (i.e., low NO_x) forest canopies.⁶ Field measurements reveal that the $\cdot\text{OH}$ radical concentrations measured therein are much higher than those evaluated from current atmospheric chemistry mechanisms and estimated VOCs emission fluxes.⁷ This notorious deficiency has led to consider the possibility, seemingly by elimination, that unspecified HPs might help close the gap.⁷ What the presumed HPs are, however, is not clear. Emerging new concepts in the physical chemistry of interfaces,⁸⁻¹¹ and newly found phenomena at the air-water interface¹²⁻²³ hint that some or all of the missing processes could not have been anticipated.

It is not easily grasped or generally realized that chemistry on the surface of water cannot be deduced, extrapolated from or assimilated to those in bulk gas or liquid phases. The key distinctive feature is that water density drops a thousand-fold within a few Angstroms through the gas-liquid interfacial region.^{8, 10} Thus, approaching

hydrophobic VOCs will likely remain in these relatively 'dry' interfacial water layers rather than proceed into bulk water.⁸ As a rule, then, most organic gases should be expected to be incorporated into condensed aqueous phases via adsorption on aqueous interfaces to extents larger than those predicted from Henry's law gas-to-bulk partition constants.^{8, 10, 24-25} We have shown that gas-phase olefins are protonated on the surface of pH < 4 water.¹⁸⁻²⁰ Thus, unsaturated hydrocarbon gases, such as most biogenic VOCs, have an additional strong chemical driving force for sticking to modestly acidic aqueous aerosol surfaces. This phenomenon increases their residence time at the interface and, hence, makes them amenable to reactive attack by gaseous atmospheric oxidants, such as ozone and hydroxyl radicals. Furthermore, there is evidence that some reactions become feasible at the gas-water interface for thermodynamic reasons related to hydration, whereas others proceed at faster rates or, in the case of competitive channels, with branching ratios different than those in bulk water.^{13, 15-16, 22-23, 26} Although some of these game-changing ideas have been floated in the literature for some time, they have been demonstrated experimentally only recently.²⁷⁻²⁸

Isoprene (ISO), the most abundant non-methane VOC, is one of the major contributors to secondary organic aerosols (SOA) formation.²⁹⁻³³ The mechanisms involved in such transformations, however, are not fully understood. Current gas-phase atmospheric chemistry mechanisms systematically underestimate SOA formation.^{2, 7} Because ISO is barely soluble in bulk water ($H_{ISO} \approx 10^{-2} \text{ M atm}^{-1}$)³⁴, its lifetime in daytime tropospheres ($\tau_{1/2} \approx 3 \text{ h}$) is deemed to be determined by its fast reaction with $\cdot\text{OH}(\text{g})$.²⁴

³⁵⁻³⁸ The products of ISO oxidation in the gas-phase are mostly water-soluble, and become incorporated into the aerosol phase where they continue to be processed.³⁹⁻⁴⁰ ·OH radicals, however, are also produced in the aerosol phase via the Fe(II)-catalyzed (Fenton) decomposition, and the solar ($\lambda < 350$ nm) photolysis of dissolved H₂O₂.⁴¹ Since atmospheric H₂O₂ is overwhelmingly enriched in water ($H_{HP} \approx 10^5$ M atm⁻¹),³⁴ the preceding considerations suggest that ISO(g), by being trapped via protonated on mildly acidic pH < 4 environmental waters, could be oxidized by ·OH(aq) radicals from the decomposition of H₂O₂(aq). Actually, the rate of ·OH-radical generation from the solar photolysis of H₂O₂ dissolved in aqueous aerosols is several orders of magnitude faster than that from the photolysis of O₃(g) in the gas-phase.⁴¹ Herein we report the results of experiments designed to explore such possibility. Our experiments are based on a novel technique developed in our laboratory that allows for the *in situ* detection of interfacial reactants and products via online electrospray ionization mass spectrometry.¹⁹

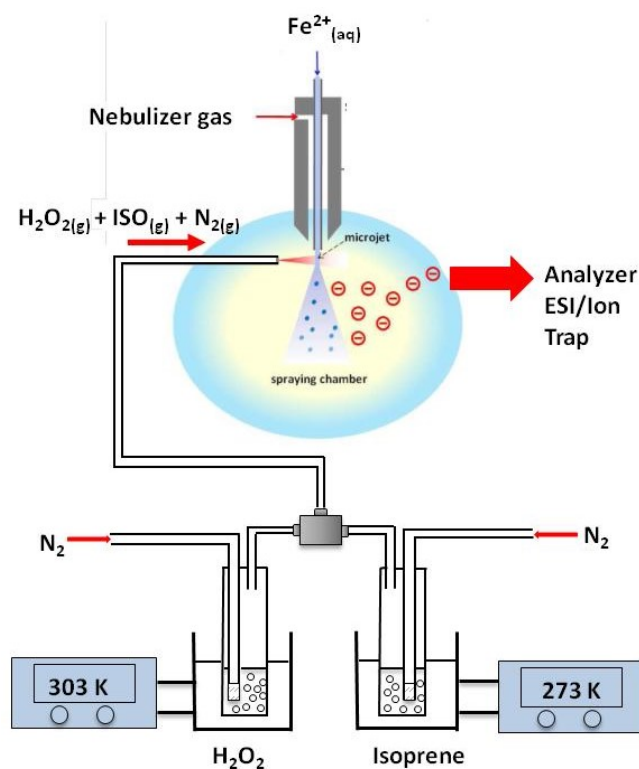
EXPERIMENTAL SECTION

Experiments were carried out by intersecting continuously flowing acidic 1 μ M FeCl₂(aq) microjets with ISO(g)/N₂(g), H₂O₂(g)/N₂(g) or ISO(g)/H₂O₂(g)/N₂(g) gas streams in the spraying chamber of an electrospray (ES) ionization mass spectrometer (Agilent 1100 Series, LC/MSD high performance ion trap mass spectrometer) maintained at ambient temperature and pressure. The structures of selected products were elucidated via MS² spectrometry in positive and negative ion modes in the 50 to 600 Da mass range

at fragmentation voltages of 1 V and 3V. The detected species are produced during encounters of gaseous ISO and/or H₂O₂ with the surface of the aqueous microjets as they emerge from the nozzle, *i.e.*, before they are broken up into submicrometer-sized droplets by the nebulizer gas.⁴²⁻⁴³ These microdroplets carry excess charges of either sign, which represent the information registered by the mass spectrometer. The experimental design is shown in Scheme 4.1. Further details on the instrument, the experiments and the evidence accumulated in our laboratory about the surface specificity of our measurements have been provided in previous reports.⁴³

Aqueous FeCl₂ solutions, prepared by dissolving FeCl₂·4H₂O (> 98 % Sigma-Aldrich) in deionized water and acidified to pH ~2.0 with HCl(aq), were continuously pumped at 25 μL/min into the spraying chamber through a grounded stainless steel needle injector. Liquid ISO (Sigma-Aldrich, 98.0%, purified by fractional distillation collecting the fraction boiling between 40 and 45 °C) was maintained at 273 K and sparged with 15 cm³/min N₂(g) gas flow. Similarly, 50 wt. % H₂O₂ (Sigma-Aldrich) kept at 303 K was sparged with 150 cm³/min N₂(g). These flows could be conveyed independently, or merged (through a T-connector) into the spraying chamber. These gas streams were directed via a Teflon catheter positioned near and toward the liquid microjet. The actual concentrations at the surface of the microjet: [ISO(g)] ~ 5 × 10¹⁵ molecules cm⁻³; [H₂O₂(g)] ~ 4 × 10¹⁴ molecules cm⁻³, were estimated from the vapor pressure of ISO(l) at 273 K, the reported composition of the vapor in equilibrium with 50 wt.% H₂O₂ solutions at 303 K, the corresponding carrier and nebulizer gas flow rates (see Supporting Information). Other

instrumental parameters were: drying gas flow rate: 8 L min^{-1} ; drying gas temperature: $325 \text{ }^\circ\text{C}$; nebulizer pressure: 3 bars; collector capillary voltage: $\pm 2.5 \text{ kV}$; fragmentation voltages: 20 V (for positive ions) and 40V (for negative ions) were chosen to optimize mass signals with minimal fragmentation of molecular ions.



SCHEME 4.1

SCHEME 4.1 - Experimental setup

The progeny of oxidation products was established by successively sparging deionized H_2O instead of H_2O_2 solution, or deionized H_2O instead of ISO while maintaining the combined gas flow rate at $165 \text{ cm}^3 \text{ min}^{-1}$. In some experiments, we

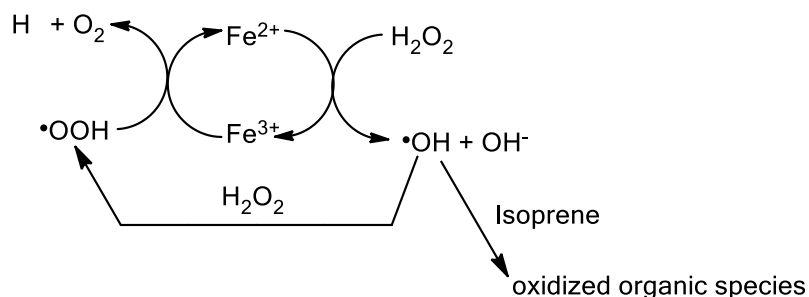
added 100 μM *tert*-butanol (an efficient $\cdot\text{OH}$ scavenger: $k_{\text{OH}+\text{t-BuOH}} = 5 \times 10^8 \text{ M}^{-1} \text{ s}^{-1}$ in bulk water)⁴⁴ to 1 μM FeCl_2 solutions to test the participation of $\cdot\text{OH}$ radicals in the formation of the observed products.

RESULTS AND DISCUSSION:

We have recently shown that the Fe(II)-catalyzed decomposition of $\text{H}_2\text{O}_2(\text{g})$ at the air-water interface is about 10^3 times faster than its counterpart in bulk water.⁴⁴ The Fenton reaction may produce $\cdot\text{OH}$ radicals via a one-electron transfer (the Haber-Weiss mechanism), reaction R1, and $\text{Fe}^{\text{IV}}\text{O}^{2+}$ species via a two-electron oxidation via O-atom transfer (the Bray-Gorin mechanism), reaction R2.⁴⁴



R1 is followed by further reactions that recycle Fe(II) and generate $\text{HOO}\cdot$ radicals⁴⁵⁻⁴⁷ and $\text{O}_2(\text{g})$ as additional reactants (Scheme 4.2). Experiments testing the effect of variable $\text{O}_2(\text{g})$ concentrations are underway. We have recently reported that R2 is the dominant channel at the air-water interface that produces mono- and poly-iron species containing the ferryl $\text{Fe}^{\text{IV}}\text{O}^{2+}$ moiety, which may disproportionate with Fe^{2+} into Fe^{3+} or react with suitable O-atom acceptors such as DMSO.⁴⁴



SCHEME 4.2

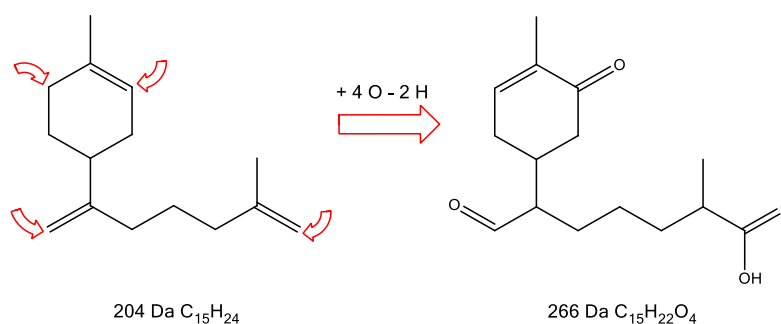
Negative ion ES mass spectra are shown in Fig. 4.1. In accordance with our previous report, we detect, in addition to the triplet at $m/z^- = 161, 163$ and 165 (arising from natural abundance $^{35}\text{Cl}/^{37}\text{Cl} = 3$ isotopes) that corresponds to the $\text{Fe}^{\text{II}}\text{Cl}_3^-$ reactant, clusters at $m/z^- = 196, 198, 200$ and 202 , which are readily assigned to the $\text{Fe}^{\text{III}}\text{Cl}_4^-$ product,⁴⁴ and $m/z^- = 303, 305$ and 307 from the mixed valence di-nuclear ferryl $\text{O}=\text{Fe}^{\text{IV}}\cdot\text{Cl}\cdot\text{Fe}^{\text{II}}\text{Cl}_4^-$.⁴⁴ We confirmed that these products disappear upon switching from $\text{H}_2\text{O}_2(\text{g})/\text{N}_2(\text{g})$ to $\text{ISO}(\text{g})/\text{N}_2(\text{g})$ mixtures, as expected. Significantly, however, exposure to $\text{ISO}(\text{g})/\text{H}_2\text{O}_2(\text{g})/\text{N}_2(\text{g})$ mixtures resulted in the appearance of a new sizable peak at $m/z^- = 265$, which we tentatively assign to the anion of a carboxylic acid product, plus a multitude of minor peaks.

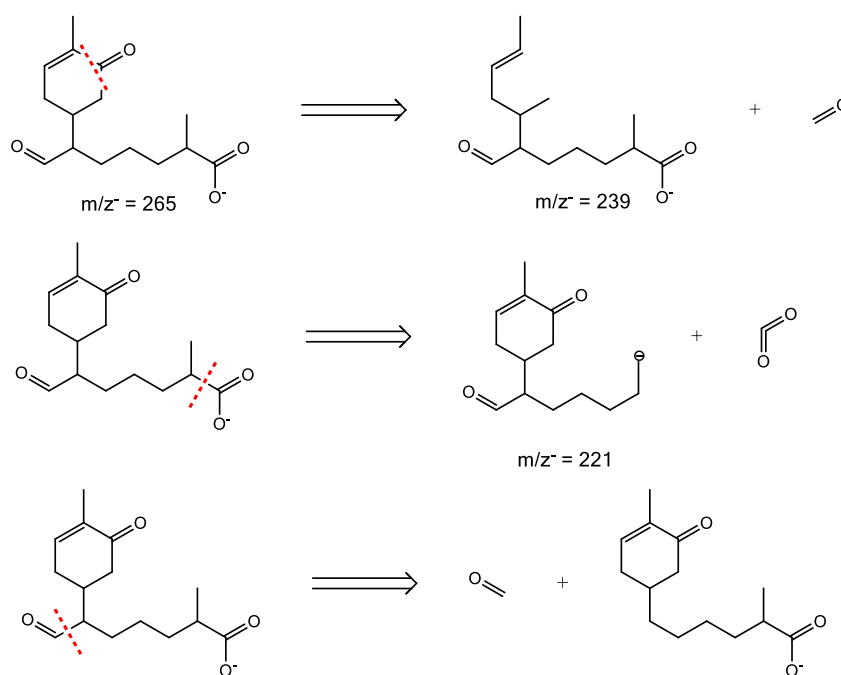
The MS^2 of the $m/z^- = 265$ anion is shown in Figure 4.2. The 44 and 28 neutral losses are consistent with the presence of both carboxylate and carbonyl groups in its structure.⁴⁸ The detection of an intense $m/z^+ = 267$ peak (see below, Figure 3B), which is the doubly protonated counterpart of $m/z^- = 265$, implies the formation of a 266 Da neutral acid produced from the oxidation of the most abundant $(\text{ISO})_3\text{H}^+$ $m/z^+ = 205$

oligomer at the air-water interface (see below). The algebra linking $(\text{ISO})_3$ with the 266 Da product: $(\text{ISO})_3 + 4 \text{ O} - 2 \text{ H} = 204 - 2 + 64 = 266$, ascribes a $\text{C}_{15}\text{H}_{22}\text{O}_4$ molecular formula to the acid giving rise to the $m/z^- = 265$ anion. Possible structures for the 204 Da $(\text{ISO})_3$ sesquiterpenes and associated 266 Da $\text{C}_{15}\text{H}_{22}\text{O}_4$ products are given in Scheme 3. The remarkable finding that $(\text{ISO})_3\text{H}^+$ would add 4 O-atoms and lose 2 H-atoms to produce $\text{C}_{15}\text{H}_{22}\text{O}_4$ species reveals that ~ 5 O-atoms per $(\text{ISO})_3$ are available at the air-water interface within $\sim 10 \mu\text{s}$ contact times. This finding implies that $\text{H}_2\text{O}_2(\text{g})$ generates oxidant species ($\cdot\text{OH}$, $\text{HOO}\cdot$, O_2 and $\text{Fe}^{\text{IV}}\text{O}^{2+}$) in excess over $(\text{ISO})_n\text{H}^+$ in the outermost interfacial layers, where they are rapidly consumed before they can diffuse away into deeper layers.

Positive ion mass spectra are more complex. Figures 4.3 A and B show positive ion ESI-MS of the surface of $1 \mu\text{M}$ FeCl_2 aqueous microjets while being exposed to $\text{ISO}(\text{g})$, $\text{H}_2\text{O}_2(\text{g})$ or $\text{ISO}(\text{g})/\text{H}_2\text{O}_2(\text{g})$ mixtures. Confirming our previous results,¹⁹ $\text{ISO}(\text{g})$ gives rise to a series of protonated oligomer homologues $(\text{ISO})_{1-8}\text{H}^+$, $m/z^+ = 137$ ($n = 2$), 205 ($n = 3$), 273 ($n = 4$), or $(68n + 1)$, via the cationic polymerization of ISO at the air-water interface (Fig. 4.3A). Notably, we found that such species are conspicuously absent from the mass spectra of ISO previously dissolved in $\text{pH} \sim 2$ water, a finding that proves the protonation of ISO, and hence the formation of the $(\text{ISO})_n\text{H}^+$ oligomers, only takes place at the air-water interface, where the acidity of interfacial H_3O^+ is magnified due to limited hydration.^{16, 18-20} The extent of oligomerization clearly increases at larger $[\text{ISO}(\text{g})]$ because our previous experiments carried at lower $[\text{ISO}(\text{g})]$ led to the formation of

(ISO)₁₋₃H⁺ species.¹⁹ Thus, the most abundant of such species under present conditions is the $m/z^+ = 205$ (ISO)₃H⁺ oligomer. The MS² fragmentation patterns of these oligomers reveal 28 (CH₂=CH₂) and 42 (Me-CH=CH₂) Da neutral losses (Figure 4.4), as expected from polyolefins possessing both terminal –CH=CH₂ and –C(Me)=CH₂ groups. Exposure of FeCl₂ microjets to H₂O₂(g)/N₂(g) did not lead to any detectable positive ion products, as expected, whereas exposure to ISO(g)/H₂O₂(g)/N₂(g) streams gave rise to the formation of myriad species (Figure 3B). We therefore associate such signals to products of the fast oxidation of (ISO)_nH⁺ initiated by ·OH additions to double bonds, followed by the combined action of ·OOH and O₂ species on the resulting free radicals (Scheme 4.2).⁴⁵⁻⁴⁷ As mentioned above, these products are deemed the result of extremely fast reactive events (within ~ 10 μs) involving multiple oxidation steps in interfacial layers where the oxidants generated from H₂O₂(g) (see Scheme 4.2) reach high concentrations therein.





SCHEME 4.3

The multitude of relatively small signals is consistent with the multiple ways in which these three oxidants can react with the myriad structural isomers of the $(\text{ISO})_{1-8}\text{H}^+$ oligomers. These signals correspond to *bona fide* products, as revealed by the evolution of signal intensities at specific m/z^+ values as functions of gas composition (Figure 4.5). Figure 4.6 shows the MS^2 fragmentation patterns of some of these oxidation products, which display the 42 Da neutral losses typical of the molecular frameworks of parent $(\text{ISO})_n\text{H}^+$ species, in addition to 16 (O), 18 (H_2O) and 28 (CO) Da losses characteristic of the fragmentation of species containing epoxide, alcohol and carbonyl functionalities.⁴⁸ The identification of all products was deemed too onerous and beyond the scope of this paper, because it is doubtful whether it would add additional insights to the observation

that most of the species on which we performed MS² analysis displayed similar fragmentation patterns.

The genealogy of the most conspicuous species can be easily traced from their molecular formulas and typical fragmentations losses. Thus, from the addition of two ·OH radicals to (ISO)₂H⁺ (C₁₀H₁₇⁺, m/z⁺ = 137) we get : C₁₀H₁₇⁺ + 2 ·OH → C₁₀H₁₉O₂⁺, m/z⁺ = 171 (Figures 5D and 6), and C₁₀H₁₉O₂⁺ - H₂O → C₁₀H₁₇O⁺, m/z⁺ = 153 (Figure 6). Alternatively, C₁₀H₁₇⁺ + ·OH + ·OOH → C₁₀H₁₉O₃⁺, m/z⁺ = 187, whose fragmentations lead to: C₁₀H₁₉O₃⁺ - H₂O → C₁₀H₁₇O₂⁺, m/z⁺ = 169, and C₁₀H₁₉O₃⁺ - O₂ → C₁₀H₁₉O⁺, m/z⁺ = 155 (Figure 4.5B and 4.5A, respectively). (ISO)₃H⁺ (C₁₅H₂₅⁺, m/z⁺ = 205), the most abundant oligomer, in similar fashion, gives rise to: C₁₅H₂₅⁺ + 2 ·OH → C₁₅H₂₇O₂⁺, m/z⁺ = 239, C₁₅H₂₅⁺ + ·OH + ·OOH → C₁₅H₂₇O₃⁺, m/z = 255, C₁₅H₂₇O₃⁺ - H₂O → C₁₅H₂₅O₂⁺, m/z⁺ = 237. Possible structures of some of these species are shown as Supporting Information. We estimated a lower limit for the overall yield of oxidation products by summing the intensities of all positive ion signals between 50 - 600 Da in the presence of ISO(g) before and after adding H₂O₂(g). Estimated yields ~ 5% are actually lower limits, because oxidation can also change the positive charge of (ISO)_nH⁺ reactants into neutral or negatively charged products.

We have demonstrated that, in addition to ·OH radicals, the interfacial Fenton reaction produces Fe(IV)=O ferryl species. We have also demonstrated, that poly-iron Fe(IV)=O species are able to transfer an O-atom to the S(IV) center of dimethyl sulfoxide.^{44, 49} The possibility that poly-iron Fe(IV)=O ferryls could add O-atoms to

(ISO)_nH⁺ double bonds was tested in experiments in which 100 μM *t*-BuOH, a standard ·OH radical scavenger, was dissolved in FeCl₂ solutions prior to injection. Figure 4.7 shows that *t*-BuOH *completely* inhibits the formation of carboxylates. Figure 4.8 further reveals that *t*-BuOH has a similar effect on protonable products. On this basis, we infer that the oxidation of ISO(g) on the surface of water is largely driven by ·OH radical addition to the double bonds of interfacial (ISO)_nH⁺ oligomers. Note that *t*-BuOH behaves as a chemical scavenger in these experiments and, therefore, quenches ISO oxidation products by generating new products of its own (Figure 4.8). These findings imply that observed products result from ·OH-initiated chemistry, and are consistent with the smaller yield of ·OH radicals (from R1) versus Fe(IV)=O ferryls (from R2) at the air-water interface.^{44, 49}

ATMOSPHERIC IMPLICATIONS

Recently, we have shown experimentally that unsaturated VOCs, such as ISO(g) and most biogenic terpenes, are protonated in inelastic collisions with the surface of pH < 4 water.¹⁸⁻²⁰ Our results were consistent with uptake coefficients in the $\gamma \sim 10^{-3} - 10^{-4}$ range.¹⁸⁻²⁰ On this basis, we could estimate $\omega_s \sim 4 \times 10^{-5} \text{ s}^{-1}$ frequencies for sticking collisions with acidic aerosol/cloud/fog droplets of typical (S/V) $\sim 3 \times 10^{-5} \text{ cm}^{-1}$ surface densities.^{18-19, 50} This ω_s value is commensurate with the first-order rate constant $\omega_g \sim 2.5 \text{ h}^{-1} = 1 \times 10^{-4} \text{ s}^{-1}$ for the removal of ISO(g) by diurnal ·OH(g).⁵¹⁻⁶⁶ Actual rates will

clearly depend on atmospheric conditions, such as actinic irradiance, relative humidity and Fe(II) content of the aerosol phase.

By scavenging hydrogen peroxide, whose Henry's law constant $H = 10^5 \text{ M atm}^{-1}$ makes it extremely soluble in water, airborne dispersed water represents a significant pool of oxidizing power in the troposphere.^{41, 67-69} Typical $\sim 1 \text{ ppbv H}_2\text{O}_2(\text{g})$ concentrations are in equilibrium with $1 \text{ mM H}_2\text{O}_2(\text{aq})$, which can generate $\cdot\text{OH}(\text{aq})$ via Fenton chemistry⁴⁴ or via photolysis under $\lambda < 350 \text{ nm}$ sunlight.^{54-55, 58, 63, 70-71} Because air masses transported from polluted sources, such as megacities and industrial conglomerates, contain significant H_2O_2 concentrations at nighttime,⁶³ interfacial Fenton chemistry can drive oxidations in the aerosol phase throughout the day.⁵⁸

In this general context, our results provide direct evidence, for the first time, that VOCs can be oxidized day and night on acidic aerosol via interfacial Fenton chemistry. This process represents an additional, hitherto unknown mechanism for the conversion of organic gases into secondary organic aerosol matter. Related experiments involving the reaction of ISO(g) with $\cdot\text{OH}$ radicals from the photolysis of dissolved H_2O_2 will be reported shortly.⁷²

ACKNOWLEDGEMENTS – F. R. K., M. R. H and A. J. C. acknowledge financial support from the National Science Foundation (U.S.A.) Grant AC-1238977. F. R. gratefully acknowledges her tutor, Prof. E. Selli and financial support from the Doctorate School in

Chemistry of the University of Milan. S.E. is grateful to Kurita Water and Environment Foundation and the Japan Science and Technology Agency (JST) PRESTO program.

SUPPORTING INFORMATION AVAILABLE - Additional data and experimental details. This information is available free of charge via the Internet at <http://pubs.acs.org>.

FIGURES

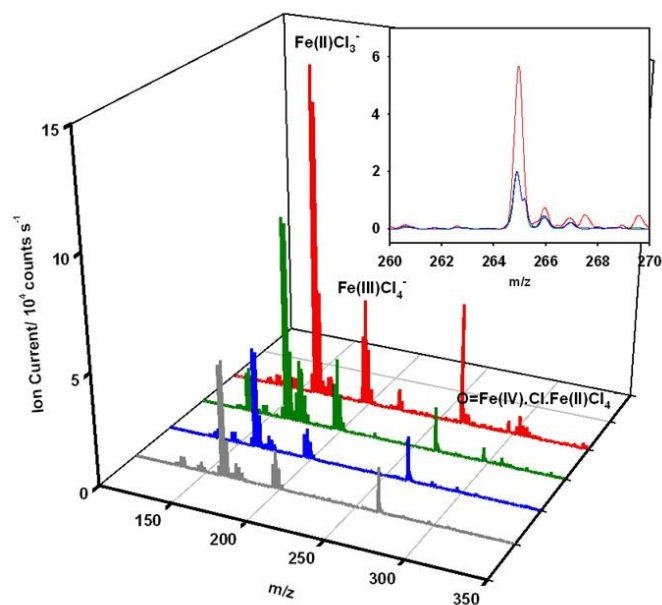


FIGURE 4.1 - Negative ESI-MS of FeCl_2 microjets exposed to: $\text{N}_2(\text{g})$ (grey trace), $\text{ISO}(\text{g})/\text{N}_2(\text{g})$ (blue trace), $\text{H}_2\text{O}_2(\text{g})/\text{N}_2(\text{g})$ (green trace), and $\text{ISO}(\text{g})/\text{H}_2\text{O}_2(\text{g})/\text{N}_2(\text{g})$ (red trace) streams. The inset zooms into the mass range where the $m/z = 265$ product appears. Note that the intensity of the $m/z = 265$ species significantly increases upon the simultaneous presence of $\text{ISO}(\text{g})$ and $\text{H}_2\text{O}_2(\text{g})$.

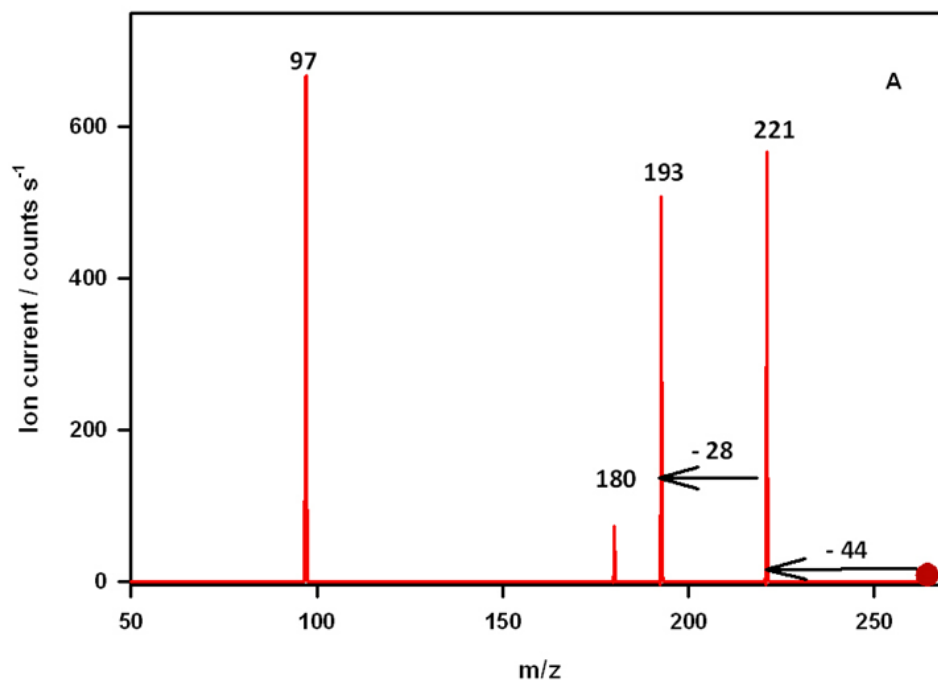
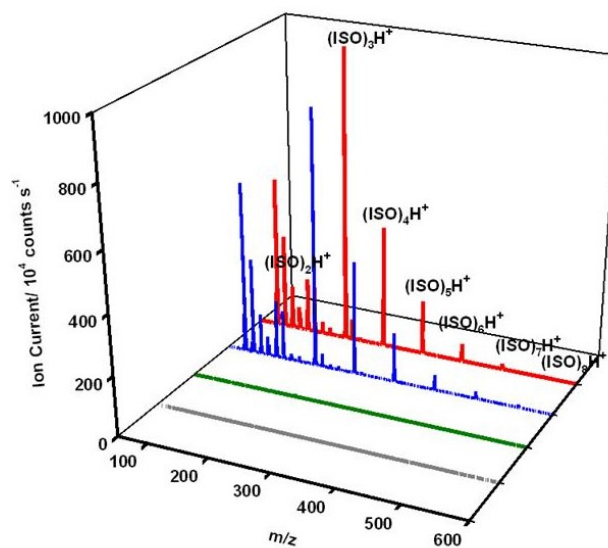
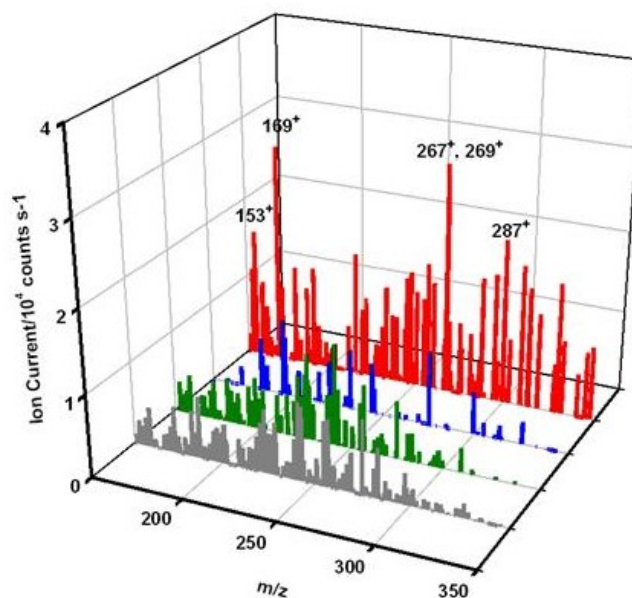


FIGURE 4.2 - MS^2 of $m/z = 265$.



4.3A



4.3 B

FIGURE 4.3 - Positive ESI-MS of 1 μM FeCl_2 at pH 2 (grey traces) exposed to $\text{ISO}(\text{g})/\text{N}_2(\text{g})$ (blue traces), $\text{H}_2\text{O}_2(\text{g})/\text{N}_2(\text{g})$ (green traces), $\text{ISO}(\text{g})/\text{H}_2\text{O}_2(\text{g})/\text{N}_2(\text{g})$ (red traces).

4.3A: spectra in the $m/z = 50 - 600$ Da range.

4.3B: spectra of the less abundant product species in the $m/z = 150 - 350$ Da range.

Note the 250:1 Y-axis scale expansion in 4.3B relative to 4.3A. The largest $(\text{ISO})_{1-8}\text{H}^+$ signals of A were subtracted from the blue and red trace spectra of 4.3B for clarity.

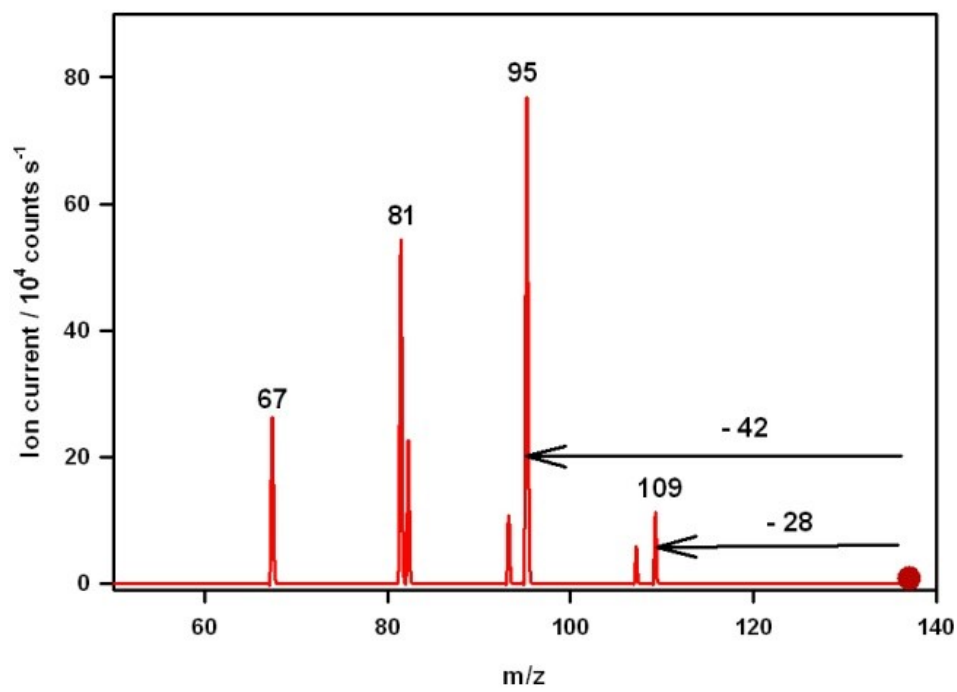


FIGURE 4.4 - MS^2 of $(ISO)_2H^+$, $m/z=137^+$.

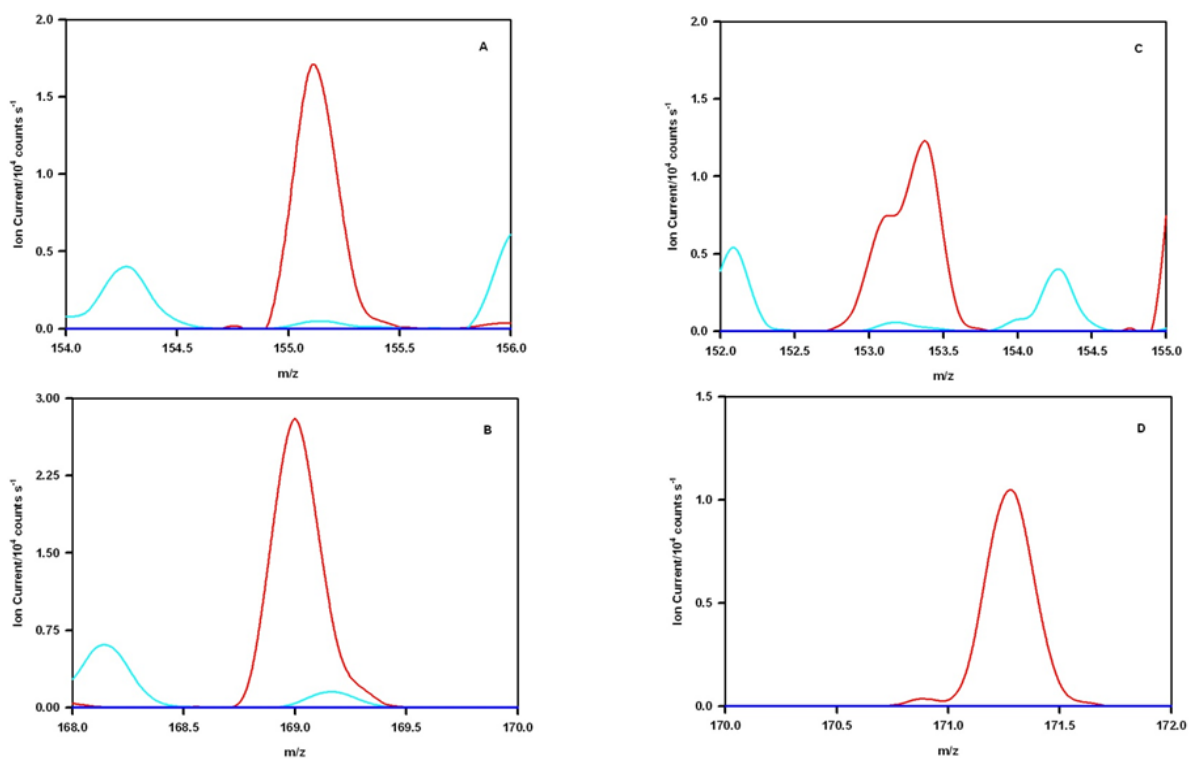


FIGURE 4.5 - Zooming in on the evolution of specific mass spectral peaks as functions of gas composition, and the presence of *t*-BuOH as ·OH radical scavenger. ISO(g): blue trace. ISO(g)/ H₂O₂(g)/N₂(g): red trace. ISO(g)/H₂O₂(g) in the presence of excess dissolved *t*-BuOH (see text): light blue trace. A: $m/z^+ = 155$. B: $m/z^+ = 169$. C: $m/z^+ = 153$. D: $m/z^+ = 171$. [ISO(g)] $\sim 5 \times 10^{15}$ molecules cm⁻³; [H₂O₂(g)] $\sim 4 \times 10^{14}$ molecules cm⁻³.

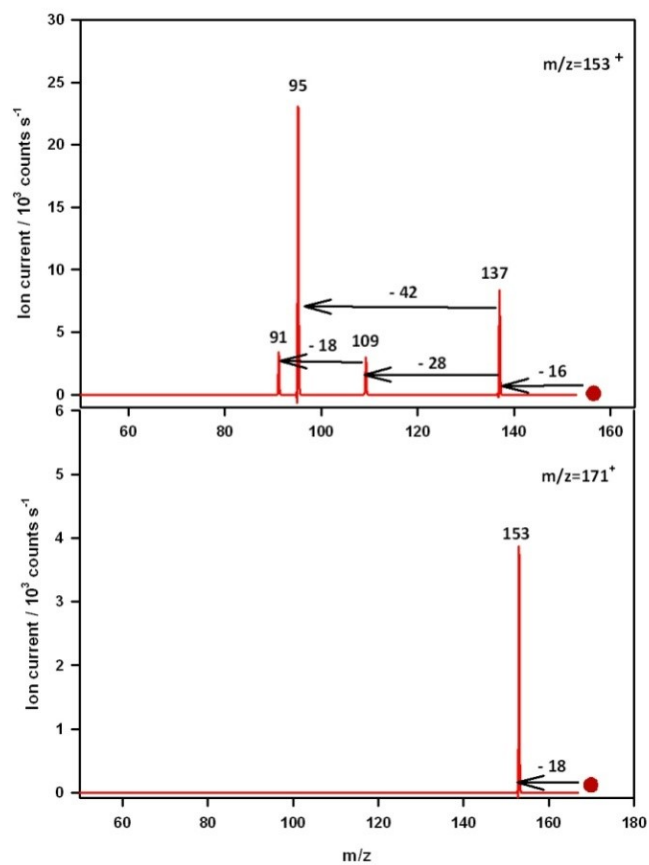


FIGURE 4.6 - MS² of the $m/z^+ = 153$ and $m/z^+ = 171$ product signals of Figure 5.

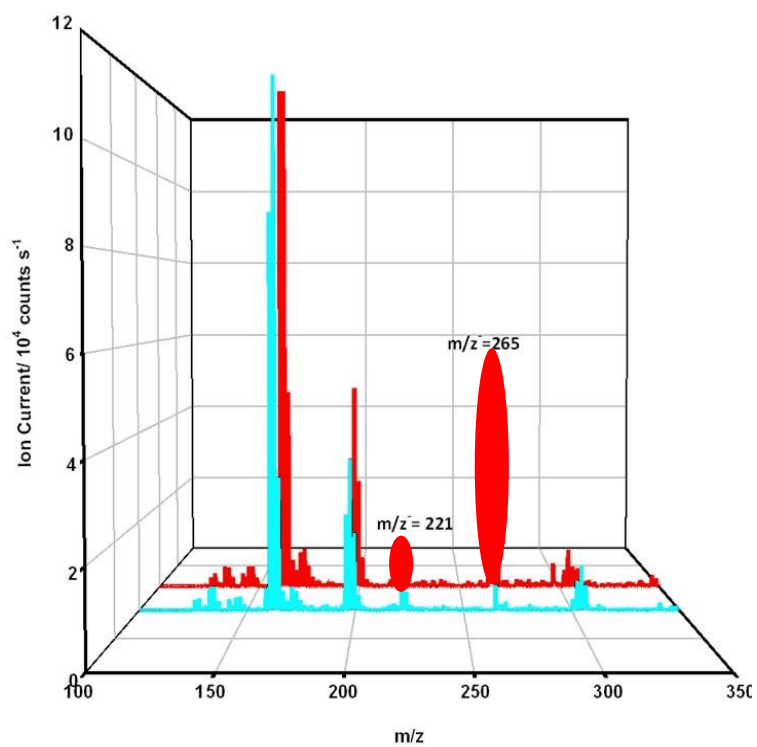


FIGURE 4.7 - Negative ES-MS of $1\mu M$ Fe^{2+} at pH 2, exposed to ISO(g)/ H₂O₂(g)/N₂(g) (red line), ISO(g)/ H₂O₂(g)/N₂(g) in the presence of excess dissolved t-BuOH ($\sim 100 \times [FeCl_2]$) (light blue line) in the $m/z=100-350$ Da range. $[ISO(g)] \sim 5 \times 10^{15}$ molecules cm^{-3} ; $[H_2O_2(g)] \sim 4 \times 10^{14}$ molecules cm^{-3} .

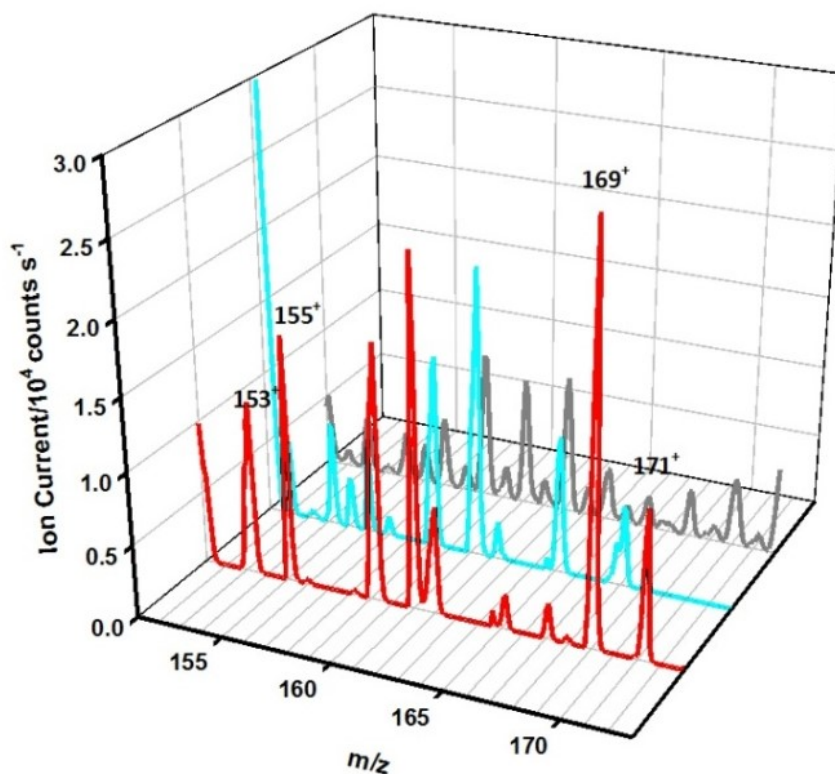


FIGURE 4.8 - Positive ES-MS of $1\mu\text{M Fe}^{2+}$ at pH 2 in the presence of excess dissolved t-BuOH ($\sim 100 \times [\text{FeCl}_2]$) (grey trace), exposed to ISO(g)/H₂O₂(g)/N₂(g) (light blue line) in the range of $m/z = 151\text{-}173$ Da range of the less abundant product species. The red trace represents the ISO(g)/H₂O₂(g)/N₂(g) beams in the absence of t-BuOH. The large (ISO)₁₋₈H⁺ large signals were subtracted from the light blue and red trace spectra for clarity. [ISO(g)] $\sim 5 \times 10^{15}$ molecules cm⁻³; [H₂O₂(g)] $\sim 4 \times 10^{14}$ molecules cm⁻³.

REFERENCE

1. Schryer, D. R., *Heterogeneous Atmospheric Chemistry*. American Geophysical Union: Washington, D.C, 1982; Vol. 26.
2. Heald, C. L.; Jacob, D. J.; Park, R. J.; Russell, L. M.; Huebert, B. J.; Seinfeld, J. H.; Liao, H.; Weber, R. J., A Large Organic Aerosol Source in the Free Troposphere Missing from Current Models. *Geophys. Res. Lett.* **2005**, *32*, L18809.
3. Kanakidou, M.; Seinfeld, J. H.; Pandis, S. N.; Barnes, I.; Dentener, F. J.; Facchini, M. C.; Van Dingenen, R.; Ervens, B.; Nenes, A.; Nielsen, C. J., et al., Organic Aerosol and Global Climate Modelling: A Review. *Atmos. Chem. Phys.* **2005**, *5*, 1053-1123.
4. Kroll, J. H.; Seinfeld, J. H., Chemistry of Secondary Organic Aerosol: Formation and Evolution of Low-Volatility Organics in the Atmosphere. *Atmos. Environm.* **2008**, *42*, 3593-3624.
5. Munger, J. W.; Jacob, D. J.; Waldman, J. M.; Hoffmann, M. R., Fogwater Chemistry in an Urban Atmosphere. *J. Geophys. Res.-Atmos.* **1983**, *88*, 5109-5121.
6. Paulot, F.; Crouse, J. D.; Kjaergaard, H. G.; Kurten, A.; St Clair, J. M.; Seinfeld, J. H.; Wennberg, P. O., Unexpected Epoxide Formation in the Gas-Phase Photooxidation of Isoprene. *Science* **2009**, *325*, 730-733.
7. Whalley, L.; Stone, D.; Heard, D., New Insights into the Tropospheric Oxidation of Isoprene: Combining Field Measurements, Laboratory Studies, Chemical Modelling and Quantum Theory. In *Atmospheric and Aerosol Chemistry*, McNeill, V. F.; Ariya, P. A., Eds. 2014; Vol. 339, pp 55-95.

8. Donaldson, D. J.; Valsaraj, K. T., Adsorption and Reaction of Trace Gas-Phase Organic Compounds on Atmospheric Water Film Surfaces: A Critical Review. *Environ. Sci. Technol.* **2010**, *44*, 865-873.
9. Valsaraj, K. T., Onn the Physicochemical Aspects of Partitioning of Non-Polar Hydrophobic Organics at the Air-Water Interface. *Chemosphere* **1988**, *17*, 875-887.
10. Valsaraj, K. T., A Review of the Aqueous Aerosol Surface Chemistry in the Atmospheric Context. *Open Journal of Physical Chemistry* **2012**, *2*, 58-66.
11. Valsaraj, K. T.; Thoma, G. J.; Reible, D. D.; Thibodeaux, L. J., On the Enrichment of Hydrophobic Organic-Compounds in Fog Droplets. *Atmos Environ* **1993**, *27*, 203-210.
12. Enami, S.; Hoffmann, M. R.; Colussi, A. J., How Phenol and α -Tocopherol React with Ambient Ozone at Gas/Liquid Interfaces. *J. Phys. Chem. B* **2009**, *113*, 7002-7007.
13. Enami, S.; Hoffmann, M. R.; Colussi, A. J., Simultaneous Detection of Cysteine Sulfenate, Sulfinate, and Sulfonate During Cysteine Interfacial Ozonolysis. *J. Phys. Chem. B* **2009**, *113*, 9356-9358.
14. Enami, S.; Hoffmann, M. R.; Colussi, A. J., Absorption of Inhaled NO₂. *J Phys Chem B* **2009**, *113*, 7977-7981.
15. Enami, S.; Hoffmann, M. R.; Colussi, A. J., Prompt Formation of Organic Acids in Pulse Ozonation of Terpenes on Aqueous Surfaces. *J. Phys. Chem. Lett.* **2010**, *1*, 2374-2379.
16. Enami, S.; Hoffmann, M. R.; Colussi, A. J., Proton Availability at the Air/Water Interface. *J Phys Chem Lett* **2010**, *1*, 1599-1604.

17. Enami, S.; Hoffmann, M. R.; Colussi, A. J., Molecular Control of Reactive Gas Uptake "on Water". *J Phys Chem A* **2010**, *114*, 5817-5822.
18. Enami, S.; Hoffmann, M. R.; Colussi, A. J., Dry Deposition of Biogenic Terpenes Via Cationic Oligomerization on Environmental Aqueous Surfaces. *J. Phys. Chem. Lett.* **2012**, *3*, 3102-3108.
19. Enami, S.; Mishra, H.; Hoffmann, M. R.; Colussi, A. J., Protonation and Oligomerization of Gaseous Isoprene on Mildly Acidic Surfaces: Implications for Atmospheric Chemistry. *J. Phys. Chem. A* **2012**, *116*, 6027-6032.
20. Enami, S.; Stewart, L. A.; Hoffmann, M. R.; Colussi, A. J., Superacid Chemistry on Mildly Acidic Water. *J Phys Chem Lett* **2010**, *1*, 3488-3493.
21. Enami, S.; Vecitis, C. D.; Cheng, J.; Hoffmann, M. R.; Colussi, A. J., Global Inorganic Source of Atmospheric Bromine. *J. Phys. Chem. A* **2007**, *111*, 8749-8752.
22. Mishra, H.; Enami, S.; Nielsen, R. J.; Hoffmann, M. R.; Goddard, W. A.; Colussi, A. J., Anions Dramatically Enhance Proton Transfer through Aqueous Interfaces. *P. Natl. Acad. Sci. USA* **2012**, *109*, 10228-10232.
23. Mishra, H.; Enami, S.; Nielsen, R. J.; Stewart, L. A.; Hoffmann, M. R.; Goddard, W. A.; Colussi, A. J., Bronsted Basicity of the Air-Water Interface. *P. Natl. Acad. Sci. USA* **2012**, *109*, 18679-18683.
24. Seinfeld, J. H.; Pandis, S. N., *Atmospheric Chemistry and Physics: From Air Pollution to Climate Change*. 2nd ed.; Wiley: Hoboken, N.J., 2006, pp. 284-302 and 932.

25. Tong, C. H.; Clegg, S. L.; Seinfeld, J. H., Comparison of Activity Coefficient Models for Atmospheric Aerosols Containing Mixtures of Electrolytes, Organics, and Water. *Atmos Environ* **2008**, *42*, 5459-5482.
26. Enami, S.; Hoffmann, M. R.; Colussi, A. J., Ozone Oxidizes Glutathione to a Sulfonic Acid. *Chem. Res. Toxicol.* **2009**, *22*, 35-40.
27. Rudich, Y., Laboratory Perspectives on the Chemical Transformations of Organic Matter in Atmospheric Particles. *Chem. Rev.* **2003**, *103*, 5097-5124.
28. Laskin, J.; Laskin, A.; Nizkorodov, S. A., New Mass Spectrometry Techniques for Studying Physical Chemistry of Atmospheric Heterogeneous Processes. *International Reviews in Physical Chemistry* **2013**, *32*, 128-170.
29. Chameides, W. L.; Fehsenfeld, F.; Rodgers, M. O.; Cardelino, C.; Martinez, J.; Parrish, D.; Lonneman, W.; Lawson, D. R.; Rasmussen, R. A.; Zimmerman, P., et al., Ozone Precursor Relationships in the Ambient Atmosphere. *J. Geophys. Res.-Atmos.* **1992**, *97*, 6037-6055.
30. Guenther, A.; Karl, T.; Harley, P.; Wiedinmyer, C.; Palmer, P. I.; Geron, C., Estimates of Global Terrestrial Isoprene Emissions Using Megan (Model of Emissions of Gases and Aerosols from Nature). *Atmos Chem Phys* **2006**, *6*, 3181-3210.
31. Carlton, A. G.; Wiedinmyer, C.; Kroll, J. H., A Review of Secondary Organic Aerosol (SOA) Formation from Isoprene. *Atmos. Chem. Phys.* **2009**, *9*, 4987-5005.
32. Carlton, A. G.; Pinder, R. W.; Bhave, P. V.; Pouliot, G. A., To What Extent Can Biogenic SOA Be Controlled? *Environ Sci Technol* **2010**, *44*, 3376-3380.

33. He, C.; Liu, J.; Carlton, A. G.; Fan, S.; Horowitz, L. W.; Levy, H.; Tao, S., Evaluation of Factors Controlling Global Secondary Organic Aerosol Production from Cloud Processes. *Atmos Chem Phys* **2013**, *13*, 1913-1926.
34. Huang, D. M.; Chen, Z. M., Reinvestigation of the Henry's Law Constant for Hydrogen Peroxide with Temperature and Acidity Variation. *Journal of Environmental Sciences-China* **2010**, *22*, 570-574.
35. Fan, J. W.; Zhang, R. Y., Atmospheric Oxidation Mechanism of Isoprene. *Environ. Chem.* **2004**, *1*, 140-149.
36. Huang, D.; Zhang, X.; Chen, Z. M.; Zhao, Y.; Shen, X. L., The Kinetics and Mechanism of an Aqueous Phase Isoprene Reaction with Hydroxyl Radical. *Atmos. Chem. Phys.* **2011**, *11*, 7399-7415.
37. Santos, L. S.; Dalmazio, I.; Eberlin, M. N.; Claeys, M.; Augusti, R., Mimicking the Atmospheric OH-Radical-Mediated Photooxidation of Isoprene: Formation of Cloud-Condensation Nuclei Polyols Monitored by Electrospray Ionization Mass Spectrometry. *Rapid Commun Mass Sp* **2006**, *20*, 2104-2108.
38. Kleindienst, T. E.; Lewandowski, M.; Offenberg, J. H.; Jaoui, M.; Edney, E. O., The Formation of Secondary Organic Aerosol from the Isoprene Plus OH Reaction in the Absence of NO_x. *Atmos Chem Phys* **2009**, *9*, 6541-6558.
39. Epstein, S. A.; Nizkorodov, S. A., A Comparison of the Chemical Sinks of Atmospheric Organics in the Gas and Aqueous Phase. *Atmos Chem Phys* **2012**, *12*, 8205-8222.

40. Nguyen, T. B.; Laskin, A.; Laskin, J.; Nizkorodov, S. A., Direct Aqueous Photochemistry of Isoprene High-NO_x Secondary Organic Aerosol. *Phys Chem Chem Phys* **2012**, *14*, 9702-9714.
41. Kameel, F. R.; Hoffmann, M. R.; Colussi, A. J., OH Radical-Initiated Chemistry of Isoprene in Aqueous Media. Atmospheric Implications. *J. Phys. Chem. A* **2013**, *117*, 5117-5123.
42. Enami, S.; Colussi, A. J., Long-Range Specific Ion-Ion Interactions in Hydrogen-Bonded Liquid Films. *J Chem Phys* **2013**, *138*.
43. Enami, S.; Mishra, H.; Hoffmann, M. R.; Colussi, A. J., Hofmeister Effects in Micromolar Electrolyte Solutions. *J. Chem. Phys.* **2012**, *136*.
44. Enami, S.; Sakamoto, Y.; Colussi, A. J., Fenton Chemistry at Aqueous Interfaces. *Proc. Natl. Acad. Sci. U. S. A.* **2014**, *111*, 623-628.
45. Stark, M. S., Addition of Peroxyl Radicals to Alkenes and the Reaction of Oxygen with Alkyl Radicals. *J. Am. Chem. Soc.* **2000**, *122*, 4162-4170.
46. Villano, S. M.; Carstensen, H. H.; Dean, A. M., Rate Rules, Branching Ratios, and Pressure Dependence of the HO₂ + Olefin Addition Channels. *J. Phys. Chem. A* **2013**, *117*, 6458-6473.
47. Zador, J.; Klippenstein, S. J.; Miller, J. A., Pressure-Dependent OH Yields in Alkene Plus HO₂ Reactions: A Theoretical Study. *J. Phys. Chem. A* **2011**, *115*, 10218-10225.

48. Kahnt, A.; Iinuma, Y.; Mutzel, A.; Boge, O.; Claeys, M.; Herrmann, H., Campholenic Aldehyde Ozonolysis: A Mechanism Leading to Specific Biogenic Secondary Organic Aerosol Constituents. *Atmos. Chem. Phys.* **2014**, *14*, 719-736.
49. Bataineh, H.; Pestovsky, O.; Bakac, A., pH-Induced Mechanistic Changeover from Hydroxyl Radicals to Iron(IV) in the Fenton Reaction. *Chem. Sci.* **2012**, *3*, 1594-1599.
50. Yabushita, A.; Enami, S.; Sakamoto, Y.; Kawasaki, M.; Hoffmann, M. R.; Colussi, A. J., Anion-Catalyzed Dissolution of NO₂ on Aqueous Microdroplets. *J. Phys. Chem. A* **2009**, *113*, 4844-4848.
51. Charbouillot, T.; Brigante, M.; Deguillaume, L.; Mailhot, G., Atmospheric Aqueous-Phase Photoreactivity: Correlation between the Hydroxyl Radical Photoformation and Pesticide Degradation Rate in Atmospherically Relevant Waters. *Photochem. Photobiol.* **2012**, *88*, 32-37.
52. Charbouillot, T.; Gorini, S.; Voyard, G.; Parazols, M.; Brigante, M.; Deguillaume, L.; Delort, A. M.; Mailhot, G., Mechanism of Carboxylic Acid Photooxidation in Atmospheric Aqueous Phase: Formation, Fate and Reactivity. *Atmos. Environ.* **2012**, *56*, 1-8.
53. Chevallier, E.; Jolibois, R. D.; Meunier, N.; Carlier, P.; Monod, A., "Fenton-Like" Reactions of Methylhydroperoxide and Ethylhydroperoxide with Fe²⁺ in Liquid Aerosols under Tropospheric Conditions. *Atmos. Environ.* **2004**, *38*, 921-933.

54. Deguillaume, L.; Leriche, M.; Chaumerliac, N., Impact of Radical Versus Non-Radical Pathway in the Fenton Chemistry on the Iron Redox Cycle in Clouds. *Chemosphere* **2005**, *60*, 718-724.
55. Deguillaume, L.; Leriche, M.; Monod, A.; Chaumerliac, N., The Role of Transition Metal Ions on HO_x Radicals in Clouds: A Numerical Evaluation of Its Impact on Multiphase Chemistry. *Atmos. Chem. Phys.* **2004**, *4*, 95-110.
56. Ervens, B.; George, C.; Williams, J. E.; Buxton, G. V.; Salmon, G. A.; Bydder, M.; Wilkinson, F.; Dentener, F.; Mirabel, P.; Wolke, R., et al., Capram 2.4 (Modac Mechanism): An Extended and Condensed Tropospheric Aqueous Phase Mechanism and Its Application. *J. Geophys. Res-Atmos.* **2003**, *108*.
57. Graedel, T. E.; Mandich, M. L.; Weschler, C. J., Kinetic Model Studies of Atmospheric Droplet Chemistry. 2. Homogeneous Transition Metal Chemistry in Raindrops. *J. Geophys. Res.-Atmos.* **1986**, *91*, 5205-5221.
58. Guo, J.; Tilgner, A.; Yeung, C.; Wang, Z.; Louie, P. K. K.; Luk, C. W. Y.; Xu, Z.; Yuan, C.; Gao, Y.; Poon, S., et al., Atmospheric Peroxides in a Polluted Subtropical Environment: Seasonal Variation, Sources and Sinks, and Importance of Heterogeneous Processes. *Environ. Sci. Technol.* **2014**, *48*, 1443-1450.
59. Jacobsen, F.; Holcman, J.; Sehested, K., Reactions of the Ferryl Ion with Some Compounds Found in Cloud Water. *Int. J. Chem. Kinet.* **1998**, *30*, 215-221.

60. Leriche, M.; Voisin, D.; Chaumerliac, N.; Monod, A.; Aumont, B., A Model for Tropospheric Multiphase Chemistry: Application to One Cloudy Event During the Cime Experiment. *Atmos. Environ.* **2000**, *34*, 5015-5036.
61. Liang, H.; Chen, Z. M.; Huang, D.; Zhao, Y.; Li, Z. Y., Impacts of Aerosols on the Chemistry of Atmospheric Trace Gases: A Case Study of Peroxides and HO₂ Radicals. *Atmos. Chem. Phys.* **2013**, *13*, 11259-11276.
62. Long, Y.; Charbouillot, T.; Brigante, M.; Mailhot, G.; Delort, A. M.; Chaumerliac, N.; Deguillaume, L., Evaluation of Modeled Cloud Chemistry Mechanism against Laboratory Irradiation Experiments: The Hxoy/Iron/Carboxylic Acid Chemical System. *Atmos. Environ.* **2013**, *77*, 686-695.
63. Marinoni, A.; Parazols, M.; Brigante, M.; Deguillaume, L.; Amato, P.; Delort, A. M.; Laj, P.; Mailhot, G., Hydrogen Peroxide in Natural Cloud Water: Sources and Photoreactivity. *Atmos. Res.* **2011**, *101*, 256-263.
64. Minero, C.; Lucchiari, M.; Maurino, V.; Vione, D., A Quantitative Assessment of the Production of (OH)-O-Center Dot and Additional Oxidants in the Dark Fenton Reaction: Fenton Degradation of Aromatic Amines. *Rsc. Advances.* **2013**, *3*, 26443-26450.
65. Tilgner, A.; Brauer, P.; Wolke, R.; Herrmann, H., Modelling Multiphase Chemistry in Deliquescent Aerosols and Clouds Using Capram3.0i. *J. Atmos. Chem.* **2013**, *70*, 221-256.

66. Vaitilingom, M.; Charbouillot, T.; Deguillaume, L.; Maisonobe, R.; Parazols, M.; Amato, P.; Sancelme, M.; Delort, A. M., Atmospheric Chemistry of Carboxylic Acids: Microbial Implication Versus Photochemistry. *Atmos. Chem. Phys.* **2011**, *11*, 8721-8733.
67. Jacob, D. J., Heterogeneous Chemistry and Tropospheric Ozone. *Atmos. Environ.* **2000**, *34*, 2131-2159.
68. Mao, J.; Fan, S.; Jacob, D. J.; Travis, K. R., Radical Loss in the Atmosphere from Cu-Fe Redox Coupling in Aerosols. *Atmos. Chem. Phys.* **2013**, *13*, 509-519.
69. Wu, S. L.; Mickley, L. J.; Jacob, D. J.; Logan, J. A.; Yantosca, R. M.; Rind, D., Why Are There Large Differences between Models in Global Budgets of Tropospheric Ozone? *J. Geophys. Res-Atmos.* **2007**, *112*.
70. Siefert, R. L.; Johansen, A. M.; Hoffmann, M. R.; Pehkonen, S. O., Measurements of Trace Metal (Fe, Cu, Mn, Cr) Oxidation States in Fog and Stratus Clouds. *Journal of the Air & Waste Management Association* **1998**, *48*, 128-143.
71. Siefert, R. L.; Webb, S. M.; Hoffmann, M. R., Determination of Photochemically Available Iron in Ambient Aerosols. *J. Geophys. Res-Atmos.* **1996**, *101*, 14441-14449.
72. Enami, S.; Hoffmann, M. R.; Colussi, A. J., In Situ Mass Spectrometric Detection of Interfacial Intermediates in the Oxidation of RCOOH(Aq) by Gas-Phase OH-Radicals *J. Phys. Chem. A* **2014**, *118*, 4130-4137.